Coupling of two chemical reactions through an oxygen transporting perovskite membrane: Thermodynamic and kinetic control

Von der Naturwissenschaftlichen Fakultät

der Gottfried Wilhelm Leibniz Universität Hannover

zur Erlangung des Grades

Doktor der Naturwissenschaften

Dr. rer. nat.

genehmigte Dissertation

von

M.Sc. Heqing Jiang

geboren am 12.09.1978 in Henan, China

Hannover, 2010

Referent: Univ.-Prof. Dr. Jürgen Caro

Korreferent: Univ.-Prof. Dr. Thomas Scheper

Tag der Promotion: 03.05.2010

Preface

The presented results of this thesis were achieved since April 16, 2007 during my Ph. D. study at the Institute of Physical Chemistry and Electrochemistry at the Gottfried Wilhelm Leibniz Universität Hannover under the supervision of Prof. Dr. Jürgen Caro. In this period, I have also been a scientific co-worker and worked for the BMBF project SynMem and the European project NASA-OTM.

Six research articles in which I am the first author are presented within this thesis. I wrote the first draft of the six papers, Prof. Dr. J. Caro and other co-authors corrected and improved them. The following statement will point out my contribution to the articles collected in this thesis. For all these articles, I would like to acknowledge the fruitful discussions and valuable comments from the co-authors and referees, particularly from Prof. Dr. J. Caro, Prof. Dr. H. Wang, Dr. S. Werth, and Priv.-Doz. Dr. A. Feldhoff. All the dense hollow fiber membranes used during my Ph. D. work were provided by Dr. T. Schiestel from the Fraunhofer Institute of Interfacial Engineering and Biotechnology (IGB) in Stuttgart.

Three articles studying the thermodynamic coupling for hydrogen production from water splitting are collected in Chapter 2. The first article, *Hydrogen production by water dissociation in surface-modified $BaCo_xFe_yZr_{1-x-y}O_{3-\delta}$ hollow fiber membrane reactor with improved oxygen permeation,* was written by me. I got support on the manuscript preparation from all the co-authors, especially from Prof. Dr. J. Caro, Priv.-Doz. Dr. A. Feldhoff and K. Efimov. The $BaCo_xFe_yZr_{0.9-x-y}Pd_{0.1}O_{3-\delta}$ (BCFZ-Pd) powder was prepared by F. Liang following my idea. Deposition of the BCFZ-Pd porous layer onto the BCFZ hollow fiber membrane and all the measurements of oxygen permeation and hydrogen production were done by myself. SEM and TEM characterizations were done by me, Priv.-Doz. Dr. A. Feldhoff, and K. Efimov. The second article, *Simultaneous production of hydrogen and synthesis gas by combining water splitting with partial oxidation of methane in a hollow-fiber membrane reactor,* was written by me. The experimental results and calculations were mainly done by myself. Prof. Dr. J. Caro and Prof. Dr. H. Wang provided strong support on the manuscript preparation. The third article, *A coupling strategy to produce hydrogen and ethylene in a membrane reactor,* was also written by me, and Prof. Dr. J. Caro improved it. The measurements were conducted by Zhengwen Cao and me in almost equal shares. SEM measurements were done by myself.

Another three articles focusing on the kinetic coupling for nitrogen oxides decomposition are collected in Chapter 3. The first article, *Highly effective NO decomposition by in situ removal of inhibitor oxygen using an oxygen transporting membrane,* was written by me. The measurements and the interpretation were carried out by Lei Xing and me. I wrote the first draft of the second article: *Direct decomposition of nitrous oxide to nitrogen by in situ oxygen removal with a perovskite membrane.* Prof. Dr. J. Caro and Prof. Dr. H. Wang spent much time on correcting and improving it. Dr. S. Werth wrote the German version of this article. All the measurements and calculations included in this article were conducted by myself under the supervision of Prof. Dr. J. Caro. The third article, *Improved water dissociation and nitrous oxide decomposition by in situ oxygen removal in perovskite catalytic membrane reactor*, was written by me with the help of Prof. Dr. J. Caro. All the measurements, calculations and interpretation were mainly carried out by myself. Additionally, I obtained support on the manuscript preparation from all co-authors.

Acknowledgement

Abstract

The equilibrium controlled water splitting and the kinetically controlled nitrogen oxides (NO and N_2O) decomposition were studied in the perovskite $BaCo_xFe_yZr_{1-x-y}O_{3-\delta}$ (BCFZ) hollow fiber membrane reactor that allows the selective permeation of oxygen. The hydrogen production rate or the conversion of NO and N_2O directly depends on the rate of oxygen removal from the system of water splitting or nitrogen oxides decomposition. To improve the oxygen permeation rate and thus the reactor performance, a series of oxygen-consuming reactions were coupled with water splitting or nitrogen oxides decomposition on the opposite sides of the BCFZ membrane reactor.

Chapter 2 demonstrated the effective hydrogen production from water splitting by in situ removing oxygen from the steam side to the other side of the BCFZ membrane, where the permeated oxygen was continuously consumed by methane combustion, partial oxidation of methane (POM), or oxidative dehydrogenation of ethane (ODE). First, when a catalytic $BaCo_xFe_yZr_{0.9-x-y}Pd_{0.1}O_{3-\delta}$ (BCFZ-Pd) porous layer was elaborately attached to the outer surface of the dense BCFZ membrane, the permeated oxygen was even more effectively consumed by methane combustion, leading to a larger gradient of oxygen partial pressure across the membrane. The oxygen permeation rate was increased by 3.5 times as compared to that of the blank BCFZ membrane, and the hydrogen production rate was increased from 0.7 to 2.1 mL min^{-1} cm^{-2} at 950 °C after depositing a BCFZ-Pd porous layer onto the BCFZ membrane. When packing a Ni-based catalyst and feeding methane to the shell side, not only a hydrogen production rate of 3.1 mL min^{-1} cm^{-2} was achieved at 950 °C on the core side, but also synthesis gas was obtained on the shell side. A lower operating temperature was achieved by coupling water splitting with the ODE process on the opposite sides of the BCFZ hollow fiber membrane. At 800 °C, not only a hydrogen production rate of 1.0 mL min^{-1} cm^{-2} was obtained, but also an ethylene yield of around 55 % was achieved on the other side of the BCFZ membrane. Moreover, the operation for the simultaneous production of hydrogen on the core side and ethylene on the shell side was conducted for 100 h without membrane failure.

During the decomposition of NO or N_2O into N_2 and O_2 over perovskite BCFZ, the produced oxygen acts as an inhibitor. The effective abatement of NO and N_2O by in situ removing the inhibitor oxygen via the perovskite BCFZ oxygen-permeable membrane was

presented in Chapter 3. It was found that the conversion of NO or N_2O on the core side is very low when no sweep gas was applied on the shell side. However, when feeding methane in combination with Ni-based catalyst to the shell side, the direct decomposition of NO over the inner surface of the BCFZ hollow fiber membrane was achieved with NO conversion of almost 100 % and N_2 yield of around 95 % even with coexisting 3 vol.% oxygen in the feed. For the N_2O decomposition in the BCFZ membrane reactor, the oxygen concentration on N_2O side can be kept at a low level by increasing the operating temperature or the pressure difference across the membrane or by feeding reducing gases like methane or ethane on permeate side. Benefiting from the effective oxygen removal via the BCFZ oxygen-permeable membrane, a complete decomposition of N_2O with the concentration of up to 50 vol.% was obtained at 875 °C. Moreover, the permeated oxygen was utilized to produce synthesis gas by the POM or ethylene by the ODE process on the shell side. A methane conversion of over 90 % and a CO selectivity of 90 % were obtained at 875 °C with the simultaneous complete decomposition of 20 vol.% N_2O.

Zusammenfassung

Die gleichgewichtskontrollierte Zersetzung von Wasser in die Elemente als auch die kinetisch kontrollierte Zersetzung von Stickstoffoxiden (NO und N_2O) wurden in einem sauerstoffleitenden perowskitischen Hohlfasermembranreaktor der Zusammensetzung $BaCo_xFe_yZr_{1-x-y}O_{3-\delta}$ (BCFZ) untersucht.

Die Bildungsgeschwindigkeit von Wasserstoff bzw. der Umsatz von NO oder N_2O hängt dabei direkt von der Geschwindigkeit ab, mit der der Sauerstoff aus dem System entfernt wird. Um den Sauerstofffluss durch die Membran und folglich die Reaktorleistung zu verbessern, wurden eine Reihe von sauerstoffverbrauchenden Reaktionen mit der Zersetzung von Wasser oder Stickstoffoxiden auf der gegenüberliegenden Seite der BCFZ-Membran gekoppelt.

Kapitel 2 beschreibt die Wasserstoffproduktion durch Wasserzersetzung in die Elemente durch In-Situ-Entfernung von Sauerstoff von der Wasserdampf-Seite zur anderen Seite der BCFZ-Membran, wo der permeierte Sauerstoff kontinuierlich durch Methanverbrennung, Partielle Oxidation von Methan (POM) oder Oxidative Dehydrierung von Ethan (ODE) verbraucht werden kann.

Wird eine poröse katalytische BCFZ-Pd-Schicht auf die äußere Oberfläche der dichten BCFZ-Membran aufgebracht, so wird der permeierte Sauerstoff sogar noch effektiver durch die Methanverbrennung umgesetzt. Dies führt zu einem größeren O_2-Partialdruckgradienten über den Querschnitt der Membran. Die Sauerstoffpermeationsrate vergrößerte sich um ein 3,5-faches, verglichen mit der unbeschichteten BCFZ-Membran. Die Wasserstoffbildungsgeschwindigkeit bei 950 °C stieg von 0.7 auf 2.1 mL min^{-1} cm^{-2} nach Beschichtung der BCFZ-Membran mit einer porösen BCFZ-Pd-Schicht. Wird um die Membran ein Festbett eines Ni-Katalysators verwendet und Methan auf die Außenseite der Faser gegeben, so wird nicht nur eine Wasserstoffbildungsgeschwindigkeit von 3.1 mL min^{-1} cm^{-2} bei 950 °C auf der Innenseite der Membran erreicht, sondern es kann zudem auf der Shell-Seite Synthesegas gebildet werden. Eine niedrigere Reaktionstemperatur konnte realisiert werden, indem die Wasserzersetzung auf der einen Seite mit der Oxidativen Dehydrierung von Ethan auf der gegenüberliegenden Seite der BCFZ-Hohlfasermembran kombiniert wurde. Bei 800 °C wurde hier nicht nur eine Wasserstoffbildungsgeschwindigkeit von 1.0 mL min^{-1} cm^{-2} erreicht, sondern auch eine Ethylenausbeute von ca. 55 % auf der anderen Seite der Membran.

Darüberhinaus konnte für diese simultane Wasserstoffproduktion auf der Core-Seite und Ethylen Produktion auf der Shell-Seite eine Langzeitstabilität des Membranreaktors von über 100 Stunden realisiert werden.

Bei der Zersetzung von NO bzw. N_2O in die Elemente über dem BCFZ-Perowskiten agiert der produzierte Sauerstoff als Inhibitor. Die effektive Entsorgung von NO und N_2O durch In-Situ-Entfernung des inhibierenden Sauerstoffs über der sauerstoffleitenden BCFZ-Perowskithohlfasermembran wird in Kapitel 3 vorgestellt. Dort konnte gezeigt werden, dass der Umsatz von NO oder N_2O auf der Inneseite sehr gering ist, sofern kein Spülgas auf der Shell-Seite verwendet wurde. Wurde jedoch Methan als Spülgas in Kombination mit einem Nickel-Katalysator auf der Shell-Seite eingesetzt, so konnte für die direkte Zersetzung von NO an der inneren Oberfläche der BCFZ-Hohlfasermembran ein NO-Umsatz von nahezu 100 % sowie eine N_2-Ausbeute von ca. 95 % bei einem 3 vol.-% Restgehalt von Sauerstoff im Feed erreicht werden. Für die Lachgaszersetzung im BCFZ-Membranreaktor konnte die O_2-Konzentration auf der Lachgas-Seite durch Erhöhung der Betriebstemperatur oder der Druckdifferenz über der Membran als auch durch Zugabe von reduzierenden Gasen wie Methan oder Ethan auf der Permeatseite gering gehalten werden.

Mit Hilfe der effektiven Sauerstoffentfernung durch die sauerstoffleitende BCFZ-Membran konnte eine komplette Zersetzung von Lachgas bei 875 °C in Konzentrationen bis zu 50 vol.-% erreicht werden. Außerdem konnte der permeierte Sauerstoff verwendet werden, um Synthesegas durch die Partialoxidation von Methan oder Ethylen durch die Oxidative Dehydrierung von Ethan auf der Shell-Seite zu produzieren. Zum Beispiel konnte ein Methanumsatz von über 90 % und eine CO-Selektivität von 90 % bei 875 °C erzielt werden, während auf der anderen Membranseite ein 20 vol.-%iger N_2O-Gasstrom komplett zersetzt werden konnte.

Schlagwörter: Perowskitischer Membranreaktor, Kopplung, Wasserzersetzung, Zersetzung von Stickstoffoxiden, Partielle Oxidation

Contents

Chapter 1

Introduction

It is predicted that human beings will face the problem of the lack of fossil oil and natural gas in the twenty-first century. Simultaneously, human beings have faced, are facing, and will face environmental problems that are strongly linked to the production, transformation, and consumption of energy. As shown in Figure 1.1, chemical industry brings us the environmental problem while it meets the basic human needs. It is necessary for the chemical industry to build innovative process-engineering technologies for the reduction of energy consumption and the minimization of waste streams.

The two most important and often the most expensive steps in a chemical process are usually the chemical reaction and the separation of the product stream. Both the process economics and the efficient use of natural resources could be improved by the combination of these two unit operations in a single device called membrane reactor, leading to potential savings in energy consumption, effective use of raw materials and reduced formation of by-products.[1] According to the IUPAC definition, a membrane reactor is a device combining a membrane based separation and a chemical reaction in one unit.[2, 3] Membranes and membrane reactor technology are expected to play a tremendous impact on the production of clean energy while safeguarding the environment.
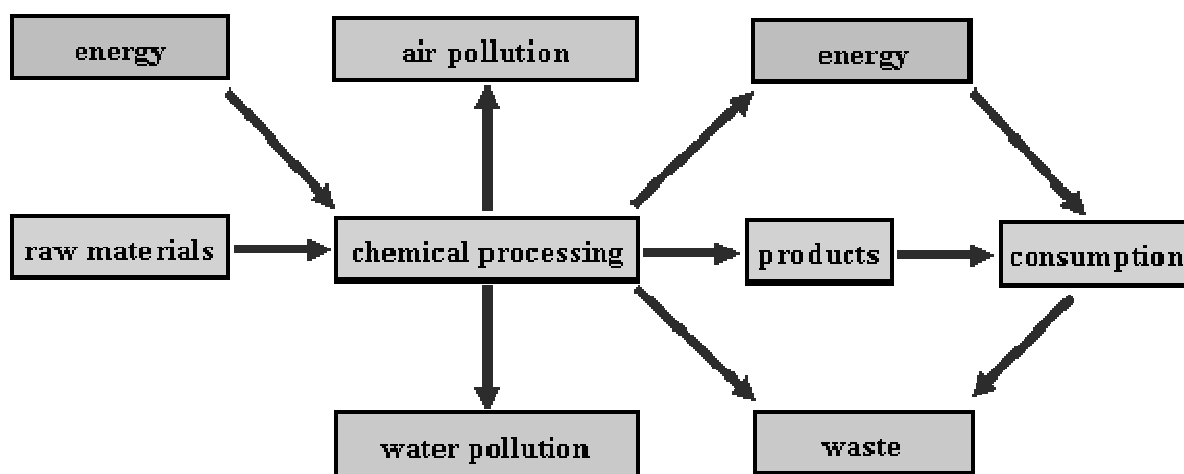
Figure 1.1 Schematic diagram of the environmental problem caused during the chemical processing of raw materials.

1.1 Basic aspects of membrane reactors

1.1.1   Types of membrane reactors

There are numerous concepts to classify membrane reactors.[3] Based on the materials used for membrane construction, the membrane reactors can be divided into inorganic and organic ones or porous and dense ones. Dense materials include solid oxide electrolyte dense membranes and palladium alloy membranes that are permeable to hydrogen. Perovskite membranes are one kind of mixed-conducting dense membranes that show high oxygen permeation rates at high temperatures, which will be discussed in the following sections. Porous inorganic membranes can be divided into macroporous ($d_p > 50$ nm), mesoporous ($50 > d_p > 2$ nm) and microporous ($d_p < 2$ nm) ones.[1] Macroporous materials, such as α-alumina membranes, are normally used to support layers of smaller pore size to form composite membranes, or as catalyst support in applications where a well-controlled reactive interface is required. Mesoporous materials for membranes have general pore sizes in the 4 - 5 nm range, so that permeation is governed by Knudsen diffusion. Microporous membranes, which should be called better nanoporous membranes, offer the potential for molecular sieving effects, with very high separation factors, and materials such as carbon molecular sieves, porous silicas, zeolites and most recently MOFs (metal-organic frameworks) have been studied.[1,4,5]

The membrane reactors can also be classified into extractors, distributors or contactors following the reactor design.[6] In addition, they can be defined as inert or catalytic membrane reactors. Of course, the inert membrane reactor can become catalytically active by packing catalyst particles in the membrane pores or outside the membrane as a fixed bed. The catalytic aspects of membrane reactors will be discussed in Section 1.1.3.

1.1.2   Advantages of membrane reactors

Removal of Product(s) For a reversible reaction

$$A + B \leftrightarrows C + D \tag{1}$$

according to thermodynamics, only a limited conversion and yield can be obtained due to the equilibrium constant. This thermodynamic restriction, however, can be overcome by

displacing the equilibrium toward more product formation. For example, if either one or both products can be in situ removed via a permselective membrane, the reversible reaction will proceed in the direction of the generation of more products. Therefore, proper product removal from the reaction zone shifts the equilibrium-limited reaction to a higher conversion.[7] Likewise, at a constant conversion degree, the operating temperatures or residence times for an endothermic equilibrium could be lowered in a membrane reactor. Because the thermodynamically unfavorable reaction can be driven closer to completion, the consumption of the feedstock can be reduced.[8] An example of this reaction type is water dissociation into oxygen and hydrogen as follows:

$$H_2O \leftrightarrows H_2 + \tfrac{1}{2} O_2 \qquad\qquad (2)$$

Due to the very small equilibrium constant of this reaction even at high temperature, only small amounts of hydrogen are generated at equilibrium. However, as shown in Figure 1.2, a hydrogen rate of 0.6 cm^3 min^{-1} cm^{-2} was obtained at 1683 °C by removing the produced oxygen via a mixed oxygen ion and electron conducting ZrO_2-TiO_2-Y_2O_3 membrane.[9]
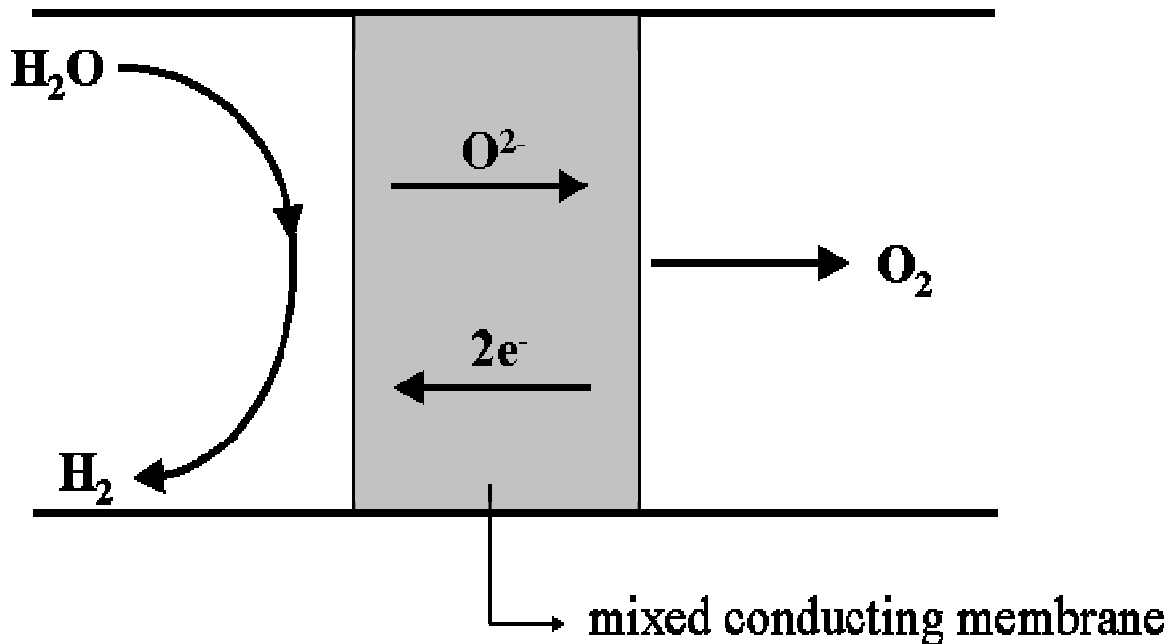
Figure 1.2 The concept of hydrogen production from direct water splitting at high temperature by removing oxygen via a mixed conducting membrane.[9, 10]

In addition to the increase of the reaction conversion, selectivity can also be enhanced in a membrane reactor. For the case that some undesirable side reactions will take place, leading to a lower yield or selectivity, when the concentration of one of the products is too high, the use of a membrane can suppress the side reactions and reduce or eliminate the formation of by-product(s).[7] An example is the dehydrogenation of isobutane to form isobutene. The selectivity to isobutene formation had a benefit by removing hydrogen via Pd membrane, since competing reactions such as hydroisomerization and hydrogenolysis could be markedly reduced.[11] Therefore, dehydrogenation in an extractor type membrane reactor with a hydrogen selective membrane is a reaction, where both conversion and selectivity are improved. Another example is the direct catalytic decomposition of NO into N_2 and O_2. Normally, the consecutive reaction between the produced O_2 and the un-reacted NO will take place, leading to the formation of undesired NO_2. However, if the direct decomposition of NO is conducted in a perovskite oxygen permeable membrane reactor, the NO_2 formation is effectively prevented benefiting from the in situ removal of the produced oxygen.[12] More details will be given in Section 3.2.

Controlled addition of reactant(s) In the conventional fixed-bed reactors, the reactants are typically premixed as a co-feed and the products are in contact with the reactants. Certain reactions that form some undesirable intermediate or side products might take place because of the uncontrolled contact between the reaction components. When a reactant is supplied through the membrane, its concentration inside the reactor can be kept at a sufficiently low and constant level, thus limiting side reactions such as deeper hydrogenations or oxidations, and avoiding the need to separate unconverted reactants.[8]

Besides, the separation of reactants allows better control of the reaction by varying the dose of each reactant independently. Moreover, the reactant supplied via the membrane can be used in a dilute, technical form rather than pure form, because the undesired compounds will be rejected by the membrane itself. For example, air instead of pure oxygen can be used for the oxidative coupling of methane on a dense oxygen-permeable membrane reactor, and nitrogen will be thus kept apart from products and unconverted reactants (the separation of methane from nitrogen is rather difficult and expensive).[13]

In addition to the potential process economic benefits, a membrane reactor can also result in a safer operation. For example, some combustion reactions involve rapid release of

energy when the reactants are mixed in a batch or bulk mode. However, when a critical reactant such as oxygen is carefully added to the reaction system (e.g., fuel) via a membrane, the potentials for the uncontrolled, massive reactions can be minimized, thus leading to safety hazards. In this way, the fuel can be used undiluted.[7]

Coupling of reactions When a reaction involves the evolution of a species while another reaction consumes the same species and a membrane can be found that is permselective to this species, it may be feasible to combine the two reactions on the opposite sides of a membrane reactor. The first proof of this concept is the simultaneous operation of an endothermic dehydrogenation and an exothermic hydrogenation upon a Pd membrane reactor. Since then most of the studies have focused on coupling dehydrogenation and hydrogenation of hydrocarbons by dense Pd-based membrane.[14, 15] Sometimes, a primary reaction is coupled to a secondary one whose purpose is to take away as soon as possible the permeating gas from the membrane so as to increase the driving force available for permeation. For example, Balachandran et al. coupled water splitting with hydrogen combustion as a model reaction in a ceramic-metal membrane reactor, by feeding hydrogen to the permeate side to consume the permeated oxygen. A maximum hydrogen production rate of 10.0 cm^3 min^{-1} cm^{-2} was obtained at 900 °C as a proof of principle.[10, 16] Since in this model reaction the amount of hydrogen produced was equivalent to the hydrogen amount consumed, the coupling of practice-relevant reactions in membrane reactors looks more attractive.

The coupled dehydrogenation/hydrogenation is also studied in fixed bed reactors, e.g. the simultaneous ethylbenzene dehydrogenation and benzene hydrogenation.[17] Recently, Kondratenko et al. reported the production of ethylene with the simultaneous almost 100 % removal of nitrous oxide (N_2O) by coupling the N_2O decomposition with the thermal dehydrogenation of ethane in a catalytic fixed bed reactor.[18] However, by the coupling of the two reactions in the fixed bed reactor, a subsequent procedure is necessary to separate the products. If the reactions are conducted in a membrane reactor, the products will be kept separated on the two sides of the membrane. Therefore, it looks attractive to search for new pairs of industrially interesting reactions in membrane reactors.

1.1.3 Catalytic considerations of membrane reactors

When following the concept of process intensification and combining the separator and the reactor functions into one unit, catalytic considerations are very important as they directly influence the conversion and selectivity of a reaction. The type of catalyst material and its dispersion might have profound impacts on the reactor performance. The choice of membrane material and its microstructure may also affect the catalytic aspects of the membrane reactor. The noble metals normally provide high catalytic activity, mechanical stability and heat conductivity. The cost, however, can be an issue. An economically feasible solution to this problem is to introduce the metal catalyst particles into a narrow region just below the surface of a less expensive porous support membrane or just as thin layer over the surface of a dense membrane. In this Ph. D. work, a Pd-doped perovskite porous layer was elaborately attached to perovskite membrane to improve the catalytic activity of membrane surface. More details are given in Section 2.2.

The placement of the catalyst in the reactor relative to the membrane can also have significant impact not only on the conversion of a reaction but also, in some case, the yield or selectivity. Three common modes of placing the catalyst are: (1) a bed of catalyst particles or pellets in a packed or fluidized state is physically separated but confined by the membrane as part of the reactor wall; (2) the catalyst in the form of particles or monolithic layers is attached to the membrane surface or inside the membrane pore; and (3) the membrane is inherently catalytic.[7]

1.2 Perovskite-type membrane reactor

1.2.1 Fundamentals of perovskite-type oxides

<u>Structure of perovskites</u> In addition to the name for the calcium titanate mineral with the formula $CaTiO_3$, perovskite in its general term defines a certain structure family.[19] In the general formula of perovskite-type oxides ABO_3, A is the larger cation and B is the smaller cation. In this structure, as shown in Figure 1.3, the B cation is 6-fold coordinated and the A cation is 12-fold coordinated with the oxygen anions. This structure can be viewed with the B cation placed in the center of an octahedron and the A cation in the center of a cube.[20]

An ideal perovskite consists of ABO_3 units, but the chemical composition can vary

depending on the valency of the A- and B-site cations. The sum of charges of A and B should be equal to the total charges of the oxygen anions. The cases $A^{1+}B^{5+}O_3$, $A^{2+}B^{4+}O_3$ or $A^{3+}B^{3+}O_3$, are commonly seen.[21]
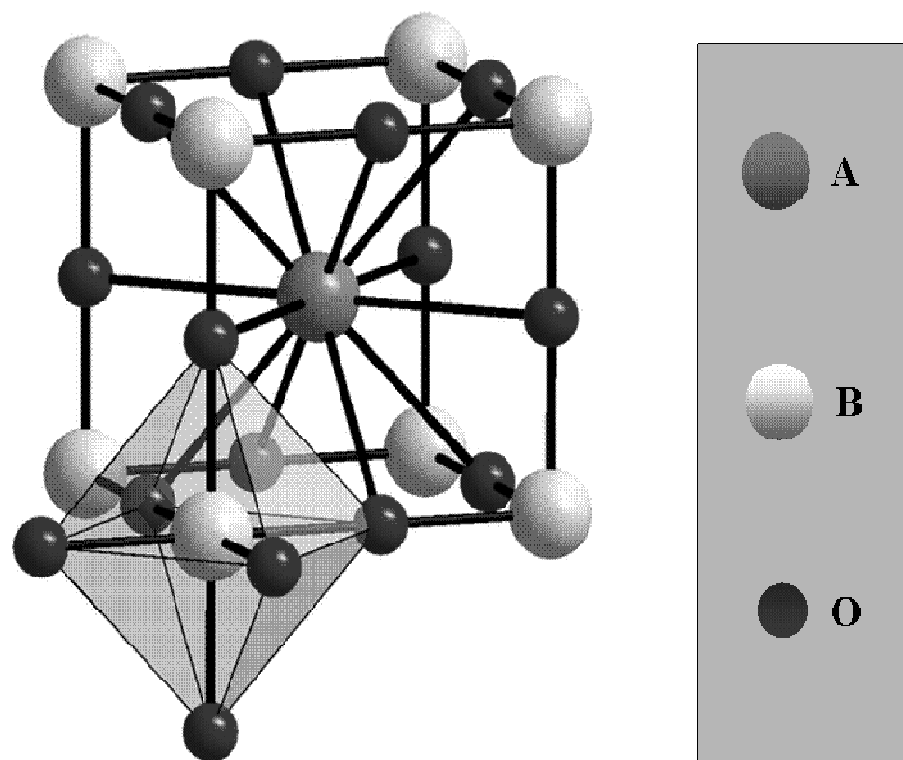
Figure 1.3 Structure of perovskite type oxide ABO_3.[22]

In a perovskite structure, the A site cation is normally larger than the B site cation due to the different coordination environment. The B-O distance is equal to a/2 (a is the cubic unit cell parameter) while the A-O distance is $a/\sqrt{2}$. For an ideal perovskite structure, it follows the equation: $r_A + r_O = \sqrt{2}(r_B + r_O)$ with r_A, r_B and r_O denoting the radii of the A-site and B-site cations and the oxygen ion. However, it was found that the cubic structure can be retained in ABO_3 compounds, even though this equation is not exactly obeyed. The tolerance factor t is defined for indicating the deviation from the ideal situation by the equation:[23, 24]

$$t = (r_A + r_O)/\sqrt{2}(r_B + r_O) \tag{3}$$

which is applicable at room temperature to the empirical ionic radii. For an ideal cubic structure, t should equal one. However, this structure is also found for lower t-values (0.75 < t < 1.0).

Formation of oxygen vacancies A perovskite with the ideal cubic structure does not have the capability to conduct oxygen ions. For the conduction or diffusion to take place, there should be a certain amount of imperfections or defects produced according to the non-stoichiometry.[25,26] Doping is a principal method to tailor the physical properties of the mixed conducting materials through formation of nonintegral stoichiometry phases or solid solutions by homogeneous doping with appropriate elements. To satisfy the requirement of electrical neutrality, the overall sum of charges in the compounds must be zero, which can be realized by decreasing the amount of oxygen anions (vacancies formation) or forming interstitial cations. For the perovskite-structured oxides ABO_3, it is often seen that a lower valence dopant B' is introduced on the B site to produce $AB_xB'_{1-x}O_{3-\delta}$.[27] Thus oxygen vacancies are present, as shown in Figure 1.4a. The symbol δ expresses the amount of the oxygen vacancies that provide a pathway for oxygen ions as shown in Figure 1.4b. In addition, a wide range of compounds with the perovskite structure can also be produced with substitutions occurring for either the A atom, the B atom, or both to form a structure of $A_xA'_{1-x}B_{1-y}B'_yO_{3-\delta}$.[28]
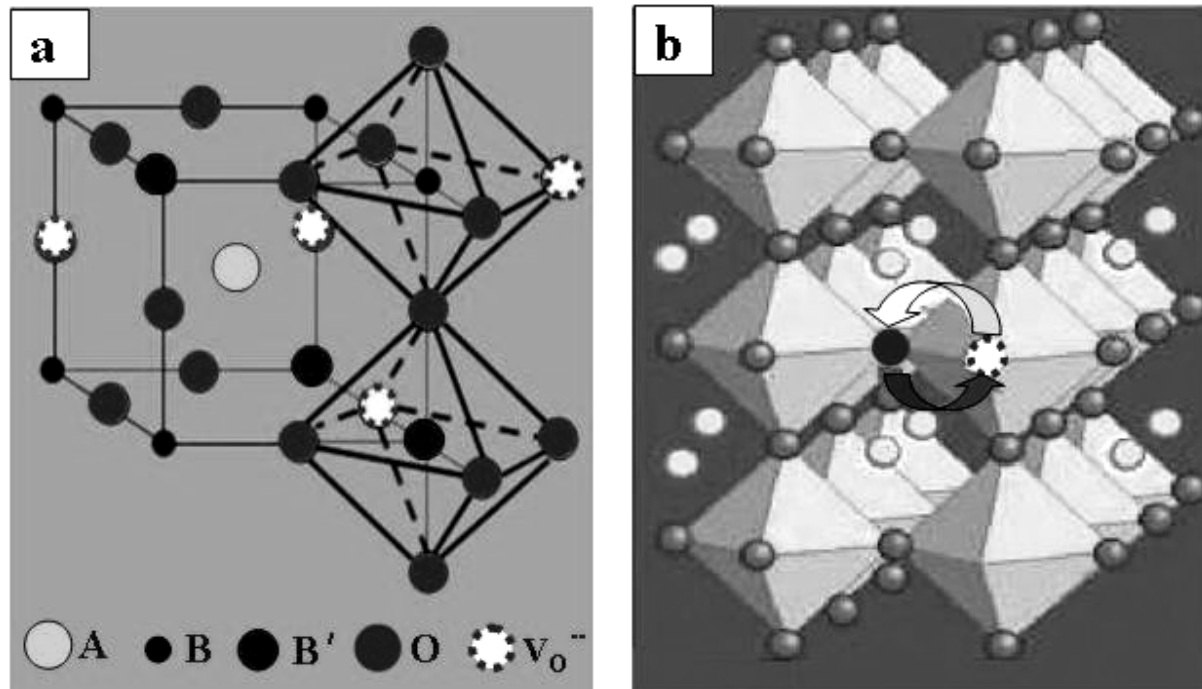
Figure 1.4 (a) The structure of perovskite $AB_xB'_{1-x}O_{3-\delta}$ with oxygen vacancies $V_O^{\cdot\cdot}$ and (b) oxygen transport through oxygen vacancies.[29,30]

Heterogeneous catalysis on perovskites Perovskite-type oxides may show good stability and high catalytic activity towards methane combustion at high temperature.[31,32,33] Partial substitution at the A-site can strongly affect catalytic activity due to stabilization of unusual oxidation states of the B component and to the simultaneous formation of structural defects that are responsible not only for part of the catalytic activity, but also for oxygen mobility within the crystal lattice. For example, Ferri and Forni studied the influence of substitution at the A-site in families of $La_{1-x}A'_xBO_3$ (B = Co, Fe, Ni) oxides on methane combustion. Substitution at the A-site with a bivalent cation (A' = Sr, Eu) or a tetravalent cation (A' = Ce) led to a decrease or an increase, respectively, of methane combustion activity.[34]

Several perovskite oxides have been exploited as catalysts for the partial oxidation of methane (POM: $CH_4 + {}^1/_2 O_2 \rightarrow CO + 2 H_2$) to synthesis gas.[35,36,37] Hayakawa et al. studied the series of perovskites $Ca_{0.8}Sr_{0.2}Ti_{1-y}Ni_yO_3$ towards methane oxidation.[38] It was found that the catalyst with a composition of y > 0.1 shows high activity for CH_4 combustion at temperatures around 600 °C but suddenly changes to synthesis gas formation at 800 °C. An increase in y results in high activity for CH_4 combustion, and the highest selectivity to synthesis gas is obtained with catalyst y = 0.2 at 800 °C. Two consecutive processes are suggested to account for the formation of synthesis gas: the first part of the catalyst bed catalyzes the CH_4 combustion under the O_2-rich atmosphere, and the second part of the bed catalyzes CH_4 reforming with the H_2O and CO_2 produced in the first part, under the O_2-deficient atmosphere.[20]

Perovskites were also employed as catalysts for the production of ethylene via oxidative dehydrogenation of ethane (ODE: $C_2H_6 + {}^1/_2 O_2 \rightarrow C_2H_4 + H_2O$).[39] For example, $CaTi_{1-x}Fe_xO_{3-\delta}$ (0 < x < 0.4) and $SrTi_{1-x}Fe_xO_{3-\delta}$ (0 < x < 1.0) have been studied for the ODE process and it was found that the latter showed higher C_2H_4 selectivity than the former.[40] In addition, Dai et al. embedded halide ions in the perovskite lattice. In this case, the deep oxidation of C_2H_6 and C_2H_4 and the leaching of the halide from the lattice were minimized. It was found that $SrFeO_{2.618}Cl_{0.443}$ showed a higher catalytic activity for the ODE reaction than $SrFeO_{2.81}$, and a C_2H_4 yield of ca. 63 % was obtained when working at 680 °C, a reactant molar ratio of $C_2H_6:O_2:N_2 = 2:1:3.7$ and at atmospheric pressure.[41]

Perovskites are also widely exploited as the catalyst for the decomposition of nitrogen oxides (NO_x). The direct decomposition of NO into N_2 and O_2 (2 NO $\rightarrow N_2 + O_2$) is thermodynamically favorable at temperatures below 1000 °C. It was found that the

decomposition rate is often inhibited by oxygen, and the oxygen desorption was found to be the rate-limiting step of the overall reaction. So, catalysts active for NO decomposition should accordingly display not only the ability to adsorb and dissociate NO but also the ability to facilitate the oxygen desorption. Some perovskites are active to the direct decomposition of NO.[42, 43] Iwakuni et al. found that the activity for NO decomposition was greatly elevated by doping La and Mg for Ba and Mn site in $BaMnO_3$, respectively. The highest N_2 yield was achieved on $Ba_{0.8}La_{0.2}Mn_{0.8}Mg_{0.2}O_3$. Moreover, N_2 yield of 40 % was sustained even under coexisting of 5 % O_2 at 850 °C.[44] In addition, the decomposition of N_2O to nitrogen and oxygen ($N_2O \rightarrow N_2 + {}^1/_2 O_2$) was also investigated over various substituted $La_{0.8}Sr_{0.2}MO_{3-\delta}$ (M = Cr, Fe, Mn, Co, Y) perovskite series. Among them, $La_{0.8}Sr_{0.2}CoO_{3-\delta}$ showed a maximum N_2O conversion of 90 % at 600 °C. However, the co-feed of 4 % O_2 to the stream led to a decrease in the conversion of N_2O by ca. 13 %.[45]

1.2.2 Preparation of perovskite membranes

Perovskites can be prepared by a range of methods, such as chemical vapor deposition, combustion synthesis, and the sol-gel method. The sol-gel process offers some advantages such as better mixing of the starting materials and excellent chemical homogeneity in the final product.[46,47,48] Moreover, the fine mixing and the tendency of partially hydrolyzed species to form extended networks facilitate the structure evolution, leading to rather low calcination and sintering temperatures. In this thesis, two perovskites $BaCo_xFe_yZr_{1-x-y}O_{3-\delta}$ (BCFZ) and $BaCo_xFe_yZr_{0.9-x-y}Pd_{0.1}O_{3-\delta}$ (BCFZ-Pd) were involved. The former was used to make the hollow fiber dense membrane, and the latter as the coating material was employed to improve the catalytic property of the membrane surface.

The sol-gel synthesis of perovskite BCFZ-Pd As shown in Figure 1.5, the perovskite BCFZ-Pd powder was prepared in this work by an adapted variant of the so-called citrate method employing EDTA and citric acid in parallel as complex formation agents.[46,47,48] Briefly, the calculated amounts of $Ba(NO_3)_2$ and $Pd(NO_3)_2$ powder were dissolved in an aqueous solution of $Co(NO_3)_2$, $Fe(NO_3)_3$, and $ZrO(NO_3)_2$, followed by the addition of EDTA acid and citric acid with the molar ratio of EDTA acid : citric acid : total of molar amounts of metal cations as 1:1.5:1. After agitation for a certain time, the pH value of the solution was adjusted at around 9 by the addition of aqueous NH_3. The solution was kept under heating and

stirring until a gel was formed. The transparent solution transformed into a dark purple gel after evaporation for several hours. Further heat treatments were applied, i. e. the pre-calcination for 2 h at ca. 700 °C and then a calcination at 950 °C for 10 h to obtain the powder of the final composition. X-ray diffraction (XRD), scanning electron microscopy (SEM), transmission electron electron microscopy (TEM), and energy-dispersive X-ray spectroscopy were used to characterize the samples.
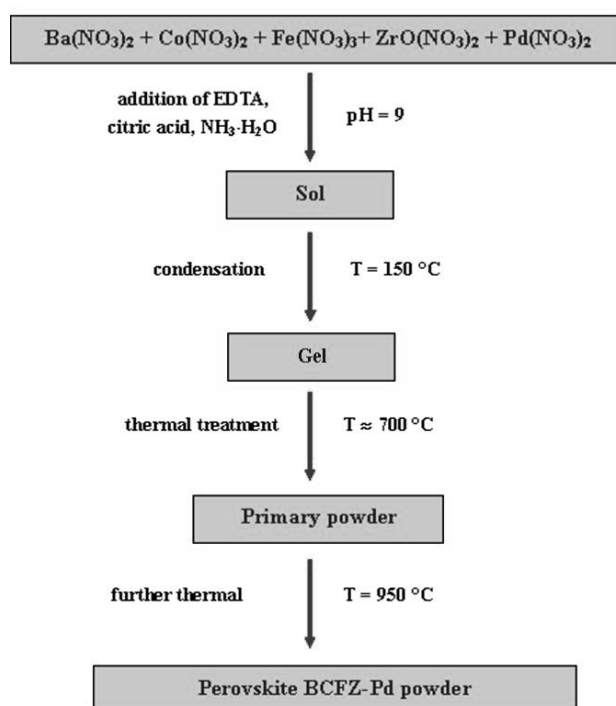
Figure 1.5 Scheme of the preparation of perovskite BCFZ-Pd powder.

Preparation of perovskite BCFZ hollow fiber membrane Perovskite BCFZ hollow fiber membranes were manufactured at the Fraunhofer Institute for Interfacial Engineering and Biotechnology (IGB) in Stuttgart by a phase inversion spinning followed by sintering.[49] The homogeneous slurry of a polymer solution and the BCFZ powder was obtained by ball milling up to 24 hours with a solid content of 50 - 60 mass %. The slurry was spun through a spinneret and the obtained infinite green hollow fiber was cut into 0.5 m long pieces before sintering the fiber in a hanging geometry. After sintering at 1300 °C for 5 h, as shown in Figure 1.6, the length of the green fiber reduced from 50 cm to ~ 32 cm and the sintered fiber had a wall thickness of around 0.17 mm with an outer diameter of 1.10 mm and an inner diameter of 0.76 mm.
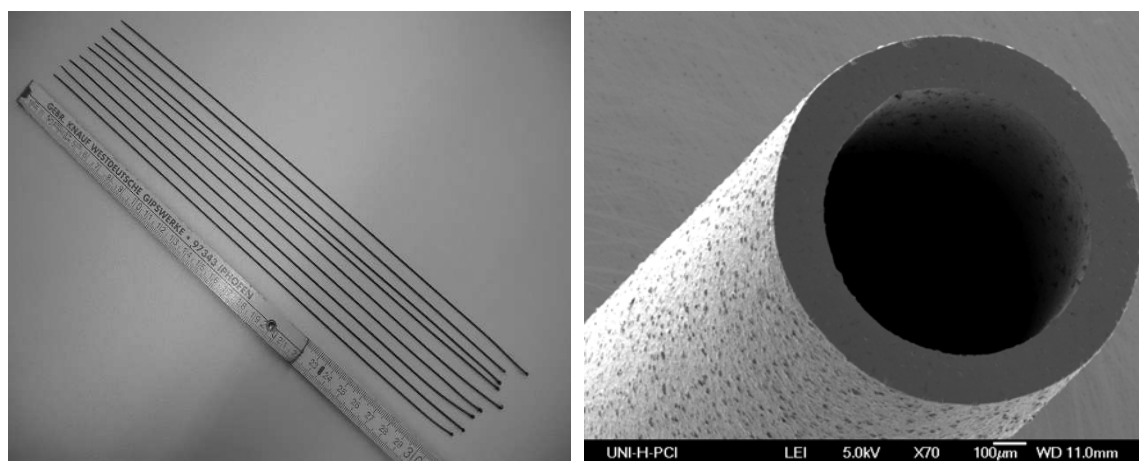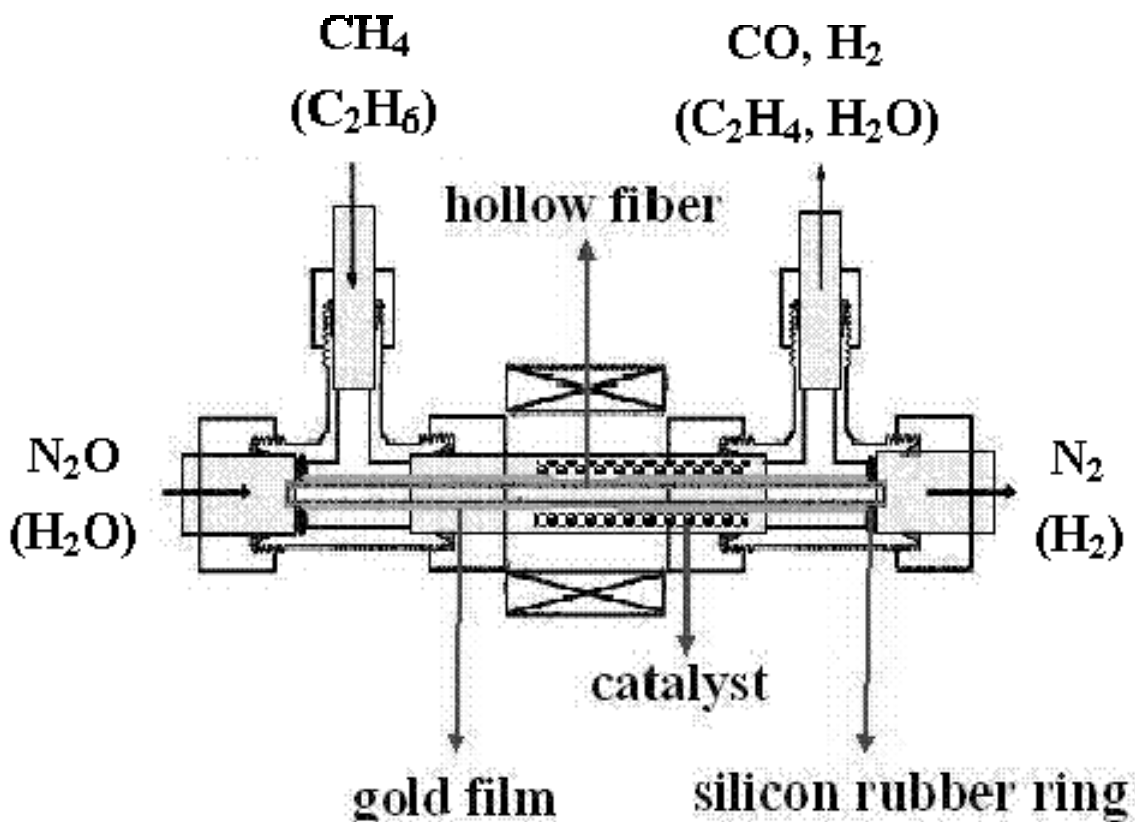
Figure 1.6 The sintered BCFZ hollow fiber membrane (SEM provided by Dr. A. Feldhoff).

<u>Deposition of BCFZ-Pd porous layer onto BCFZ hollow fiber membrane</u> The BCFZ-Pd powders were crushed in a mortar. The BCFZ-Pd pastes for coating were obtained by adding several drops of water to the crushed fine powder. The paste was coated on the surface of the dense membrane BCFZ using a fine brush. These coated membranes were sintered at 1050 °C for 1 h in air atmosphere with a heating and cooling rate of 3 °C/min.[50]

<u>Hollow fiber membrane reactor</u> Figure 1.7 shows a scheme of the BCFZ hollow fiber membrane reactor used in this Ph D. work.[51,52,53] In order to obtain the isothermal condition, the two ends of the hollow fiber were coated by Au paste and then sintered at 950 °C for 5 h. The coating and sintering procedure was repeated three times and a dense Au film, which is not permeable to oxygen was obtained on BCFZ membrane surface. Such Au-coated hollow fiber can be sealed by silicon rubber ring and the uncoated part (the effective length is 3 cm, and the effective membrane area is 0.86 cm^2), which is permeable to the oxygen, can be kept in the middle of the oven ensuring isothermal conditions. The mixture of N_2O (or H_2O) and He was fed to the core side and a mixture of CH_4 (or C_2H_6), Ne, and He was fed to the shell side. A Ni-based steam reforming (SR) catalyst (Süd Chemie AG) was packed around and behind the hollow fiber membrane when methane was used as the reducing gas on the shell side. N_2O, CH_4, C_2H_6, He, and Ne flow rates were controlled by gas mass flow controllers (Bronkhorst). H_2O flow rate was controlled by the liquid mass flow controller (Bronkhorst) and was completely evaporated at 180 ^{o}C before it was fed to the reactor. All gas lines to the reactor and the gas chromatograph were heated to 180 ^{o}C.

14

Figure 1.7 Scheme of the hollow fiber membrane reactor used in this work.[51]

The flow rate at inlet for all the gases was obtained by using a soap bubble meter. The total flow rates of the effluents at outlet (F_{total}^{out}) were determined by using Ne as an internal standard. The calculation is based on the facts that the inert Ne didn't take part in the reactions and the flow rate of Ne at inlet should be equal to that at exit:

$$F_{total}^{in} c_{Ne}^{in} = F_{total}^{out} c_{Ne}^{out} \qquad (4)$$

where F_{total}^{in} is the total flow rates of the stream at inlet, c_{Ne}^{in} and c_{Ne}^{out} are the concentrations of Ne at inlet and outlet, respectively. The concentrations of the gases at the exit of the reactor were determined by an on-line gas chromatograph (Agilent 6890) equipped with the Carboxen 1000 column (Supelco). The details about the calculation of conversions, selectivity and yields are given in Chapter 2 and Chapter 3.

15

1.2.3   Oxygen transport through perovskite membranes

Perovskite membranes show mixed oxygen ion and electron conductivity. If there is a gradient $\nabla\mu_{O2}$ of the oxygen chemical potential across the dense perovskite membrane, the oxygen can be transported from the side with a high oxygen partial pressure p_{O2}' to the side with a low oxygen partial pressure p_{O2}''. It is generally accepted that the oxygen permeation through the dense perovskite membrane, as shown in Figure 1.8, involves three progressive steps: (1) oxygen insertion on air side, (2) the simultaneous bulk diffusion of oxygen ion and electron in the bulk phase, and (3) oxygen release on the permeate side. The slowest step is expected to limit the overall oxygen permeation rate. Different perovskite membranes of varying thickness tend to have different determining steps.
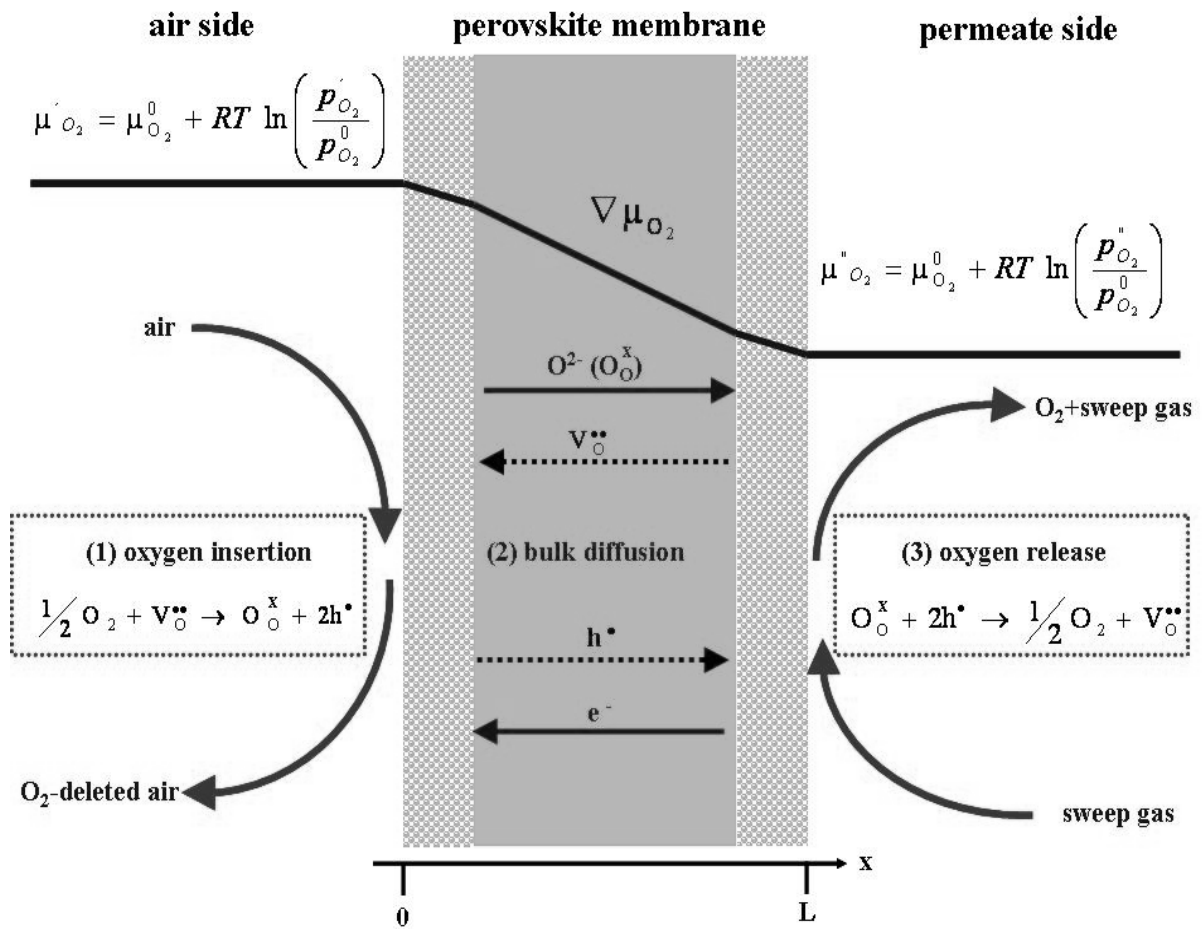

Figure 1.8 Schematic diagram of oxygen transport through a perovskite membrane.[54]

16

Bulk diffusion For a relatively thick membrane, the bulk diffusion process is commonly the determining step. In this case, the oxygen permeation through the membrane is commonly described by Wagner's theory,[55, 56] which is restricted to the simultaneous transport of oxygen ions and electrons that are ideally diluted and do not interact. The oxygen permeation flux $j(O_2)$ can be described by Wagner's equation as follows:

$$j(O_2) = -\frac{1}{(4F)^2} \cdot \frac{\sigma_{el}\sigma_{ion}}{\sigma_{el} + \sigma_{ion}} \nabla \mu_{O_2} \quad \text{with} \quad \nabla \mu_{O_2} = \frac{\partial RT \ln a_{O_2}}{\partial x} \tag{5}$$

where σ_{el} and σ_{ion} are the electronic and ionic conductivities, respectively, F the Faraday constant and $\nabla \mu_{O2}$ the gradient of the chemical potential of oxygen across the membrane. Assuming that $\sigma_{el} \gg \sigma_{ion}$ and that the $\partial \ln a_{O2}/\partial x$ can be approximated by $\ln (p_{O2}' - p_{O2}'')/L$ with p_{O2}' and p_{O2}'' denoting the oxygen partial pressure of the high chemical potential side and the low chemical potential side, respectively, of the membrane of thickness L, Wagner's equations reads

$$j(O_2) = \frac{RT}{(4F)^2} \sigma_{ion} \frac{\ln(p_{O_2}' - p_{O_2}'')}{L} \tag{6}$$

Based on the above equation, the oxygen permeation rate can be enhanced by increasing the operating temperature, the pressure gradient across the membrane, or by decreasing the thickness of the membrane.

Surface exchange Below a critical value L_c of membrane thickness, the Wagner equation is not applicable, and the surface exchange rate would become the limiting step in the oxygen permeation. The surface exchange reaction is a complex process, which includes the adsorption, oxygen reduction (charge transfer), surface diffusion of intermediate species, and the incorporation of oxygen into the perovskite lattice.[57] Many studies indicated that the surface exchange rate can be increased by coating the membrane with materials that show a high surface exchange rate such as cobalt-containing perovskite or noble metal particles.[58, 59]

When a perovskite membrane is used as a reactor for the oxidation of light hydrocarbons, the surface process on the permeate side is the reaction between the permeated oxygen species and the reactive gas such as CH_4. In this case, a better reactor performance can be expected by coating the membrane with a catalytically active layer. The catalytic coating can accelerate the oxidation of hydrocarbon. In other words, the permeated oxygen is consumed quickly and

a larger driving force for oxygen permeation will be built, leading to a higher oxygen permeation rate.

1.2.4   Applications of perovskite membranes

Perovskite membranes show high oxygen ion and electronic conductivity, and can be used to separate oxygen from air. In the past decades, many researchers demonstrate the production of pure oxygen or oxygen-enriched air using perovskite membranes. Also the separated oxygen can be used, in a perovskite membrane reactor, for the in situ partial oxidations of hydrocarbons such as the POM to synthesis gas, the ODE to ethylene, or the oxidative coupling of methane (OCM) to C_{2+} hydrocarbons.

Production of pure oxygen and oxygen-enriched air Oxygen is ranking among the top five in the production of commodity chemicals in the world. To get cheap, high-purity oxygen is a very important demand in industry. The oxygen transport through the perovskite membrane is in the form of oxygen ion instead of oxygen molecules, so pure oxygen can be obtained in principle. In the published work, most researchers, employing perovskite membrane as the oxygen separator, used the inert gas such as He or Ar to sweep the permeated oxygen. Wang et al. used steam as the sweep gas and the high-purity oxygen can be produced after the steam condensation.[60] Evacuation by a pump is an alternative to the use of sweep gas for pure oxygen production using the perovskite membrane.

Oxygen-enriched air with typically 40 – 50 % oxygen content is also needed in a number of industrial processes, for example, in the preparation of synthesis gas for ammonia production. Perovskite BCFZ membrane has also been exploited to produce oxygen-enriched air by transporting oxygen from slightly pressured air through the membrane to the air at lower pressure. When increasing the pressure difference from 0.5 bar to 3 bar, the oxygen content in the air on the permeate side almost doubled, from 30 % to 55 %, and the oxygen permeation rate rises from 0.5 to 2.2 mL min^{-1} cm^{-2}. In oxygen-enrichment mode, there is no problem with the stability of perovskite membrane, because both sides of the membrane are exposed to an oxidizing atmosphere. This is confirmed by a period of stable operation of perovskite hollow fiber membrane in excess of 800 h at 875 °C, to produce 42 % oxygen-enriched air.[61]

Partial oxidation of methane (POM) to synthesis gas Among all the potential applications for perovskite membranes, the POM to syngas ($CO+H_2$) is thought to be one of the commercially most important applications. Using mixed-conducting perovskite membranes, air is used as the oxidant on one side, and the permeated oxygen can be utilized for the N_2-free syngas production on the other side of membrane. By coupling the oxygen separation and POM in the membrane reactor, syngas production costs can be potentially reduced. The ceramic membrane further aids in safety management, since it avoids the premixing of oxygen and natural gas and reduces the formation of hot spots as encountered in a co-feed reactor. Moreover, compared to steam reforming, a lower H_2/CO ratio of 2 is obtained during POM process, which is required for methanol synthesis or the Fischer-Tropsch process.

Developing a mixed conducting perovskite membrane with a high oxygen flux and long-term phase stability is the main challenge for successful application in the syngas production process. Although membranes made from La-Sr-Co-Fe family materials exhibit a high oxygen permeation rate, considerable doubts on these cobalt-containing perovskite membranes still remain due to their poor phase stability under a reducing environment.[21] Several concepts are being followed to improve the membrane stability, such as reducing the relative amount of cobalt in the perovskite and co-doping the material with less-reducible metals such as Zr^{4+} or Ga^{3+}.[62] Tsai et al. reported the syngas production by POM in a disk-type membrane reactor based on $La_{0.2}Ba_{0.8}Co_{0.2}Fe_{0.8}O_{3-\delta}$.[63] They successfully used this membrane in syngas generation experiments for 850 h at 850 ^{o}C. Yang et al. studied the direct conversion of methane to syngas in $Ba_{0.5}Sr_{0.5}Co_{0.8}Fe_{0.2}O_{3-\delta}$ tubular membranes.[64] This reactor was successfully operated for the POM reaction in pure methane stream at 875 ^{o}C for more than 500 h without failure. In addition, the material $BaCo_{0.4}Fe_{0.4}Zr_{0.2}O_{3-\delta}$ was developed. The membrane reactor made of this material in syngas production experiments at 850 ^{o}C can be operated steadily for more than 2200 h.[65]

Beside the intrinsic property of the membrane material, the mechanism of POM in the membrane reactor is another factor for the long-term operation for perovskite membrane. The reaction of methane with oxygen in the membrane reactor is called "partial oxidation". However, there is experimental evidence that methane is first oxidized to CO_2 and H_2O, after which the products of total oxidation are reduced by un-reacted methane on conventional Ni-based catalyst to CO and H_2 according to steam reforming and dry reforming (CO_2), respectively. Yang et al. think that the gases directly contacted with the $Ba_{0.5}Sr_{0.5}Co_{0.8}Fe_{0.2}O_{3-\delta}$

membrane tube wall are CO_2 and H_2O rather than the reductive gases H_2 and CO, which might be one of the reasons why the membrane reactor can be operated steadily for long time during the POM reaction.[64] Recently, Wang et al. studied the POM process in BCFZ hollow fiber membrane reactor, and found that the so-called partial oxidation of methane to syngas in the reactor is possibly first a total oxidation followed by steam and dry reforming steps, as shown in Figure 1.9**.**[66] In addition, Chen et al. proposed and verified that the reaction via a combustion-reforming mechanism can really improve the stability of BSCF membrane materials.[67]
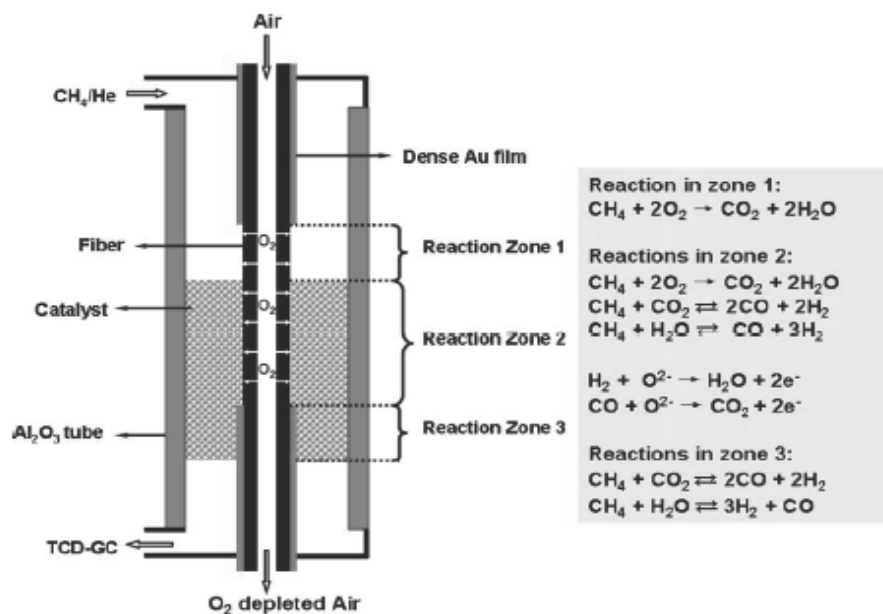
Figure 1.9 Suggested reaction pathways of POM in a hollow fiber membrane reactor.[66]

Oxidative dehydrogenation of ethane (ODE) to ethylene Currently, ethylene is produced by steam cracking of ethane in a highly endothermic and energy-consuming process in which the dilution of ethane with steam reduces the formation of coke.[68] ODE is considered a promising alternative due to the reduced demand of energy and to the fact that there is no equilibrium constraint on the conversion. One of challenges for the process is how to achieve a high selectivity for ethylene, because it is easier to be deeply oxidized to CO_x by O_2. One way to overcome these difficulties is to use lattice oxide (O^{2-}) as oxidant. Wang et al. used an oxygen permeable membrane based on $Ba_{0.5}Sr_{0.5}Co_{0.8}Fe_{0.2}O_{3-\delta}$ to continuously supply lattice oxygen for oxidative dehydrogenation of ethane to ethylene, as shown in Figure 1.10.[69] The selectivity of 90 % was obtained at 650 °C. The ODE in this disk-type membrane reactor was

also investigated at temperatures higher than 800 °C. Per pass an ethylene yield of 67 % at an ethylene selectivity of 80 % was achieved, while only 53.7 % ethylene selectivity was obtained using a conventional fixed-bed reactor under the same reaction conditions with the same catalyst at 800 °C. Lin et al. also studied the ODE process in a dense tubular ceramic membrane reactor made of fluorite structured $Bi_{1.5}Y_{0.3}Sm_{0.2}O_3$ (BYS) at temperatures 825–875 °C.[70] A dead-end tube and shell configuration was used where ethane was fed inside the tube and air was fed into the shell side of the membrane reactor. At 875 °C, per pass ethylene yield of 56 % at an ethylene selectivity of 80 % was obtained in the membrane reactor. However, the thermal dehydrogenation of ethane should be considered when the reaction temperature is higher than 800 °C.
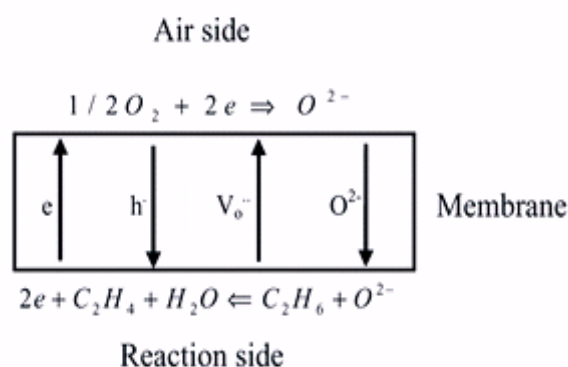
Figure 1.10 Mechanism of oxidative dehydrogenation of ethane to ethylene in an oxygen permeable membrane reactor.[69]

1.3 Aims of the thesis

It is the aim of this thesis to demonstrate the coupling of two reactions via an oxygen-transporting membrane. Two energy/environment related model reactions have been selected:

1. The hydrogen production by thermal water splitting, which is coupled with methane combustion, the POM to synthesis gas, or the ODE to ethylene.

2. The nitrogen oxides (NO and N_2O) abatement by its decomposition into nitrogen and oxygen, which is coupled with the POM to synthesis gas or the ODE to ethylene.

Hydrogen is gaining more and more attention because it is regarded as an important future fuel. Today, hydrogen is mainly produced from nonrenewable natural gas and petroleum. With concerns over worldwide energy demands and global climate change, alternative sources must be found. Water is recommended as the ideal source for the generation of hydrogen. Although water dissociation into oxygen and hydrogen is conceptually simple, efficient hydrogen production from water remains difficult as a result of the low equilibrium constant of $K_p \approx 2 \times 10^{-8}$ at the relatively high temperature of 950 °C.[71]

As discussed in Section 1.1.2, one technique to enhance the hydrogen production rate from the equilibrium-limited water splitting is the in situ removal of the simultaneously produced oxygen using a mixed oxygen ion and electron conducting membrane. Previous studies had shown that an operating temperature of 1683 °C was necessary to obtain a hydrogen production rate of 0.6 cm^3 min^{-1} cm^{-2} in a mixed-conducting ZrO_2-TiO_2-Y_2O_3 membrane.[9] In order to lower the operating temperature, Balachandran et al. fed hydrogen on the permeation side of a ceramic-metal membrane reactor to consume the permeated oxygen.[10] Although a maximum hydrogen production rate of 10.0 cm^3 min^{-1} cm^{-2} was obtained at 900 °C, the amount of hydrogen produced was equivalent to the amount consumed, which makes it unpractical. Therefore, it would be attractive for both the feed and permeate stream to yield a valuable compound.

At the Fraunhofer IGB in Stuttgart in cooperation with Caro's group under the auspieces of the BMBF projects "Tool-Box: Ceramic membranes for Catalysis" (2003-2006) and the successor project "SynMem: Synthesis Gas Production in Membrane Reactors" (2006-2009), a novel BCFZ perovskite hollow fiber membrane with high oxygen permeability has been developed for e.g. oxygen separation, the POM to synthesis gas, and the ODE to ethylene.[49,72,73] One aim of my Ph. D. work was to exploit the feasibility of hydrogen production from water splitting by removing the simultaneously produced oxygen via BCFZ hollow fiber membrane. Clearly, the hydrogen production rate depends directly on the rate of oxygen removal from the water dissociation system. Besides operating temperature and membrane thickness, according to Wagner's theory as discussed in Section 1.2.3, the oxygen permeation rate is related to the oxygen partial pressure gradient across the BCFZ membrane. By feeding the reducing gas to the permeate side of the membrane, a larger driving force will be provided for the fast removal of oxygen from the steam side, thus increasing the hydrogen production rate. The strategy used here to improve the hydrogen production rate is to couple

water splitting with practice-related reactions on the opposite sides of the BCFZ membrane reactor. Specifically, three reactions such as methane combustion, POM, and ODE were employed, respectively, to consume the permeated oxygen on the permeate side. In addition, a catalytic porous layer onto BCFZ membrane was fabricated or a Ni-based reforming catalyst was put around and behind the BCFZ membrane to accelerate the rate of oxygen consumption. Based on this novel coupling strategy, not only a higher hydrogen production rate from water splitting on the one side, but also valuable chemical products such as synthesis gas or ethylene on the other side of the membrane were obtained.

Another aim of this Ph. D. work was to abate nitrogen oxides in a perovskite BCFZ membrane reactor, which are mainly produced by automobiles and stationary power plants and among the major atmospheric pollutants. As discussed in Section 1.2.1, the catalytic decomposition of nitrogen oxides over perovskite catalysts is strongly inhibited by the produced oxygen, leading to a lower conversion. To avoid the inhibition by the produced oxygen, the decomposition of nitrogen oxides were conducted in the BCFZ oxygen permeable membrane reactor in this work. Here, the BCFZ membrane fulfills a double role: it can catalyze the decomposition of nitrogen oxides, and transport the produced oxygen to the other side of membrane, thus overcoming the inhibition by oxygen. In addition, to get a larger driving force for oxygen removal and thus a complete conversion of nitrogen oxides, the decomposition of nitrogen oxides was coupled with POM or ODE in the BCFZ membrane reactor.

In summary, by using a perovskite-type BCFZ oxygen-permeable hollow fiber membrane, oxygen from water dissociation can be continually removed and this reaction was continuously shifted to the product side. When coupling the equilibrium-controlled water splitting with POM or ODE, a larger driving force was provided for oxygen transport through the membrane, and accordingly significant amounts of hydrogen was achieved. Simultaneously, valuable chemical products such as synthesis gas or ethylene can be obtained on the other side of membrane. For the kinetically controlled nitrogen oxides decomposition, the inhibitor oxygen can be in situ removed via BCFZ hollow fiber membrane. When coupling this reaction with POM or ODE, a complete decomposition of nitrogen oxides was obtained due to the effective removal of the inhibitor oxygen.

1.4 Bibliography

[1] A. G. Dixon, Int. J. Chem. Rea*ctor Eng.,* **2003**, *1*, 1.

[2] W. J. Koros, Z. H. Ma, T. Shimidzu, http://www.che.utexas.edu/nams/IUPAC/iupac.html.

[3] R. Dittmeyer, J. Caro in *Handbook of Heterogeneous Catalysis*, *Vol. 4* (Eds.: G. Ertl, H. Knözinger, F. Schüth, J. Weitkamp), Wiley-VCH, Weinheim, **2008**, p. 2198.

[4] Y. S. Li, F. Y. Liang, H. Bux, A. Feldhoff, W. S. Yang, J. Caro, *Angew. Chem. Int. Ed.*, **2010**, *49*, 548.

[5] H. Bux, F. Y. Liang, Y. S. Li, J. Cravillon, M. Wiebcke, J. Caro, *J. Am. Chem. Soc.*, **2009**, *131*, 16000.

[6] J. A. Dalmon, A. Cruz-Lopez, D. Farrusseng, N. Guilhaume, E. Iojoiu, J. C. Jalibert, S. Miachon, C. Mirodatos, A. Pantazidis, M. Rebeilleau-Dassonneville, Y. Schuurman, A. C. van Veen, *Appl. Catal. A,* **2007**, *325*, 198.

[7] H. P. Hsieh, *Inorganic Membranes for Separation and Reaction*, Elsevier, **1996**, p. 299.

[8] G. Saracco, V. Specchia, *Catal. Rev. - Sci. Eng.*, **1994**, *36*, 305.

[9] H. Naito, H. Arashi, *Solid State Ionics*, **1995**, *79*, 366.

[10] U. Balachandran, T. H. Lee, S. Wang, S. E. Dorris, *Int. J. Hydrog. Energy* **2004**, *29*, 291.

[11] T. Matsuda, I. Koike, N. Kubo, E. Kikuchi, *Appl. Catal.*, **1993**, *96*, 3.

[12] H. Q. Jiang, L. Xing, O. Czuprat, H. H. Wang, S. Schirrmeister, T. Schiestel, J. Caro, *Chem. Commun.* **2009**, 6738

[13] K. Omata, S. Hasshimoto, H. Tominaga, K. Fujimoto, *Appl. Catal.*, **1989**, *52*, L1.

[14] T. M. Moustafa, S. S. E. H. Elnashaie, *J. Membr. Sci.,* **2000**, *178*, 171.

[15] M. H. Khademi, A. Jahanmiri, M. R. Rahimpour, *Int. J. Hydrog. Energy,* **2009**, *34*, 5091.

[16] U. Balachandran, T. H. Lee, S. E. Dorris, *Int. J. Hydrog. Energy*, **2007**, *32*, 451.

[17] M. E. E. Abashar, *Chem. Eng. Proc.* **2004**, *43*, 1195

[18] E. V. Kondratenko, O. Ovsitser, *Angew. Chem.* **2008**, *120*, 3271; *Angew. Chem. Int. Ed.*, **2008**, *47*, 3227.

[19] A. S. Bhalla, R. Guo, R. Roy, *Mater. Res. Innovat.,* **2000,** *4,* 3.

[20] M. A. Pena, J. L. G. Fierro, *Chem. Rev.*, **2001**, *101*, 1981.

[21] Y. T. Liu, X. Y. Tan, K. Li, *Catal. Rev -Sci. Eng.,* **2006**, *48*, 145

[22] http://commons.wikimedia.org/wiki/File:Kristallstruktur_Perovskit.png.

[23] V. M. Goldschmidt, *Naturwissenschaften*, **1926**, *14*, 477.

[24] H. Hayashi, H. Inaba, M. Matsuyama, N. G. Lan, M. Dokiya, H. Tagawa, *Solid State Ionics*, **1999**, *122*, 1.

[25] P. J. Gellings, H. J. M. Bouwmeester, *Catal. Today*, **1992**, *12* 1.

[26] A. Thursfield, I. S. Metcalfe, *J. Mater. Chem.*, **2004**, *14*, 2475.

[27] V. V. Kharton, A. V. Kovalevsky, V. N. Tikhonovich, E. N. Naumovich, A. P. Viskup, *Solid State Ionics*, **1998**, *110*, 53.

[28] Y. Teraoka, H. M. Zhang, S. Furukawa, N. Yamazoe, *Chem. Lett.*, **1985**, *11*, 1743.

[29] http://commons.wikimedia.org/wiki/File:Perovskite.PNG.

[30] J. Martynczuk, *Mixed conducting perovskites and their solid state chemistry*, Ph. D. thesis, Leibniz Universität Hannover, **2008**.

[31] H. Arai, T. Yamada, K. Eguchi, T. Seiyama, *Appl. Catal.*, **1986**, *26*, 265.

[32] J. C. McCarty, H. Wise, *Catal. Today,* **1990**, *8*, 231.

[33] A. Civera, G. Negro, S. Specchia, G. Saracco, V. Specchia, *Catal. Today*, **2005**, *100*, 275.

[34] D. Ferri, L. Forni, *Appl. Catal. B*, **1998**, *16*, 119.

[35] R. Lago, G. Bini, M. A. Pena, J. L. G. Fierro, *J. Catal.*, **1997**, *167*, 198.

[36] A. Slagtern, U. Olsbye, *Appl. Catal. A*, **1994**, *110*, 99.

[37] T. Hayakawa, A. G. Andersen, M. Shimizu, K. Suzuki, K. Takehira, *Catal. Lett.,* **1993**, *22*, 307.

[38] T. Hayakawa, H. Harihara, A. G. Andersen, K. Suzuki, H. Yasuda, T. Tsunoda, S. Hamakawa, A. P. E. York, Y. S. Yoon, M. Shimizu, K. Takehira, *Appl. Catal. A*, **1997**, *149*, 391.

[39] G. H. Yi, T. Hayakawa, H. Harihara, A. G. Andersen, K. Suzuki, S. Hamakawa, A. P. E. York, M. Shimizu, K. Takehira, *Catal. Lett.*, **1996**, *38*, 189.

[40] T. Hayakawa, A. G. Andersen, H. Orita, M. Shimizu, K. Takehira, *Catal. Lett.,* **1992**, *16*, 373.

[41] H. X. Dai, C. F. Ng, C. T. Au, *Catal. Lett.,* **1999**, *57*, 115.

[42] H. Yasuda, N. Mizuno, M. Misono, *Chem. Commun.,* **1990**, 1094.

[43] H. J. Hwang, J. Moon, J. Moon, *J. Am. Ceram. Soc.,* **2005**, *88*, 79.

[44] H. Iwakuni, Y. Shinmyou, H. Yano, H. Matsumoto, T. Ishihara, *Appl. Catal. B,* **2007**, *74*, 299.

[45] N. Gunasekaran, S. Rajadurai, J. J. Carberry, *Catal. Lett.,* **1995**, *35*, 373.

[46] A. Feldhoff, J. Martynczuk, H. Wang, *Prog. Solid State Chem.,* **2007**, *35*, 399.

[47] J. Martynczuk, M. Arnold, H. Wang, J. Caro, A. Feldhoff, *Adv. Mat.,* **2007**, *19*, 2134.

[48] A. Feldhoff, M. Arnold, J. Martynczuk, T. M. Gesing, H. Wang, *Solid State Sci.,* **2008**, *10*, 689.

[49] T. Schiestel, M. Kilgus, S. Peter, K. J. Caspary, H. H. Wang, J. Caro, *J. Membr. Sci.,* **2005**, *258*, 1.

[50] H. Q. Jiang, F. Y. Liang, O. Czuprat, K. Efimov, A. Feldhoff, S. Schirrmeister, T. Schiestel, H. H. Wang, J. Caro, *Chem. Eur. J.* **2010**, accepted.

[51] H. Q. Jiang, H. H. Wang, F. Y. Liang, S. Werth, T. Schiestel, J. Caro, *Catal. Today,* **2010**, doi: 10.1016/j.cattod.2010.02.027.

[52] J. Caro, H. H. Wang, C. Tablet, A. Kleinert, A. Feldhoff, T. Schistel, M. Kilgus, P. Kölsch, S. Werth, *Catal. Today*, **2006**, 128.

[53] H. Q. Jiang, H. H. Wang, F. Y. Liang, S. Werth, T. Schiestel, J. Caro, *Angew. Chem.* **2009,** *121*, 3027; *Angew. Chem. Int. Ed.* **2009**, *48*, 2983.

[54] A. Feldhoff, *Solid state chemical aspects of oxygen ion and electron mixed conducting perovskites*, Habilitation thesis, Leibniz Universität Hannover, **2009**.

[55] C. Wagner, *Z. Phys. Chem. B*, **1933**, *21*, 25.

[56] C. Wagner, *Z. Phys. Chem. B*, **1936**, *32*, 447.

[57] R. Merkle, J. Maier, *Angew. Chem.* **2008,** *120*, 3936; *Angew. Chem. Int. Ed.* **2008**, *47*, 3874.

[58] J. F. Vente, W. G. Haije, Z. S. Rak, *J. Membr. Sci.,* **2006**, *276*, 178.

[59] A. Thursfield, I. S. Metcalfe, *J. Membr. Sci.,* **2007**, *288*, 175.

[60] H. H. Wang, P. K;lsch, T. Schiestel, C. Tablet, S. Werth, J. Caro, *J. Mem. Sci.,* **2006**, *284*, 5.

[61] H. H. Wang, S. Werth, T. Schiestel, J. Caro, *Angew. Chem.,* **2005**, *117*, 7066; *Angew. Chem. Int. Ed.,* **2005**, *44*, 6906.

[62] W. Yang, H. Wang, X. Zhu, L. Lin, *Topics Catal.,* **2005**, *35*, 155.

[63] C. Y. Tsai, A. G. Dixon, W. R. Moster, Y. H. Ma, *AIChE J.,* **1997**, *43*, 2741.

[64] H. H. Wang, Y. Cong, W. Yang, *Catal. Today*, **2003**, *82*, 157.

[65] J. H. Tong, W. S. Yang, R. Cai, B. C. Zhu, L. W. Lin, *Catal. Lett.,* **2002**, *78*, 129.

[66] H. H. Wang, C. Tablet, T. Schiestel, S. Werth, J. Caro, *Catal. Commun.,* **2006**, *7,* 907.

[67] C. Chen, S. J. Feng, S. Ran, D. C. Zhu, W. Liu, H. J. M. Bouwmeester, *Angew. Chem.,* **2003**, *115*, 5354; *Angew. Chem. Int. Ed.,* **2003**, *42*, 5196.

[68] H. Zimmermann, R. Walzl, *Ullmann's Encyclopedia of Industrial Chemistry*, 7th Edition, Wiley-VCH, Winheim, **2009**.

[69] H. H. Wang, Z. Cong, W. S. Yang, *Chem. Commun.,* **2002**, 1468.

[70] F. T. Akin, Y. S. Lin, *J. Mem. Sci.*, **2002**, *209*, 457.

[71] S. Ihara, *Bull. Electrotech. Lab.,* **1977**, *41*, 259.

[72] C. Hamel, A. Seidel-Morgenstern, T. Schiestel, S. Werth, H. H. Wang, C. Tablet, J. Caro, *AIChE J.*, **2006**, *52*, 3118.

[73] J. Caro, K. J. Caspary, C. Hamel, B. Hoting, P. Kölsch, B. Langanke, K. Nassauer, T. Schiestel, A. Schmidt, R. Schomcker, A. Seidel-Morgenstern, E. Tsotsas, I. Voigt, H. H. Wang, R. Warsitz, S. Werth, A.Wolf, *Ind. Eng. Chem. Res.,* **2007**, *46*, 2286.

Chapter 2

Thermodynamic coupling for hydrogen production

2.1 Summary

As mentioned in Section 1.1.2, one technique to produce more hydrogen from the equilibrium-limited water splitting is the in situ removal of the simultaneously produced oxygen via a perovskite oxygen-permeable membrane. The hydrogen production rate directly depends on the rate of oxygen removal from the water splitting system. In this chapter, the effective hydrogen production from water splitting was demonstrated by coupling water splitting with three oxygen-consuming reactions on the opposite sides of BCFZ hollow fiber membrane.

In the first article, water splitting was coupled with methane combustion. A BCFZ-Pd porous layer with the thickness of around 40 μm was elaborately attached to the outer surface of the dense BCFZ membrane to catalyze methane combustion. The oxygen permeation rate was increased by 3.5 times as compared to that of the blank BCFZ membrane, and the hydrogen production rate from water splitting was increased from 0.7 to 2.1 cm^3 min^{-1} cm^{-2} at 950 °C after depositing a BCFZ-Pd porous layer onto the dense BCFZ membrane.

In the second article, water splitting was coupled with the POM to synthesis gas (a mixture of CO and H_2). A Ni-based catalyst was packed on the shell side. It was found that the hydrogen production rate was increased by increasing the operating temperature or methane concentration on the shell side. A hydrogen production rate of 3.1 cm^3 min^{-1} cm^{-2} was obtained on the core side at 950 °C. Simultaneously, a methane conversion of 70 % and CO selectivity of 60 % were obtained on the shell side.

In the third article, water splitting was coupled with the ODE to ethylene. In this case, the hydrogen production from water splitting was conducted at moderate temperature. At 800 °C, not only a hydrogen production rate of 1.0 cm^3 min^{-1} cm^{-2} was obtained, but also an ethylene yield of around 55 % was achieved on the other side of the BCFZ membrane. Moreover, the operation for the simultaneous production of hydrogen on the core side and ethylene on the shell side was conducted for 100 h without membrane failure.

2.2 Hydrogen production by water dissociation in surface-modified BaCo$_x$Fe$_y$Zr$_{1-x-y}$O$_{3-\delta}$ hollow fiber membrane reactor with improved oxygen permeation

Heqing Jiang, Fangyi Liang, Oliver Czuprat, Konstantin Efimov, Armin Feldhoff, Steffen Schirrmeister, Thomas Schiestel, Haihui Wang, and Jürgen Caro

Hydrogen production by water dissociation in surface-modified BaCo$_x$Fe$_y$Zr$_{1-x-y}$O$_{3-\delta}$ hollow fiber membrane reactor with improved oxygen permeation

Heqing Jiang,*[a] Fangyi Liang,[a] Oliver Czuprat,[a] Konstantin Efimov,[a] Armin Feldhoff,[a] Steffen Schirrmeister,[b] Thomas Schiestel,[c] Haihui Wang,[d] and Jürgen Caro*[a]

Abstract: A porous perovskite BaCo$_x$Fe$_y$Zr$_{0.9-x-y}$Pd$_{0.1}$O$_{3-\delta}$ (BCFZ-Pd) coating was deposited onto the outer surface of a BaCo$_x$Fe$_y$Zr$_{1-x-y}$O$_{3-\delta}$ (BCFZ) perovskite hollow fiber membrane. The surface morphology of the modified BCFZ fiber was characterized by scanning electron microscopy (SEM), indicating the formation of a BCFZ-Pd porous layer onto the outer surface of a dense BCFZ hollow fiber membrane. The oxygen permeation flux of the BCFZ membrane with BCFZ-Pd porous layer has been increased by 3.5 times as compared with that of the blank BCFZ membrane when feeding the reactive CH$_4$ on the permeation side. The blank BCFZ membrane and surface-modified

Keywords: perovskite phases · water splitting · oxygen separation · hollow fiber membranes · heterogeneous catalysis

BCFZ membrane were respectively used as reactor to shift the equilibrium of thermal water dissociation for hydrogen production because they allow the selective removal of the produced oxygen from the water dissociation system. It was found that the hydrogen production rate has been increased from 0.7 to 2.1 mL H$_2$ min^{-1} cm^{-2} at 950 °C after depositing a BCFZ-Pd porous layer onto the BCFZ membrane.

Introduction

Dense perovskite membranes with mixed oxygen ion and electron conductivity[1,2] have been intensively investigated as separator material to produce pure oxygen from air[3] or in membrane reactors for the partial oxidation of methane (POM) to synthesis gas,[4] the oxidative dehydrogenation of light hydrocarbons (ODH) to olefins,[5]

[a] H.Q. Jiang, F.Y. Liang, O. Czuprat, K. Efimov, Dr. A. Feldhoff, Prof. J. Caro
Institute of Physical Chemistry and Electrochemistry
Leibniz University of Hannover
Callinstr. 3A, D-30167 Hannover, Germany
Fax: (+) 49-511-76219121
E-mail: heqing.jiang@pci.uni-hannover.de and juergen.caro@pci.uni-hannover.de

[b] Dr. S. Schirrmeister
Uhde GmbH
Friedrich-Uhde-Str. 15, D-44141 Dortmund, Germany

[c] Dr. T. Schiestel
Fraunhofer Institute of Interfacial Engineering and Biotechnology (IGB)
Nobelstr 12, D-70569 Stuttgart, Germany

[d] Prof. H.H. Wang
School of Chemistry and Chemical Engineering
South China University of Technology, Guangzhou, 510640, China

Supporting information for this article is available on the WWW under http://www.chemeurj.org/ or from the author.

or in the Ostwald process.[6] It is well accepted that oxygen permeation through the membrane involves (i) surface exchange between molecular oxygen and oxygen ions on the membrane surface and (ii) bulk diffusion of the oxygen ion.[1] The diffusion-controlled oxygen permeation flux can be increased by reducing the thickness of the membrane until its thickness reaches a critical value. Below the critical thickness, the surface exchange processes become rate-limiting. In this case, the oxygen permeation flux can be enhanced by coating the membrane with materials that show a high exchange rate such as cobalt-containing perovskites[7] or noble metal particles.[8] It is worth noting that the surface reaction accelerated by the active materials in the above work[7,8] is the oxygen ionization O$_2$ + 4e$^-$ $\leftrightarrows$ 2 O^{2-} because only the inert gas He was used to sweep the permeated oxygen.

In another application of perovskite membrane as reactor for the oxidation of light hydrocarbons,[1,5] the surface process is the reaction between the permeated oxygen species and the reactive gas such as CH$_4$. In this case, a better reactor performance can be expected by coating the membrane with a catalytically active layer. However, to the best of our knowledge, no attention was paid so far on the surface modification of perovskite hollow fiber membrane by a catalytically active porous layer. When the catalytic coating accelerates the hydrocarbon oxidation, oxygen is consumed quickly, the driving force for oxygen permeation is increased and a higher oxygen flux can be expected.

Recently, a novel BaCo$_x$Fe$_y$Zr$_{1-x-y}$O$_{3-\delta}$ (BCFZ) perovskite hollow fiber membrane with high oxygen permeability has been developed in our group for e.g. oxygen separation, partial oxidation of methane to synthesis gas.[9] In this contribution, BCFZ hollow

1

fiber membrane is surface-modified by $BaCo_xFe_yZr_{0.9-x-y}Pd_{0.1}O_{3-\delta}$ (BCFZ-Pd) catalytic porous layer. The choice of BCFZ-Pd as the coating material is based on the following considerations. Compared to the common catalysts such as Pd/Al_2O_3 that can lead to the membrane failure due to the diffusion of Al and Co between the catalyst and membrane,[10] BCFZ-Pd shows a better compatibility with BCFZ membrane, and has almost the same melting point as the perovskite BCFZ, which make it possible to obtain a surface coating with good mechanical strength onto BCFZ membrane surface. Co-containing perovskites and noble metal Pd catalysts are well known for their activity towards methane combustion.[11] The noble metal Pd modified perovskites are expected to combine the advantages of the above two kinds of catalysts such as catalytic activity and thermal resistance. In addition, it was reported that the presence of Pd can increase the reducibility of cobalt ions in $Pd-Co/Al_2O_3$,[12] which leads to a better catalytic performance for methane oxidation. It can be expected, therefore, that the fine mixing of Pd and Co in the perovskite lattice will favour the interaction between them. The ionic radius of $Pd^{2+} = 80$ pm allows the modification of the B site of the $ABO_{3-\delta}$ structure according to the Goldschmidt tolerance concept. So a pure phase of Pd-Co-containing perovskite (BCFZ-Pd) was first prepared in this work.
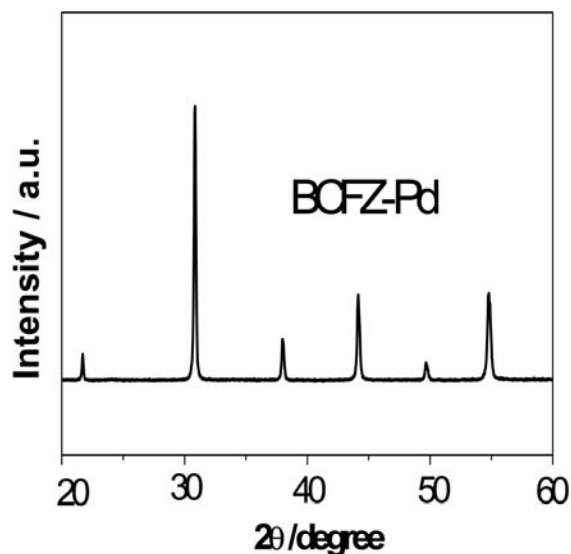

Figure 1 XRD pattern of the BCFZ-Pd powder used for coating the BCFZ hollow fiber membranes.
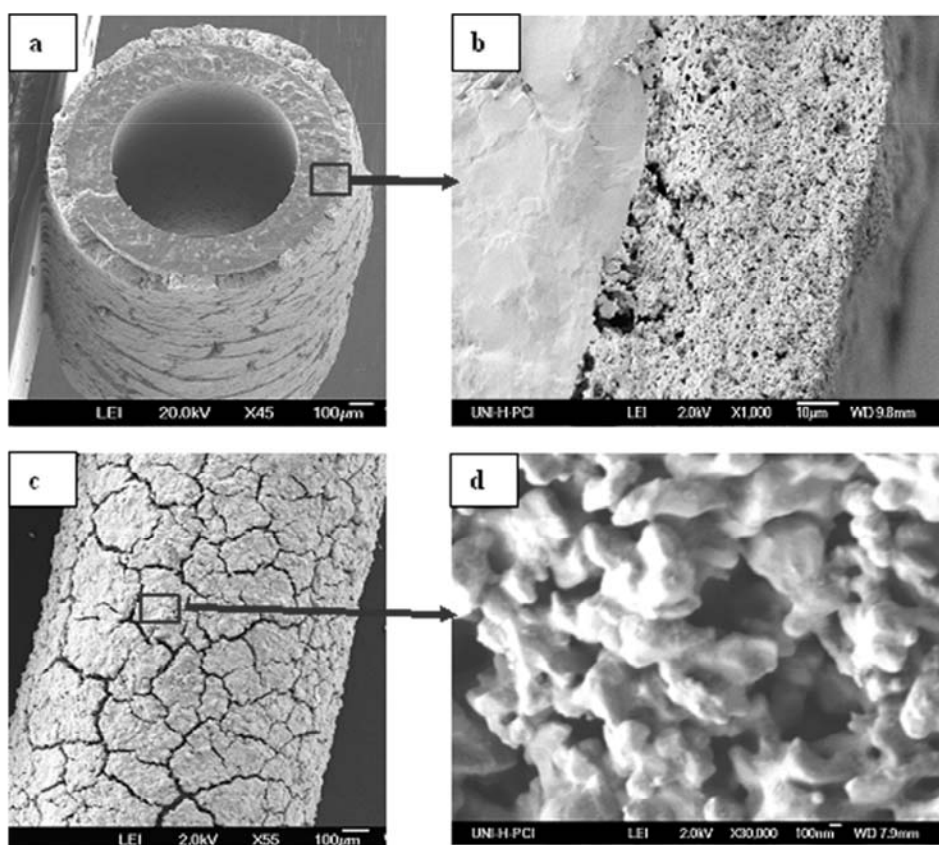

Figure 2 SEM micrographs of BCFZ hollow fiber membrane with BCFZ-Pd layer treated at 1050 °C for 1 h. (a, b) cross-section, and (c, d) outer surface of the modified hollow fiber membrane before use in the membrane reactor.

2

Results and Discussion

Figure 1 presents the X-ray diffraction (XRD) pattern of BCFZ-Pd (4.2 mass% Pd) powder used in this work. From the absence of signals different from a pure perovskite phase, it is concluded that a one-phase material has been formed with Pd successfully incorporated into the BCFZ lattice. This can be further proven by scanning transmission electron microscopy (STEM) results. Figure S1a and Figure S1b (see Supporting Information) show the dark-field micrograph of BCFZ-Pd particles and the energy-dispersive X-ray spectrum (EDXS) of the particles, respectively, demonstrating the presence of Ba, Co, Fe, Zr, Pd, and O. The corresponding elemental distribution images (Figure S1c to h, Supporting Information) show that all the elements were homogenously distributed in the particles. Electron diffractions pattern from selected area of BCFZ-Pd particle (Figure S2a and b, Supporting Information) indicates that BCFZ-Pd is a singular crystal structure. Moreover, the crystal orientation can be observed from the high-resolution transmission electron microscopy (HRTEM) micrograph (Figure S2c, Supporting Information). The results of XRD and TEM demonstrated the formation of a pure perovskite phase BCFZ-Pd and the homogeneous distribution of Co and Pd in the perovskite lattice.

It was experimentally found that the mechanical strength and porosity of the BCFZ-Pd coating layer onto the surface of the BCFZ fiber can be adjusted by controlling the temperature and time of calcination. The optimal condition for the formation of a porous layer with good mechanical strength was found in a treatment of the coated fiber at 1050 °C for 1 h. Figure 2 presents the scanning electron microscopy (SEM) images of the BCFZ hollow fiber membrane coated by BCFZ-Pd. It can be seen from Figure 2a,b that BCFZ-Pd layer with the thickness of about 40 μm is tightly attached to the outer surface of the BCFZ hollow fiber membrane. And no development of any crack was observed on the dense part of BCFZ membrane after the coating process. Moreover, the outer BCFZ-Pd layer sintered at 1050 °C for 1 h is still porous. So a larger surface area is obtained and a higher catalytic activity can be expected.
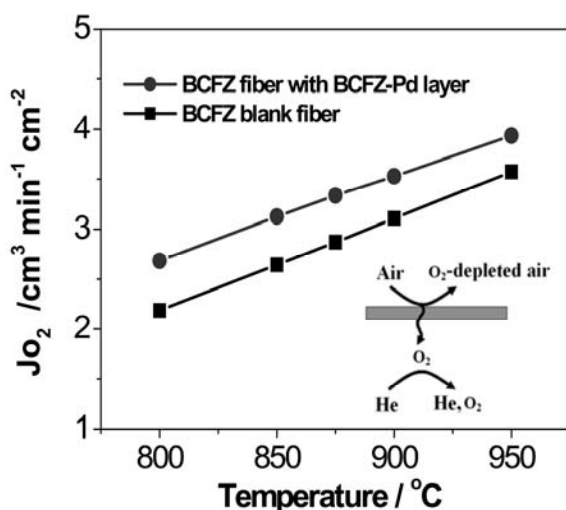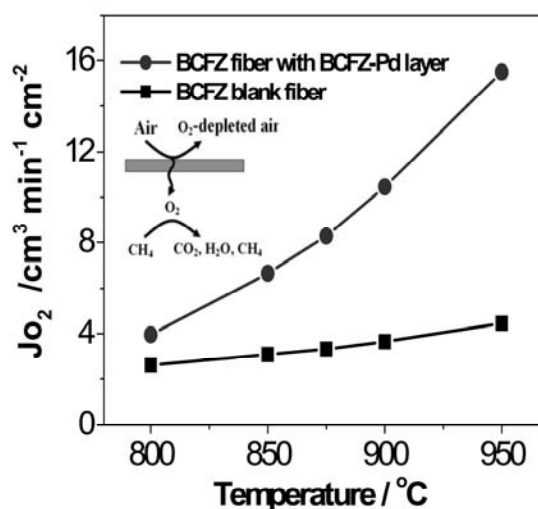
Figure 4 Oxygen permeation fluxes (J$_{O_2}$) of a BCFZ hollow fiber membrane with/without a BCFZ-Pd porous layer as a function of temperature having the diluted methane on the permeation side for oxygen consumption. Core side: F$_{air}$=150 cm^3 min^{-1}. Shell side: F$_{He}$=39 cm^3 min^{-1}, F$_{CH4}$=10 cm^3 min^{-1} and F$_{Ne}$=1.0 cm^3 min^{-1}. Membrane area: 0.86 cm^2.

Figure 2c demonstrates the surface morphology of BCFZ hollow fiber membrane coated by BCFZ-Pd surface layer. It can be seen that the outer side of the hollow fiber is well coated by surface layer (BCFZ-Pd) along the whole length although some cracks are observed due to shrinking of the coating by the heat treatment. The magnified image (Figure 2d) shows that the BCFZ-Pd particles are connected with each other forming a three dimensional network which ensures the necessary mechanical strength and porosity.

It is very important to make sure that the hollow fiber membrane along the whole length after the catalyst coating process is still gastight. Here, after the fiber was installed into the high-temperature reactor, a large pressure gradient across the membrane was established by increasing the pressure on the core side. It was found that, at room temperature, there is not any increase of the pressure on the shell side when the pressure on the core side was increased from 1 bar to 5 bar, indicating the membrane after the coating process is still gastight. During the measurements, air was fed to the core side. At high temperature, oxygen can be selectively transported from the core side to the shell side, but nitrogen can not if the membrane is gastight. So nitrogen from air can work as the non-permeable gas to indicate whether the membrane is gastight or not. There is almost no obvious nitrogen detected by gas chromatography from the shell side for all the following investigated hollow fiber membranes, indicating they are all gastight.

Figure 3 demonstrates the temperature dependence of the oxygen permeation flux J$_{O_2}$ of the blank and surface-modified BCFZ membranes, respectively, using He as the sweep gas. It can be seen that J$_{O_2}$ increases with increasing temperature for both membranes. However, J$_{O_2}$ of the coated membrane is only by about 10 % higher than that of the uncoated one. According to our previous studies,[13] the permeation flux through the BCFZ hollow fiber membrane is controlled by both the bulk diffusion of oxygen
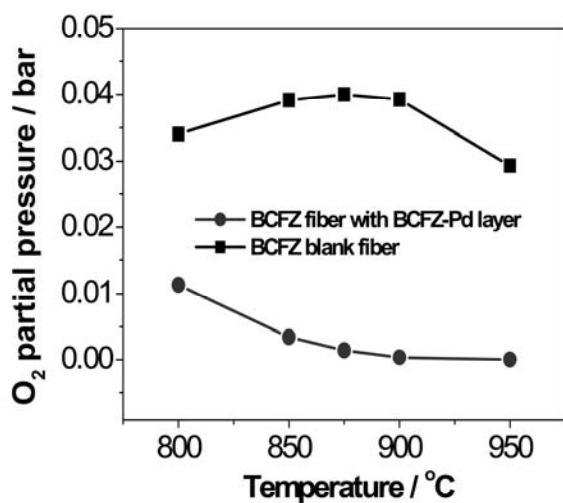

Figure 3 Oxygen permeation fluxes (J$_{O_2}$) of a BCFZ hollow fiber membrane with/without a BCFZ-Pd porous layer as a function of temperature using He as the sweep gas. Core side: F$_{air}$=150 cm^3 min^{-1}. Shell side: F$_{He}$=49 cm^3 min^{-1}, and F$_{Ne}$=1.0 cm^3 min^{-1}. Membrane area: 0.86 cm^2.

3

Figure 5 Temperature dependence of the residual oxygen partial pressure on the permeation side of BCFZ membrane with/without BCFZ-Pd porous coating measured by gas chromatography (see experimental conditions in Figure 4).

ions and the surface exchange processes. The BCFZ-Pd porous layer on the permeation side can provide more sites for the association of oxygen ions to molecular oxygen followed by desorption, leading to a higher surface exchange rate. So a slight increase of the oxygen permeation flux is observed due to surface enlargement by the BCFZ-Pd porous layer onto BCFZ membrane surface.

One promising application of the perovskite membranes will be their use as reactor for the partial oxidation of hydrocarbons.[4,5] In this case, another kind of surface reaction between the permeated oxygen species and hydrocarbon will be involved. So it is interesting to investigate the effect of surface modification of perovskite membrane on the oxygen permeation rate by using a reactive gas like CH_4 as sweep gas. Figure 4 presents J_{O_2} at different temperatures of the blank and coated BCFZ hollow fiber membranes when feeding diluted methane on the permeation side. In comparison with the blank BCFZ membrane, J_{O_2} increased dramatically from 4.5 to 15.5 mL min^{-1} cm^{-2} at 950 °C after coating with a porous BCFZ-Pd layer. This experimental finding can be understood as follows. When feeding diluted methane to the permeation side, the main surface reaction is the methane oxidation ($CH_4 + 4 O^{2-} \rightarrow CO_2 + 2 H_2O + 8e^-$). In the case of coating by the catalytically active BCFZ-Pd porous layer with a large surface area,
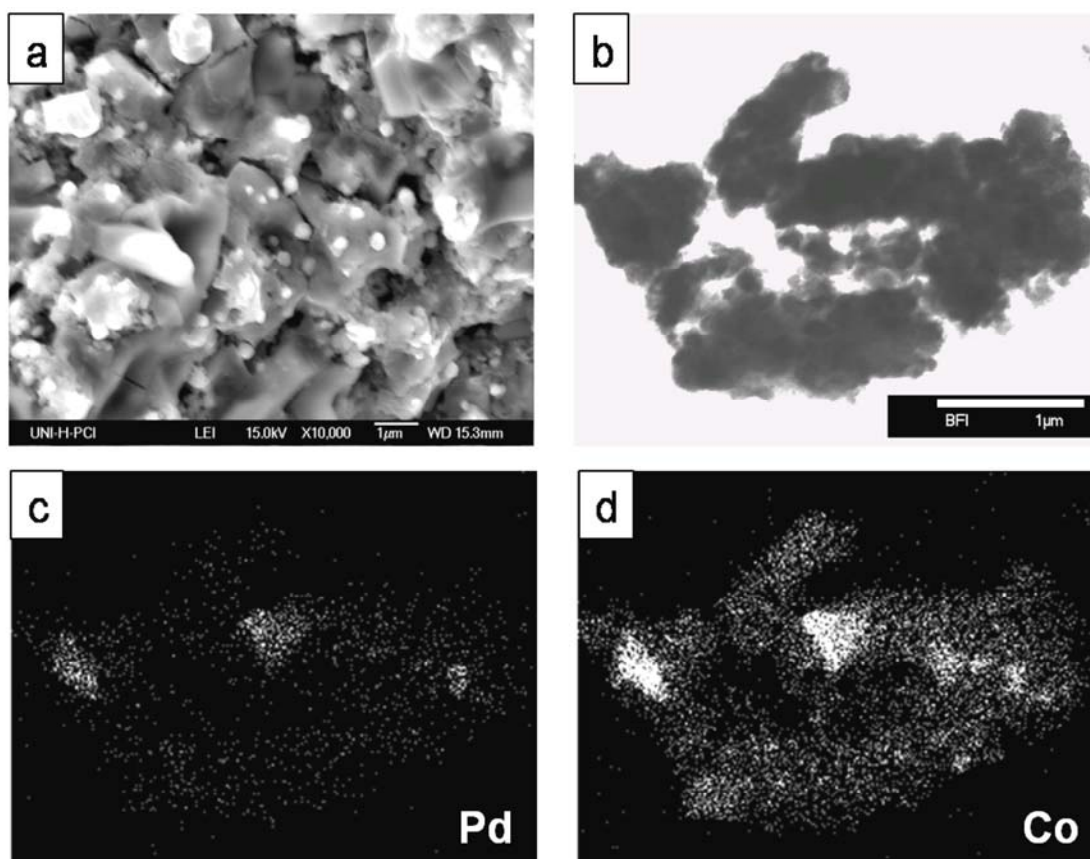

Figure 6 Spent BCFZ-Pd coating after studying the oxygen permeation at 950 °C (see Figure 4): a) Secondary electron micrograph, b) STEM bright-field micrograph and (c, d) the corresponding elemental distribution images of palladium and cobalt.

4

the permeated oxygen species can be consumed faster due to the higher catalytic activity of surface layer for methane oxidation. So a lower oxygen partial pressure can be obtained, which could be measured by gas chromatography, as shown in Figure 5. It can be seen from Figure 5 that the oxygen partial pressure above the coated membrane on the methane side is obviously lower than that of the blank BCFZ membrane. This experimental finding shows that the Pd-containing BCFZ coating catalyses effectively the combustion of methane. Thus a larger oxygen partial pressure gradient was established across the coated membrane and the oxygen permeation rate is enhanced based on Wagner equation[1].

Methane combustion over cobalt-containing perovskite, which is one of the most reducible perovskites, has been extensively investigated in the past years. The partial reduction of Co^{3+} to Co^{2+} in perovskite will lead to large amounts of active sites (oxygen vacancies) for oxygen adsorption and, thus, a high catalytic activity towards methane oxidation.[14] When comparing the fresh (Figure 2d) and spent (Figure 6a) one can see that the spent coating contains spherical particles of about 100 -200 nm . From the light appearance of the spherical particles due to a higher emission of secondary electrons can be concluded that they are enriched with heavy metals. Correspondingly, EDXS of the spent coating in STEM modus shows an inhomogeneous distribution of Pd and Co (Fig. 6 b-d). Different to the fresh particles before measurement, in which all the related elements were homogeneously distributed (see Figure S1c to h, Supporting Information), the Co-enriched phase and Co-Pd co-enriched phase were identified (Figure 6c to d). The presence of Co-Pd co-enriched phase implies the interaction between Co and Pd. It is reported that the presence of Pd increased the reducibility of cobalt ions in a Pd-Co/Al_2O_3 catalyst.[12] Here, the addition of Pd into Co-containing perovskite lattice enhances reducibility of cobalt ions and, thus, leads to a higher catalytic activity towards methane oxidation.
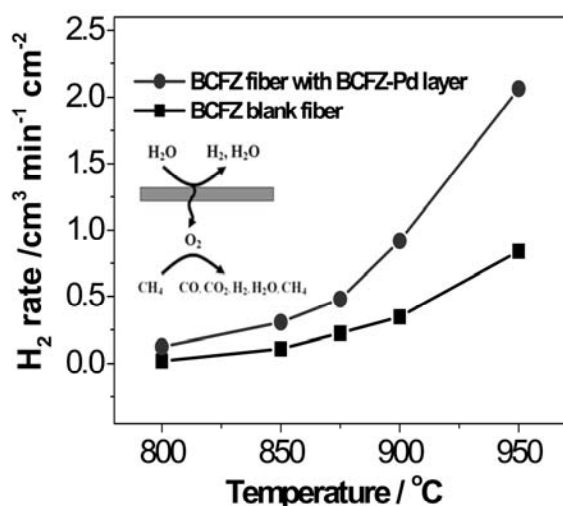
From the above results, it can be seen that the BCFZ hollow fiber membrane with BCFZ-Pd catalytic porous layer exhibits higher oxygen permeability, so a better performance can be expected when it is used as membrane reactor. In this paper, we have evaluated the catalytically modified BCFZ hollow fiber membrane for hydrogen production by water splitting in a membrane reactor: on one side of the membrane, water is thermally dissociated into hydrogen and oxygen according to $H_2O \leftrightarrows H_2 + \frac{1}{2} O_2$. The latter can be in situ removed by the oxygen-permeable membrane and then consumed by methane oxidation on the other side according to $CH_4 + 2 O_2 \rightarrow CO_2 + 2 H_2O$. Obviously, the hydrogen production rate after steam condensation in the retentate is related to three processes: water dissociation, oxygen transport through the membrane and oxygen consumption on the permeation side. Figure 7 shows the temperature dependence of hydrogen production rates for the blank and surface-modified BCFZ membrane reactors, respectively. It was found that the hydrogen production rate increases as the temperature rises from 800 to 950 °C for both membranes. With increasing temperature, the equilibrium constant of the endothermic water splitting will increase, and the oxygen removal rate from the water dissociation system will also increase due to the increased oxygen permeability of the membrane. So, the hydrogen production rate becomes higher with increasing temperature. As discussed above, compared to the blank BCFZ membrane, the surface-modified BCFZ hollow fiber membrane shows higher catalytic activity towards methane oxidation, leading to higher oxygen permeation rate. So a higher hydrogen production rate was obtained after the surface of BCFZ membrane was modified by BCFZ-Pd catalytic porous layer. It can be seen from Figure 7, that the hydrogen production rate has been improved from 0.7 to 2.1 mL min^{-1} cm^{-2} at 950 °C after depositing a BCFZ-Pd porous layer onto the BCFZ membrane

Conclusion

In summary, a BCFZ hollow fiber membrane is surface-modified by a catalytically active BCFZ-Pd porous layer that shows a high catalytic activity in hydrocarbon combustion. The oxygen permeation flux of the surface-modified BCFZ membrane has been increased by 3.5 times as compared with that of the blank BCFZ membrane when feeding the oxygen consuming CH_4 instead of an inert sweep gas like He on the permeation side. When the surface-modified BCFZ membrane was used as the reactor to shift the equilibrium of water dissociation for hydrogen production, a higher H_2 production rate was obtained due to its higher oxygen permeability. This paper demonstrates that, by modifying the oxygen-permeable hollow fiber BCFZ perovskite membrane with a proper catalytic porous layer, not only the oxygen permeation flux can be enhanced, but also a better reactor performance can be obtained.

Figure 7 H_2 production rates as a function of temperature on a BCFZ hollow fiber membrane with/without a BCFZ-Pd porous layer. Core side: F_{H2O}=30 cm^3 min^{-1} and F_{He}=10 cm^3 min^{-1}. Shell side: F_{He}=39 cm^3 min^{-1}, F_{CH4}=10 cm^3 min^{-1} and F_{Ne}=1.0 cm^3 min^{-1}. Membrane area: 0.86 cm^2.

Experimental Section

BCFZ-Pd perovskite powder was prepared by a combined citric acid and ethylenediaminetetraacetic acid (EDTA) complexing method.[15] The calculated amounts of Ba(NO$_3$)$_2$, Pd(NO$_3$)$_2$ and ZrO(NO$_3$)$_2$ powder were dissolved in an aqueous solution of Co(NO$_3$)$_2$ and Fe(NO$_3$)$_3$ followed by the addition of EDTA acid and citric acid with the molar ratio of EDTA acid : citric acid : total of metal cations = 1:1.5:1. After agitation for a certain time, the pH value of the solution was adjusted at around 9 by adding NH$_4$OH. The solution was then heated in the temperature range of 120-150 °C under constant stirring to obtain a gel. Further heat treatment was applied at 950 °C for 10 h to obtain BCFZ-Pd perovskite powder with the final composition.

5

The crystal structure of BCFZ-Pd perovskite powder was investigated using a Philips X'pert-MPD instrument with Cu Kα radiation. TEM was performed on a field-emission instrument of the type JEOL JEM-2100F. An Oxford Instruments INCA-200-TEM system with an ultra-thin window was attached to the microscope that allowed for elemental analysis using EDXS. The surface morphology of BCFZ hollow fiber membrane coated by BCFZ-Pd layer was characterized using a field-emission SEM of the type JEOL JSM-6700F.

The dense BCFZ hollow fiber membranes were manufactured by phase inversion spinning followed by sintering.[13] The sintered fiber had a wall thickness of around 0.17 mm with an outer diameter of 1.10 mm and an inner diameter of 0.76 mm. The BCFZ-Pd slurry was prepared by mixing BCFZ-Pd powder with water in a mortar followed by milling. The BCFZ-Pd porous layer can be obtained by brushing the above slurry onto the outer surface of the central 3 cm of BCFZ membrane followed by heating at 1050 °C for 1 h. In order to obtain the isothermal condition, two ends of the fiber were coated by Au paste followed by sintering at 950 °C and thus a dense Au film that is not permeable to oxygen was obtained.

The oxygen permeation experiments were carried out in a high-temperature permeator as described in our previous work.[16] Synthetic air or steam diluted by He was fed to the core side and a mixture of CH_4, Ne and He was fed to the shell side. All gas flows were controlled by mass flow controllers (Bronkhorst), which were calibrated by using a soap bubble meter before measurements. The total flow rate of the effluents on shell side was calculated by using Ne as an internal standard. The concentrations of the gases at the exit of the reactor were determined by an on-line gas chromatograph (Agilent 6890). The oxygen permeation rate can be obtained based on the change of oxygen concentration on air side between the inlet and outlet. H_2 production rate on the core side was calculated from the total flow rate F_{core} (mL.min^{-1}), hydrogen concentration c (H_2), and membrane area S (cm^2) based on the following equation:

$$J(H_2) = \frac{F_{core} \times c(H_2)}{S}$$

Acknowledgements

[1] a) W. S. Yang, H. H. Wang, X. F. Zhu, L. W. Lin, *Topic Catal.* **2005**, *35*, 155-167. b) J. Sunarso, S. Baumann, J. M. Serra, W. A. Meulenberg, S. Liu, Y. S. Lin, J. D. Costa, *J. Membr. Sci.* **2008**, *320*, 13-41. c) Y. T. Liu, X. Y. Tan, K. Li, *Catal. Rev -Sci. Eng.* **2006**, *48*, 145-198. d) C. S. Chen, S. J. Feng, S. Ran, D. C. Zhu, W. Liu, H. J. M. Bouwmeester, *Angew. Chem. Int. Ed.* **2003**, *42*, 5196-5198. e) R. Merkle, J. Maier, *Angew. Chem. Int. Ed.* **2008**, *47*, 3874-3894.

[2] a) J. Caro, K. J. Caspary, C. Hamel, B. Hoting, P. Kölsch, B. Langanke, K. Nassauer, T. Schiestel, A. Schmidt, R. Schomäcker, A. Seidel-Morgenstern, E. Tsotsas, I. Voigt, H. H. Wang, R. Warsitz, S. Werth, A. Wolf, *Ind. Eng. Chem. Res.* **2007**, *46*, 2286-2294. b) H. H. Wang, C. Tablet, A. Feldhoff, J. Caro, *Adv. Mater.* **2005**, *17*, 1785-1788. c) J. Martynczuk, M. Arnold, H. H. Wang, J. Caro, A. Feldhoff, *Adv. Mater.* **2007**, *19*, 2134-2140.

[3] P. N. Dyer, R. E. Richards, S. L. Russek, D. M. Taylor, *Solid State Ionics* **2000**, *134*, 21-33.

[4] a) H. J. M. Bouwmeester, *Catal. Today* **2003**, *82*, 141-150. b) J. T. Ritchie, J. T. Richardson, D. Luss, *AIChE Journal* **2001**, *47*, 2092-2101.

[5] a) F. T. Akin, Y. S. Lin, *J. Membr. Sci.* **2002**, *209*, 457-467. b) H. H. Wang, Y. Cong, W. S. Yang, *Catal. Lett.* **2002**, *84*, 101-106.

[6] J. P. Perez-Ramirez, B. Vigeland, *Angew. Chem. Int. Ed.* **2005**, *44*, 1112-1115.

[7] a) J. F. Vente, W. G. Haije, Z. S. Rak, *J. Membr. Sci.* **2006**, *276*, 178-184. b) H. Kusaba, Y. Shibata, K. Sasaki, Y. Teraoka, *Solid State Ionics* **2006**, *177*, 2249-2253. c) V. V. Kharton, A. Kovalevsky, A. A. Yaremchenko, F. M. Figueiredo, E. N. Naumovich, A. L. Shaulo, F. M. B. Marques, *J. Membr. Sci.* **2002**, *195*, 277-287. d) S. Lee, K. S. Lee, S. K. Woo, J. W. Kim, T. Ishihara, D. K. Kim, *Solid State Ionics* **2003**, *158*, 287-296. e) A. Thursfield, I. S. Metcalfe, *J. Membr. Sci.* **2007**, *288*, 175-187.

[8] K. Gerdes, D. Luss, *AIChE Journal* **2007**, *53*, 1389-1391.

[9] a) H. Q. Jiang, H. H. Wang, F. Y. Liang, S. Werth, T. Schiestel, J. Caro, *Angew. Chem. Int. Ed.* **2009**, *48*, 2983-2986. b) H. Q. Jiang, H. H. Wang, S. Werth, T. Schiestel, J. Caro, *Angew. Chem. Int. Ed.* **2008**, *47*, 9341-9344. c) H. H. Wang, C. Tablet, T. Schiestel, S. Werth, J. Caro, *Catal. Commun.* **2006**, *7*, 907-912. d) H. H. Wang, S. Werth, T. Schiestel, J. Caro, *Angew. Chem. Int. Ed.* **2005**, *44*, 6906-6909. e) H. H. Wang, T. Schiestel, C. Tablet, M. Schroeder, J. Caro, *Solid State Ionics* **2006**, *177*, 2255-2259.

[10] a) S. D. Peter, E. Garbowski, V. Perrichon, M. Primet, *Cataly. Lett.* **2000**, *70*, 27-33. b) H. H. Wang, A. Feldhoff, J. Caro, T. Schiestel, S. Werth, *AIChE Journal* **2009**, *55*, 2657-2664.

[11] a) O. Demoulin, M. Navez, P. Ruiz, *Catal. Lett.* **2005**, *103*, 149-153. b) K. Persson, A. Ersson, K. Jansson, J. L. G. Fierro, S. G. Jaras, *J. Catal.* **2006**, *243*, 14-24. c) B. Bialobok, J. Trawczynski, W. Mista, M. Zawadzki, *Appl. Catal. B-Environmental*, **2007**, *72*, 395-403.

[12] A. Sarkany, Z. Zsoldos,G. Stefler, J. W. Highttower, L. Guczi, *J. Catal.* **1995**, *157*, 179-189.

[13] T. Schiestel, M. Kilgus, S. Peter, K. J. Caspary, H. H. Wang, J. Caro, *J. Membr. Sci.* **2005**, *258*, 1-4.

[14] M. Arnold, Q. Xu, F. D. Tichelaar, A. Feldhoff, *Chem. Mater.* **2009**, *21*, 635-640.

[15] a) Z. P. Shao, W. S. Yang, Y. Cong, H. Dong, J. H. Tong, G. X. Xiong, *J. Membr. Sci.* **2000**, *172*, 177-188. b) L. Yang, Z. T. Wu, W. Q. Jin, N. P. Xu, *Ind. Eng. Chem. Res.* **2004**, *43*, 2747-2752.

[16] H. H. Wang, P. Kölsch, T. Schiestel, C. Tablet, S. Werth, J. Caro, *J. Membr. Sci.* **2006**, *284*, 5-8.

6

Supporting Information for

Chemistry - A European Journal

Hydrogen production by water dissociation in surface-modified BaCo$_x$Fe$_y$Zr$_{1-x-y}$O$_{3-\delta}$ hollow fiber membrane reactor with improved oxygen permeation[**]

Heqing Jiang[a, *], Fangyi Liang[a], Oliver Czuprat[a], Konstantin Efimov[a], Armin Feldhoff[a], Steffen Schirrmeister[b], Thomas Schiestel[c], Haihui Wang[d], Jürgen Caro[a, *]

[a]*Institute of Physical Chemistry and Electrochemistry, Leibniz University of Hannover, Callinstr. 3A, D-30167 Hannover, Germany*

[b]*Uhde GmbH, Friedrich-Uhde-Str. 15, D-44141 Dortmund, Germany*

[c]*Fraunhofer Institute of Interfacial Engineering and Biotechnology (IGB), Nobelstr 12, D-70569 Stuttgart, Germany*

[d]*School of Chemistry and Chemical Engineering, South China University of Technology, Guangzhou, 510640, PR China*

37
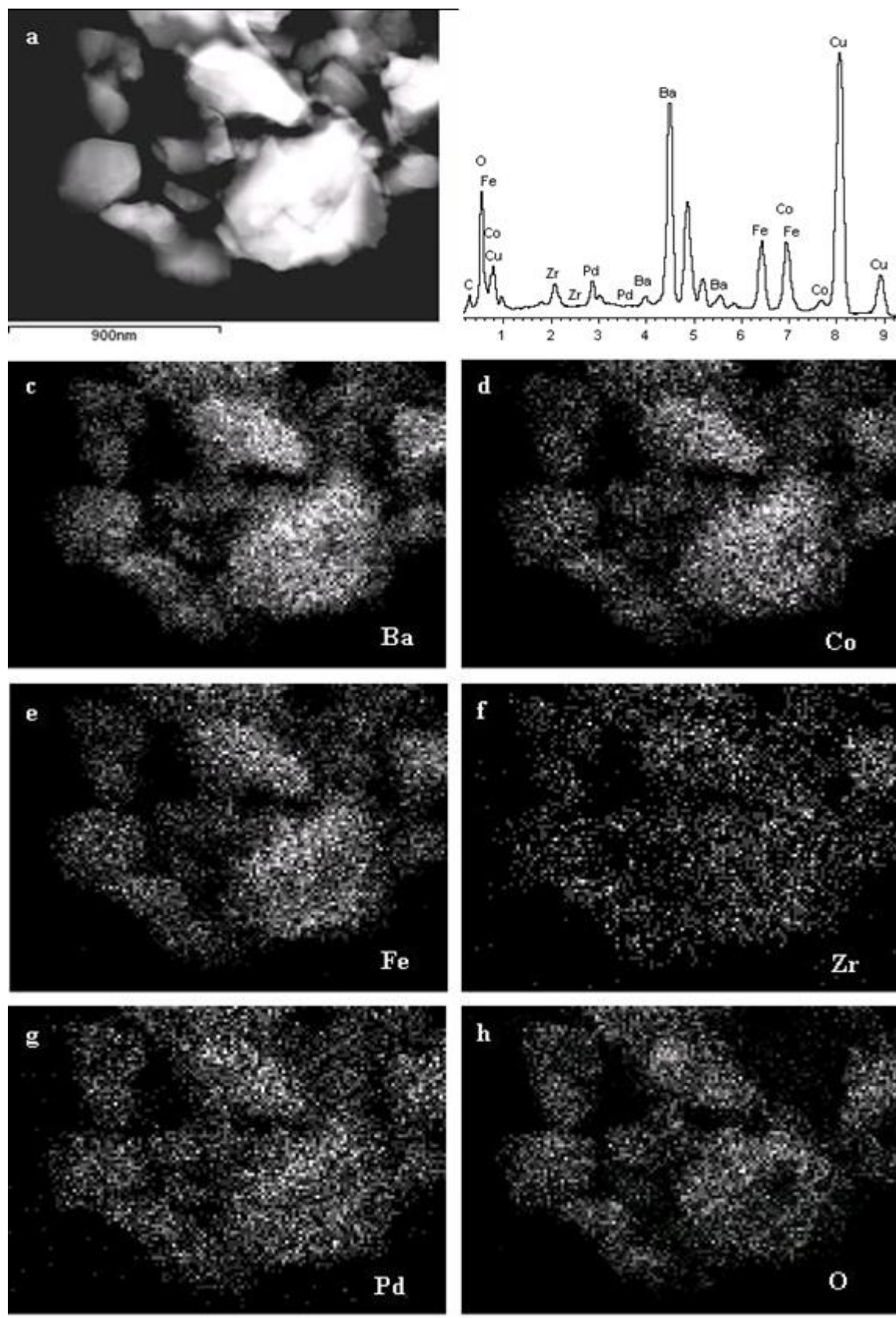
Figure S1 TEM analysis of BCFZ-Pd particles: (a) dark-field micrograph, (b) energy-dispersive X-ray spectrum (EDXS), and (c-h) corresponding elemental distribution images.
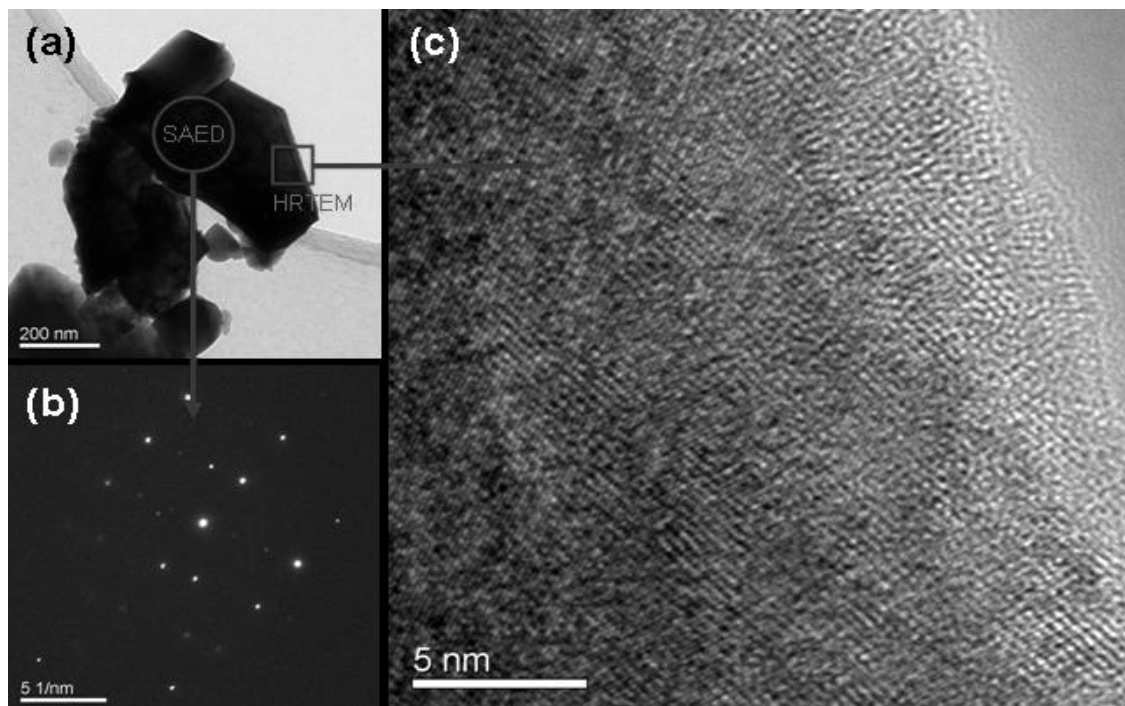
Figure S2 (a) TEM bright-field micrograph of the BCFZ-Pd powder, (b) electron diffraction pattern from the selected area, and (c) HRTEM micrograph from the selected area.

2.3 Simultaneous production of hydrogen and synthesis gas by combining water splitting with partial oxidation of methane in a hollow-fiber membrane reactor

Heqing Jiang, Haihui Wang, Steffen Werth, Thomas Schiestel, and Jürgen Caro

Hydrogen Production

Simultaneous Production of Hydrogen and Synthesis Gas by Combining Water Splitting with Partial Oxidation of Methane in a Hollow-Fiber Membrane Reactor**

Heqing Jiang, Haihui Wang, Steffen Werth, Thomas Schiestel, and Jürgen Caro*

Hydrogen is gaining more and more attention because it is regarded as an important future fuel. Today, hydrogen is mainly produced from nonrenewable natural gas and petroleum. With concerns over worldwide energy demands and global climate change, alternative sources must be found. Obviously, water is recommended as the ideal source for the generation of large amounts of hydrogen.[1] In addition to electrolysis, recently several new processes, such as photovoltaic–photoelectrochemical water splitting[2–4] and one-step or multistep thermochemical water splitting[5,6] based on focused solar[7–9] or nuclear[10] heat, have been developed. Although water dissociation into oxygen and hydrogen is conceptually simple [Eq. (1)], efficient hydrogen production

$$H_2O \rightleftharpoons H_2 + \tfrac{1}{2}O_2 \qquad (1)$$

from water remains difficult as a result of the low equilibrium constant of $K_p \approx 2 \times 10^{-8}$ at the relatively high temperature of 950 °C.[11]

However, the hydrogen production rate can be significantly improved by extracting oxygen with an oxygen-permeable membrane. One possible type of membrane for the efficient removal of oxygen at high temperatures is a mixed oxygen-ion- and electron-conducting membrane (MIECM) with high oxygen permeability.[12–16] Early studies demonstrated the possibility of hydrogen production through direct water decomposition by using MIECMs at the extremely high temperature of 1400–1800 °C.[17–20] However, the hydrogen production rate was relatively low because of

the poor oxygen permeability of these membranes, and only a modest rate of $0.6\ cm^3 min^{-1} cm^{-2}$ could be obtained at 1683 °C.[19] To obtain a higher hydrogen production rate, one possible way is to increase the rate of oxygen removal. Balachandran et al. fed hydrogen on the permeation side of a MIECM to consume the permeated oxygen.[21,22] In this case, a high oxygen partial pressure gradient across the membrane was established and a maximum hydrogen production rate of $10.0\ cm^3 min^{-1} cm^{-2}$ at 900 °C was obtained.[21,22] However, the amount of hydrogen produced was equivalent to the amount consumed, which makes it unpractical. Therefore, it would be attractive for both the feed and permeate stream to yield a valuable compound.

Herein, for the first time we report the simultaneous production of hydrogen and synthesis gas in a hollow-fiber perovskite MIECM reactor using methane to consume the permeated oxygen (see Figure 1). At high temperatures,
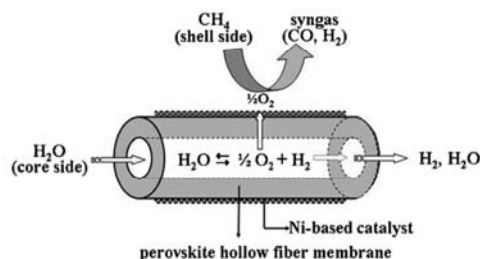
Figure 1. The concept of simultaneous production of hydrogen and synthesis gas by combining water splitting with POM in a perovskite oxygen-permeable hollow-fiber membrane.

water dissociates into hydrogen and oxygen on the membrane surface of the core side. Oxygen permeates from the core to the shell side of the hollow fiber, where it is consumed by the partial oxidation of methane (POM) to form synthesis gas according to $CH_4 + \tfrac{1}{2}O_2 \rightarrow CO + 2H_2$. Thus, when operating under equilibrium-controlled conditions, the water dissociation proceeds continuously as the oxygen is continuously consumed by the POM to produce synthesis gas. The advantage of this process is to give pure hydrogen as well as synthesis gas, which can be used to synthesize a wide variety of valuable hydrocarbons (for example, by Fischer–Tropsch synthesis) and oxygenates (methanol).

A novel $BaCo_xFe_yZr_{1-x-y}O_{3-\delta}$ (BCFZ) perovskite hollow-fiber membrane was applied for the in situ removal of the oxygen that is produced by high-temperature water splitting,

[*] Prof. Dr. H. Wang
School of Chemistry & Chemical Engineering
South China University of Technology
Wushan Road, Guangzhou 510640 (P.R. China)
Fax: (+86) 20-87110131
E-mail: hhwang@scut.edu.cn
H. Jiang, Prof. Dr. J. Caro
Institute of Physical Chemistry and Electrochemistry, Leibniz University of Hanover (Germany)
Dr. S. Werth
Uhde GmbH, Dortmund (Germany)
Dr. T. Schiestel
Fraunhofer Institute of Interfacial Engineering and Biotechnology (IGB), Stuttgart (Germany)

Communications

because it exhibits a high oxygen permeation rate[23–25] and has already been used, for example, in the production of oxygen-enriched air[26,27] and the partial oxidation of hydrocarbons.[28,29] Figure 2 shows the influence of temperature on
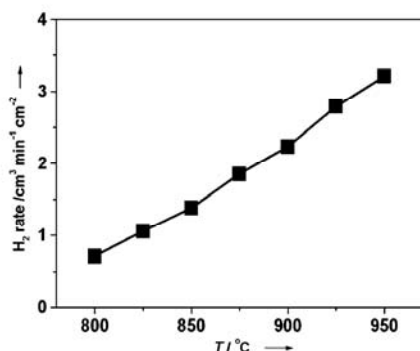
Figure 2. H_2 production rate on the core side as a function of temperature. Core side: flow rate $F_{H_2O}=30$ and $F_{He}=10$ cm³ min⁻¹; shell side: 50 cm³ min⁻¹ ($F_{He}=45$, $F_{Ne}=3$, and $F_{CH_4}=2$ cm³ min⁻¹). Amount of packed Ni/Al₂O₃ catalyst: 0.8 g. Effective membrane area: 0.86 cm².

the hydrogen production rate. This rate increases as the temperature rises from 800 to 950°C and a hydrogen flux of 3.1 cm³ min⁻¹ cm⁻² was obtained at 950°C. It was also found that the hydrogen production rate is very low (< 0.026 cm³ min⁻¹ cm⁻² at 900°C, see Figure S1 in the Supporting Information) if a sweep gas, such as He, is used on the permeate side.

Clearly, the hydrogen production rate depends directly on the rate of oxygen removal from the water dissociation system. The oxygen transport can be described by the Wagner equation for the oxygen flux $j(O_2)$ [Eq. (2)],[30,31] where σ_{el} and σ_{ion} are the electronic and ionic conductivities, respectively, F the Faraday constant, and $\nabla\mu_{O_2}$ the gradient of the chemical potential of oxygen across the membrane. Assuming that $\sigma_{el} \gg \sigma_{ion}$ and that $\partial\ln a_{O_2}/\partial x$ can be approximated by $\ln(p'_{O_2}/p''_{O_2})/L$ with p'_{O_2} and p''_{O_2} denoting the oxygen partial pressures on the shell and core sides and L the membrane thickness, the Wagner equation reads [Eq. (3)]:

$$j(O_2) = -\frac{1}{(4F)^2}\frac{\sigma_{el}\,\sigma_{ion}}{\sigma_{el}+\sigma_{ion}}\nabla\mu_{O_2} \quad \text{with} \quad \nabla\mu_{O_2} = \frac{\partial R\,T\ln a_{O_2}}{\partial x} \quad (2)$$

$$j(O_2) = -\frac{R\,T}{(4F)^2}\sigma_{ion}\frac{\ln(p'_{O_2}/p''_{O_2})}{L} \quad (3)$$

The oxygen partial pressure p'_{O_2} on the permeate side can be reduced much more efficiently when feeding methane in combination with a Ni-based catalyst (Süd Chemie AG) to the shell side. The permeated oxygen on the shell side is then consumed very quickly by the oxidation of methane. As a result of the increased oxygen partial pressure gradient across the membrane, a higher hydrogen production rate of about 2.3 cm³ min⁻¹ cm⁻² at 900°C is obtained, which is two orders of

magnitude higher than the rate of a nonreactive sweep gas such as He.

From the above discussion it follows that the hydrogen production rate is related to three reactions: water splitting, oxygen transport through the membrane, and POM. When the temperature is increased, the equilibrium constant of the endothermic water splitting will increase according to the Van't Hoff equation. So the equilibrium is shifted towards water dissociation and more hydrogen can be produced. Moreover, with increasing temperature, both the rate of the POM and the permeability of the BCFZ hollow-fiber membrane will increase. Thus, the hydrogen production rate becomes higher with increasing temperature.

With increasing concentration of steam in the feed gas on the core side, the equilibrium partial pressures of oxygen and hydrogen will increase, thus providing a higher driving force for oxygen permeation. As a result, the amount of hydrogen obtained is expected to increase. As shown in Figure 3, the
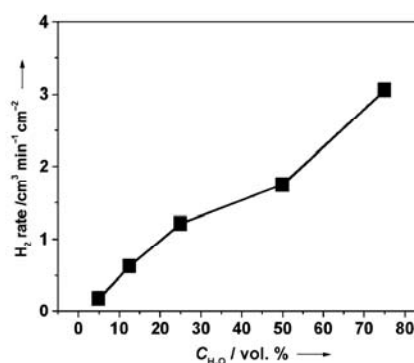

Figure 3. H_2 production rate on the core side at different steam concentrations. Core side (steam + He): 40 cm³ min⁻¹; shell side: 50 cm³ min⁻¹ ($F_{He}=45$, $F_{Ne}=3$, and $F_{CH_4}=2$ cm³ min⁻¹). Amount of packed Ni/Al₂O₃ catalyst: 0.8 g. Effective membrane area: 0.86 cm². $T=950°C$.

hydrogen production rate increased from about 0.2 to 3.1 cm³ min⁻¹ cm⁻² when the steam concentration was changed from 5 to 75 vol.%. In addition, the hydrogen production rate can be enhanced by increasing the methane concentration (Figure 4), because a higher oxygen partial pressure gradient across the perovskite membrane is established, which leads to a higher oxygen permeation rate.

At the same time as hydrogen is produced on the core side of the BCFZ hollow fiber by water dissociation, synthesis gas can be produced on the shell side. Figure 5 shows the methane conversion and the CO selectivity for feeding different methane concentrations. When the amount of the feed gas methane was small, most of the methane was totally oxidized to give CO₂ and H₂O. On feeding more methane, the methane conversion decreased gradually and the CO selectivity increased. When 2 cm³ min⁻¹ methane diluted by 48 cm³ min⁻¹ inert gases was fed to the shell side, about 70% methane conversion and 60% CO selectivity were obtained. However, for high methane concentrations the calculated selectivities became lower again. This is probably
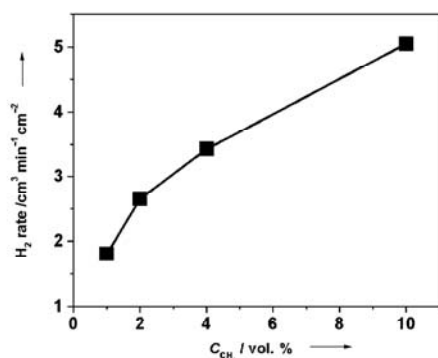
Figure 4. H₂ production rate on the core side at different methane concentrations. Core side: $F_{H_2O} = 30$ and $F_{He} = 10$ cm³min⁻¹; shell side: 50 cm³min⁻¹ ($F_{Ne} = 3$ and $F_{CH_4} + F_{He} = 47$ cm³min⁻¹). Amount of packed Ni/Al₂O₃ catalyst: 0.8 g. Effective membrane area: 0.86 cm². $T = 950$°C.
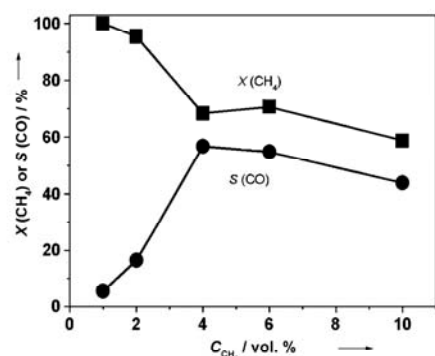
Figure 5. Conversion X of methane and selectivity S of CO on the shell side at different methane concentrations. Core side: $F_{H_2O} = 30$ and $F_{He} = 10$ cm³min⁻¹; shell side: 50 cm³min⁻¹ ($F_{Ne} = 3$ and $F_{CH_4} + F_{He} = 47$ cm³min⁻¹). Amount of packed Ni/Al₂O₃ catalyst: 0.8 g. Effective membrane area: 0.86 cm². $T = 950$°C.

caused by the formation of coke, which is expected to occur under these reaction conditions.

The net reaction in our concept is conventional methane steam reforming according to $H_2O + CH_4 \rightarrow 3H_2 + CO$ with a H₂/CO ratio of 3, which is unsuitable for the methanol or Fischer–Tropsch syntheses. However, in our process we obtain pure hydrogen on the core side as well as synthesis gas with a H₂/CO ratio of around 2 on the shell side. Synthesis gas with such a ratio is usually produced by oxygen-blown autothermal reforming, which requires a costly oxygen separation plant. Therefore, our concept provides a new way to obtain a Fischer–Tropsch synthesis gas. Furthermore, the pure hydrogen produced by our method can be used to operate the hydrocracking step in the product refinery section of the Fischer–Tropsch plant.

Hydrogen can also be produced with a hydrogen-selective membrane reactor in which methane steam reforming takes place with a reforming catalyst. The technology of steam reforming with hydrogen-selective Pd membranes has been developed since 1992 by Mitsubishi Heavy Industries and Tokyo Gas. The membrane reactor operates at 550°C and produces 40 m³ (STP) hydrogen h⁻¹.[32] However, the Pd/Pd alloy membrane can be poisoned by CO; therefore, a subsequent water-gas shift stage is needed to convert CO to CO₂, which makes the operation more complex. On the other hand, in the hydrogen-selective membrane reactor, only H₂ rather than synthesis gas can be obtained. In our concept, we can get both pure hydrogen, with an industrially interesting flux (ca. 3 m³h⁻¹m⁻²) without further water-gas shift reaction, and synthesis gas. Compared to conventional steam reforming and hydrogen-selective membrane-reactor-based steam reforming, our multifunctional reactor contributes to the concept of process intensification.

In conclusion, it is possible to produce significant amounts of hydrogen from water splitting at around 900°C by using a novel BCFZ oxygen-permeable hollow-fiber membrane. By combining high-temperature water splitting with POM, not only hydrogen but also synthesis gas can be obtained. This process presents new insight into the interplay of catalysis and separation in a membrane reactor. Besides, abundant raw materials, such as water and methane (natural gas), were used, which is of broad interest.

Experimental Section

The dense BCFZ perovskite hollow-fiber membranes were manufactured by phase-inversion spinning followed by sintering.[23–29] The sintered fiber had a wall thickness of around 0.17 mm with an outer diameter of 1.10 mm and an inner diameter of 0.76 mm. Figure S2 in the Supporting Information shows a schematic diagram of the membrane reactor used in this study. Two ends of the hollow fiber were coated with Au paste. After sintering at 950°C, a dense Au film that was not permeable to oxygen was obtained. Such an Au-coated hollow fiber was sealed by a silicon rubber ring and the uncoated part (3.0 cm), which was permeable to oxygen, was kept in the middle of the oven thus ensuring isothermal conditions. A mixture of steam and He was fed to the core side and a mixture of CH₄, Ne, and He was fed to the shell side. A Ni-based catalyst (Süd Chemie AG) was packed around and behind the hollow-fiber membrane. The CH₄, He, and Ne flow rates were controlled by gas mass-flow controllers (Bronkhorst). The H₂O flow was controlled by a liquid mass-flow controller (Bronkhorst) and completely evaporated at 180°C before it was fed to the reactor. All gas lines to the reactor and the gas chromatograph were heated to 180°C. The concentrations of the gases at the exit of the reactor were determined by an online gas chromatograph (Agilent 6890). Assuming that the oxygen from water splitting on the core side was totally removed and the flow rate at the outlet was equal to that at the inlet, the H₂ production rate after steam condensation in the retentate on the core side was calculated from the total flow rate F_{core} (cm³min⁻¹), the hydrogen concentration $c(H_2)$, and the effective membrane area S (cm²) based on Equation (4).

$$J(H_2) = \frac{F_{core}\, c(H_2)}{S} \tag{4}$$

The CH₄ conversion $X(CH_4)$ and the CO selectivity $S(CO)$ on the shell side were calculated as Equations (5) and (6), where $F(i)$ is the

$$X(CH_4) = \left(1 - \frac{F(CH_4,\text{out})}{F(CH_4,\text{in})}\right) \times 100\% \tag{5}$$

43

Communications

$$S(CO) = \frac{F(CO,out)}{F(CH_4,in) - F(CH_4,out)} \times 100\% \tag{6}$$

flow rate of species i on the shell side, calculated based on the measured concentration of the respective species and the total flow rate measured by a bubble flowmeter.

[1] J. A. Turner, *Science* **2004**, *305*, 972–974.
[2] O. Khaselev, J. A. Turner, *Science* **1998**, *280*, 425–427.
[3] C. Srinivasan, *Curr. Sci.* **2006**, *90*, 756–757.
[4] D. Lu, T. Takata, N. Saito, Y. Inoue, K. Domen, *Nature* **2006**, *440*, 295–297.
[5] O. Coskuner, E. A. A. Jarvis, T. C. Allison, *Angew. Chem.* **2007**, *119*, 7999–8001; *Angew. Chem. Int. Ed.* **2007**, *46*, 7853–7855.
[6] Y. Tamaura, R. Uehara, N. Hasegawa, H. Kaneko, H. Aoki, *Solid State Ionics* **2004**, *172*, 121–124.
[7] H. Ishihara, N. Hasegawa, H. Aoki, H. Kaneko, A. Suzuki, Y. Tamaura, *Solid State Ionics* **2004**, *172*, 117–119.
[8] P. Ritterskamp, A. Kuklya, M.-A. Wüstkamp, K. Kerpen, C. Weidenthaler, M. Demuth, *Angew. Chem.* **2007**, *119*, 7917–7921; *Angew. Chem. Int. Ed.* **2007**, *46*, 7770–7774.
[9] H. Aoki, H. Kaneko, N. Hasegawa, H. Ishihara, A. Suzuki, Y. Tamaura, *Solid State Ionics* **2004**, *172*, 113–116.
[10] X. Wu, K. Onuki, *Tsinghua Sci. Technol.* **2005**, *10*, 270–276.
[11] S. Ihara, *Bull. Electrotech. Lab.* **1977**, *41*, 259–280.
[12] R. Hartung, H.-H. Möbius, *Chem. Ing. Tech.* **1968**, *40*, 592–600.
[13] Y. T. Liu, X. Y. Tan, K. Li, *Catal. Rev. Sci. Eng.* **2006**, *48*, 145–198.
[14] J. Pére-Ramirez, B. Vigeland, *Angew. Chem.* **2005**, *117*, 1136–1139; *Angew. Chem. Int. Ed.* **2005**, *44*, 1112–1116.
[15] Z. P. Shao, W. S. Yang, Y. Cong, H. Dong, J. H. Tong, G. X. Xiong, *J. Membr. Sci.* **2000**, *172*, 177–188.
[16] C. Chen, S. J. Feng, S. Ran, D. C. Zhu, W. Liu, H. J. M. Bouwmeester, *Angew. Chem.* **2003**, *115*, 5354–5356; *Angew. Chem. Int. Ed.* **2003**, *42*, 5196–5198A.
[17] B. Cales, J. F. Baumard, *High Temp. High Pressures* **1982**, *14*, 681.
[18] J. Lede, F. Lapicque, J. Villermaux, B. Cales, A. Ounalli, J. F. Baumard, A. M. Anthony, *Int. J. Hydrogen Energy* **1982**, *7*, 939–950.
[19] H. Naito, H. Arashi, *Solid State Ionics* **1995**, *79*, 366–370.
[20] Y. Nigara, K. Watanabe, K. Kawamura, J. Mizusaki, M. Ishigame, *J. Electrochem. Soc.* **1997**, *144*, 1050–1055.
[21] U. Balachandran, T. H. Lee, S. Wang, S. E. Dorris, *Int. J. Hydrogen Energy* **2004**, *29*, 291–296.
[22] U. Balachandran, T. H. Lee, S. E. Dorris, *Int. J. Hydrogen Energy* **2007**, *32*, 451–456.
[23] T. Schiestel, M. Kilgus, S. Peter, K. J. Caspary, H. H. Wang, J. Caro, *J. Membr. Sci.* **2005**, *258*, 1–4.
[24] H. H. Wang, P. Kölsch, T. Schiestel, C. Tablet, S. Werth, J. Caro, *J. Membr. Sci.* **2006**, *284*, 5–8.
[25] H. H. Wang, T. Schiestel, C. Tablet, M. Schroeder, J. Caro, *Solid State Ionics* **2006**, *177*, 2255–2259.
[26] H. H. Wang, S. Werth, T. Schiestel, J. Caro, *Angew. Chem.* **2005**, *117*, 7066–7069; *Angew. Chem. Int. Ed.* **2005**, *44*, 6906–6909.
[27] C. Hamel, A. Seidel-Morgenstern, T. Schiestel, S. Werth, H. H. Wang, C. Tablet, J. Caro, *AIChE J.* **2006**, *52*, 3118–3125.
[28] H. H. Wang, C. Tablet, T. Schiestel, S. Werth, J. Caro, *Catal. Commun.* **2006**, *7*, 907–912.
[29] J. Caro, K. J. Caspary, C. Hamel, B. Hoting, P. Kölsch, B. Langanke, K. Nassauer, T. Schiestel, A. Schmidt, R. Schomäcker, A. Seidel-Morgenstern, E. Tsotsas, I. Voigt, H. H. Wang, R. Warsitz, S. Werth, A. Wolf, *Ind. Eng. Chem. Res.* **2007**, *46*, 2286–2294.
[30] M. Schroeder, *Phys. Chem. Chem. Phys.* **2005**, *7*, 166–172.
[31] R. Merkle, J. Maier, H. J. M. Bouwmeester, *Angew. Chem.* **2004**, *116*, 5179–5183; *Angew. Chem. Int. Ed.* **2004**, *43*, 5069–5073.
[32] R. Dittmeyer, J. Caro in *Handbook of Heterogeneous Catalysis*, Vol. 4 (Eds.: G. Ertl, H. Knözinger, F. Schüth, J. Weitkamp), Wiley-VCH, Weinheim, **2008**, p. 2221.

44

Supporting Information for

Simultaneous production of hydrogen and synthesis gas by combining water splitting with partial oxidation of methane in a hollow fiber membrane reactor[**]

Heqing Jiang[a], Haihui Wang[a,b*]，Steffen Werth[c], Thomas Schiestel[d], Jürgen Caro[a]

[a]*Institute of Physical Chemistry and Electrochemistry, Leibniz University of Hannover, Callinstr. 3-3A, D-30167 Hannover, Germany*

[b] *College of Chemistry and Chemical Engineering, South China University of Technology, Guangzhou, 510640, PR China*

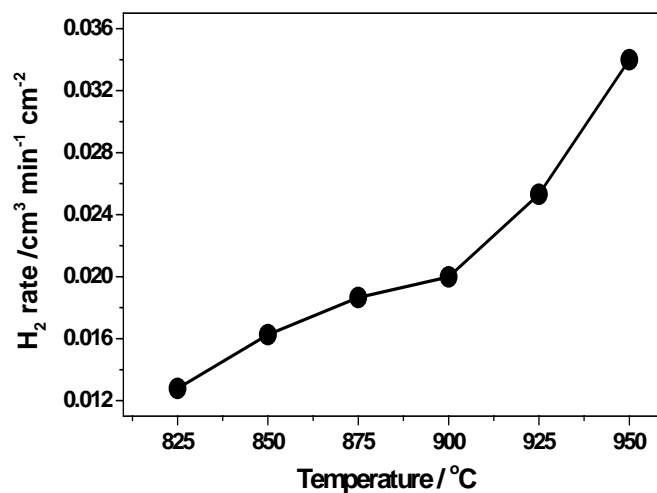[c]*Uhde GmbH, Friedrich-Uhde-Str. 15, D-44141 Dortmund, Germany*

[d]*Fraunhofer Institute of Interfacial Engineering and Biotechnology (IGB), Nobelstr 12, D-70569 Stuttgart, Germany*

[*] Corresponding author.
E-mail address: hhwang@scut.edu.cn or Haihui.Wang@pci.uni-hannover.de

Figure S1 Hydrogen flux as a function of temperature during water splitting using BCFZ hollow fiber membrane. Core side: F_{H2O} = 20 cm^3 min^{-1}; Shell side: F_{He} = 20 cm^3 min^{-1}.

Helium was used as a sweep gas and the resulting hydrogen fluxes were found to be two orders of magnitude smaller than those obtained using methane as the sweep gas with Ni-based catalyst.
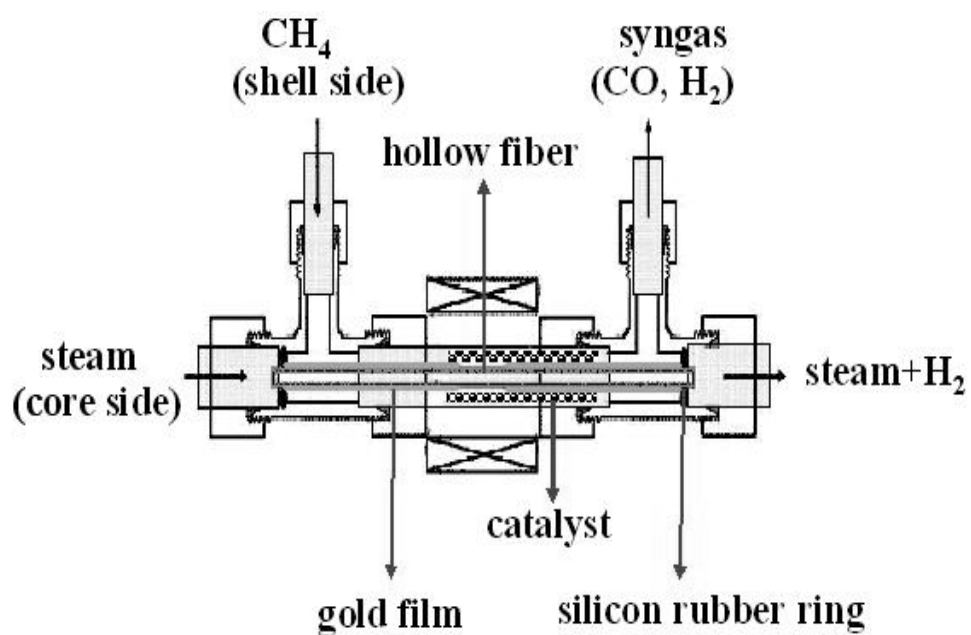
Figure S2 The schematic diagram of the experimental apparatus for hydrogen and synthesis gas production by combining water splitting with POM processes.
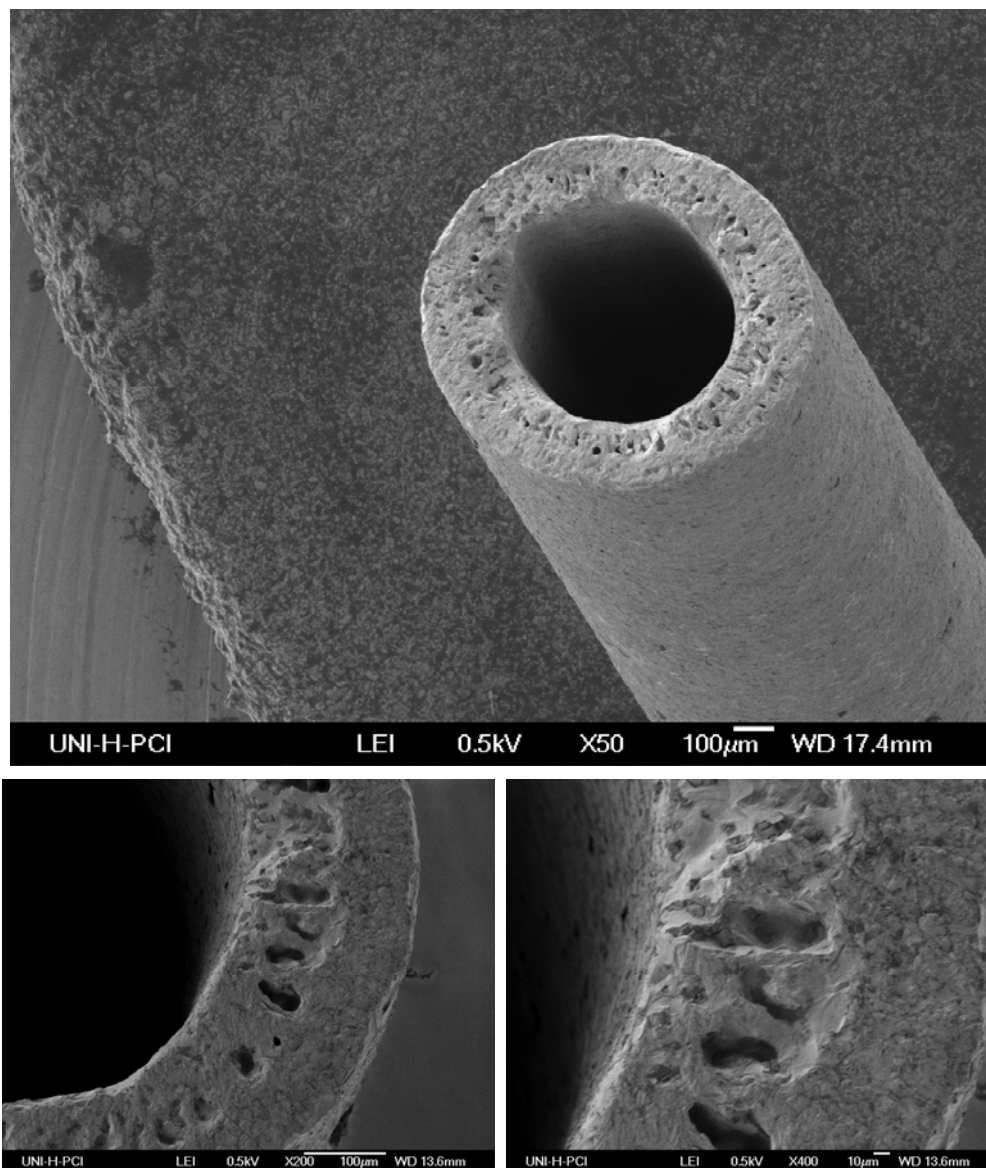
Figure S3 SEM pictures of the cross section of the fresh hollow fiber membranes Our BCFZ hollow fiber membranes exhibit an asymmetric structure with a porous layer of around 100 μm and a thin dense layer of only 50 -100 μm, which reduces the resistance to the oxygen bulk permeation. Furthermore, the porous layer facilitates the oxygen surface exchange due to its large surface area. Both effects lead to higher oxygen fluxes of our perovskite hollow fiber membrane.
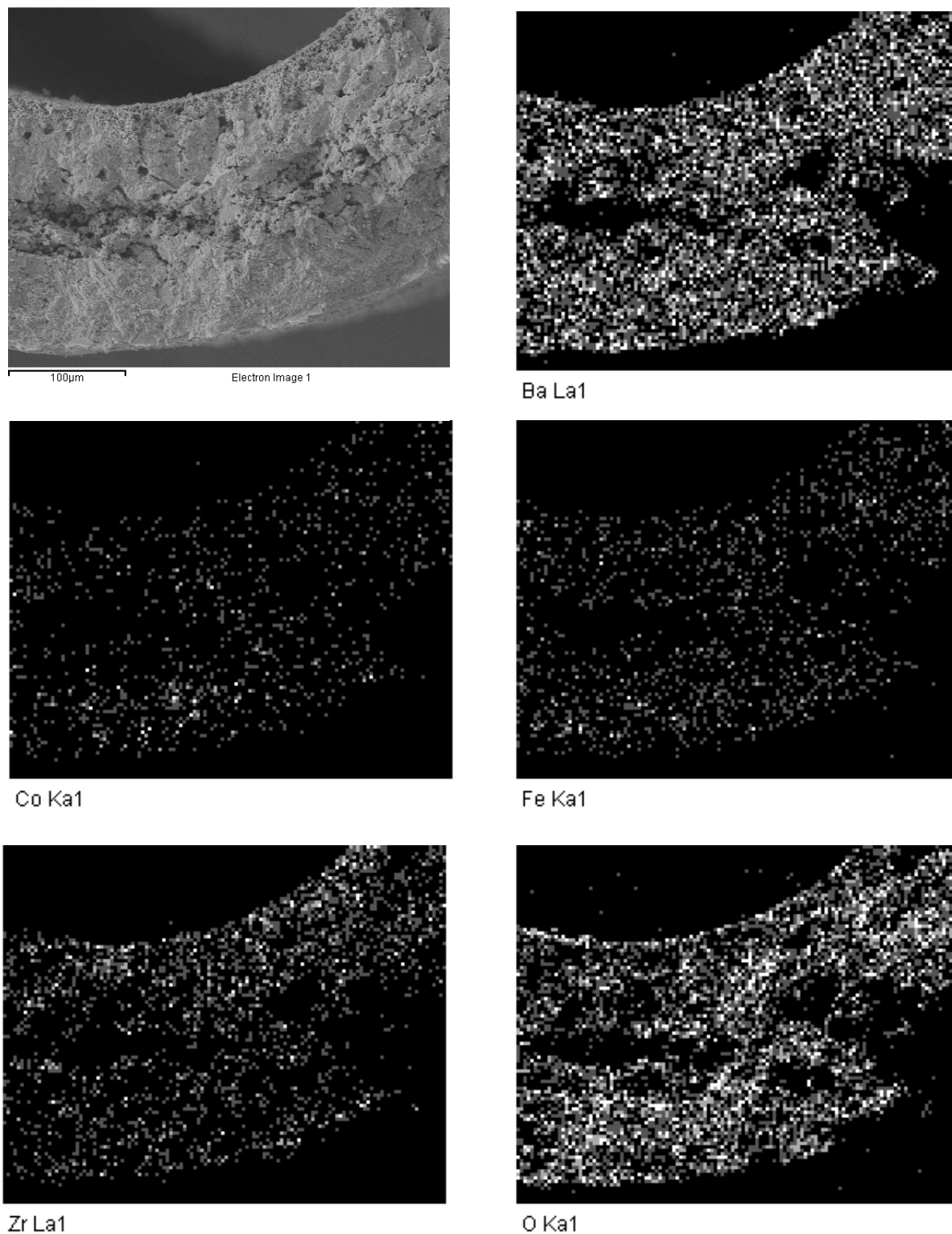
Figure S4 SEM-EDX element maps for the spent fiber. Only Fe, Co, Zr, Ba and O were found in the EDX spectrum. No significant elements segregation was observed on the both membrane surfaces and the bulk by quantitatively analyzing the element maps.

2.4 A coupling strategy to produce hydrogen and ethylene in a membrane reactor

Heqing Jiang, Zhengwen Cao, Steffen Schirrmeister, Thomas Schiestel, and Jürgen Caro
Angew. Chem. Int. Ed. **2010**, **revised.**

Membrane Reactor

A coupling strategy to produce hydrogen and ethylene in a membrane reactor**

Heqing Jiang,* Zhengwen Cao, Steffen Schirrmeister, Thomas Schiestel, and Jürgen Caro*

Following the concept of process intensification,[1,2] the effective coupling of two chemical reactions in one apparatus is gaining increasing interest from both academia and industry.[3-5] In the past years, most of theses studies have focused on the combination of an endothermic dehydrogenation with an exothermic hydrogenation of hydrocarbons in a Pd membrane reactor.[6,7] This coupled dehydrogenation/hydrogenation is also studied in fixed bed reactors, e.g. the simultaneous ethylbenzene dehydrogenation and benzene hydrogenation.[8] Recently, Kondratenko et al. reported the production of ethylene with the simultaneous almost 100 % removal of nitrous oxide (N_2O) by coupling the N_2O decomposition with the thermal dehydrogenation of ethane in a catalytic fixed bed reactor.[9] However, by the coupling of the two reactions in the fixed bed reactor, a subsequent procedure is necessary to separate the products. If the reactions are conducted in a membrane reactor, the products will be kept separated on the two sides of the membrane. Therefore, it looks attractive to search for new pairs of industrially interesting reactions in membrane reactors.

Hydrogen production from water splitting has attracted much attention in the past decades because hydrogen is considered as a promising alternative to fossil fuels.[10,11] One technique to enhance the hydrogen production rate from the equilibrium-limited water splitting is the in situ removal of the simultaneously produced oxygen using a mixed oxygen ion and electron conducting membrane.[12-16] Previous studies had shown that an operating
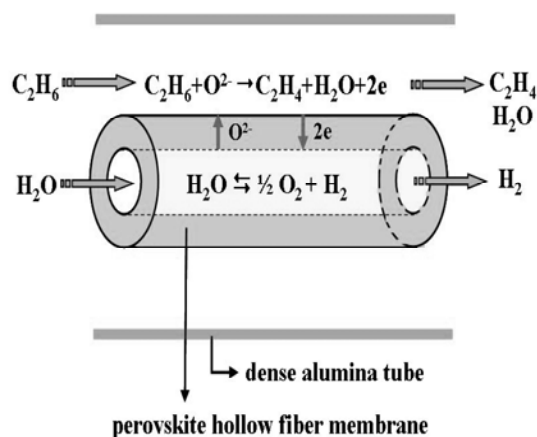
Figure 1. Schematic diagram of coupling water splitting with ethane dehydrogenation in a perovskite oxygen-permeable membrane reactor.
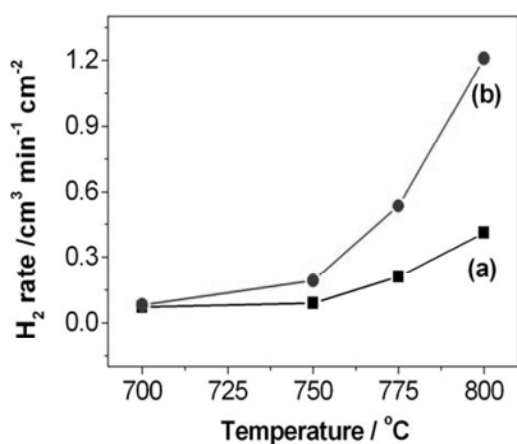
[*]   H. Jiang, Z. Cao, Prof. Dr. J. Caro
        Institute of Physical Chemistry and Electrochemistry
        Leibniz University of Hannover
        Callinstr. 3A, D-30167 Hannover, Germany
        Fax: (+49)-511-76219121
        E-mail: heqing.jiang@pci.uni-hannover.de and
        juergen.caro@pci.uni-hannover.de

        Dr. S. Schirrmeister
        Uhde GmbH
        Friedrich-Uhde-Str. 15, D-44141 Dortmund (Germany)

        Dr. T. Schiestel
        Fraunhofer Institute of Interfacial Engineering and
        Biotechnology (IGB)
        Nobelstr. 12, D-70569 Stuttgart, Germany

Supporting information for this article is available on the WWW under http://www.angewandte.org or from the author.

temperature of 1683 °C was necessary to obtain a hydrogen production rate of 0.6 cm^3 min^{-1} cm^{-2} in a mixed-conducting ZrO_2-TiO_2-Y_2O_3 membrane.[17] In order to lower the operating temperature, Balachandran et al. coupled water splitting with hydrogen combustion as a model reaction in a ceramic-metal membrane reactor, by feeding hydrogen to the permeate side to consume the permeated oxygen.[18] A maximum hydrogen production rate of 10.0 cm^3 min^{-1} cm^{-2} was obtained at 900 °C as a proof of principle. Since in this model reaction the amount of hydrogen produced was equivalent to the hydrogen amount consumed, we were looking for practice-relevant coupled reactions in membrane reactors. Recently, we reported the coupling of water splitting with partial oxidation of methane for the simultaneous production of hydrogen and synthesis gas (a mixture of CO and H_2) at temperatures between 850 to 950 °C in a perovskite $BaCo_xFe_yZr_{1-x-y}O_{3-\delta}$ (BCFZ) hollow fiber membrane reactor.[19] The BCFZ hollow fiber membrane shows a high oxygen permeation rate and has been used for the production of oxygen-enriched air and abatement of nitrogen oxides.[20-22]

In this contribution, we combine water splitting and ethane oxi-dehydrogenation in the BCFZ oxygen-permeable membrane reactor at moderate temperatures (700 to 800 °C). Figure 1 shows the concept of water splitting coupled with the oxi-dehydrogenation of ethane in the perovskite hollow fiber membrane reactor. First, water dissociates into hydrogen and oxygen on the core side of the perovskite BCFZ membrane. The produced oxygen is then removed as oxygen ion (O^{2-}) to the ethane side of the membrane, where it is consumed to convert ethane to ethylene according to $C_2H_6 + O^{2-} \rightarrow C_2H_4 + H_2O + 2e$. Local charge neutrality is maintained by the

1

Figure 2. H_2 production rate on the core side as a function of temperature. Core side: F_{H2O} = 30 cm^3 min^{-1} and F_{He} = 10 cm^3 min^{-1}; shell side: F_{total} = 40 cm^3 min^{-1} with an ethane concentration of (a) 7.5 % and (b) 20 %, respectively.

Figure 3. The 100 h operation for the H_2 production on the core side and the simultaneous ethylene production on the shell side at 800 °C. Core side: F_{H2O} = 30 cm^3 min^{-1} and F_{He} = 10 cm^3 min^{-1}; shell side: 40 cm^3 min^{-1} (F_{C2H6} = 3 cm^3 min^{-1}, F_{He} = 36 cm^3 min^{-1} and F_{Ne} = 1 cm^3 min^{-1}).
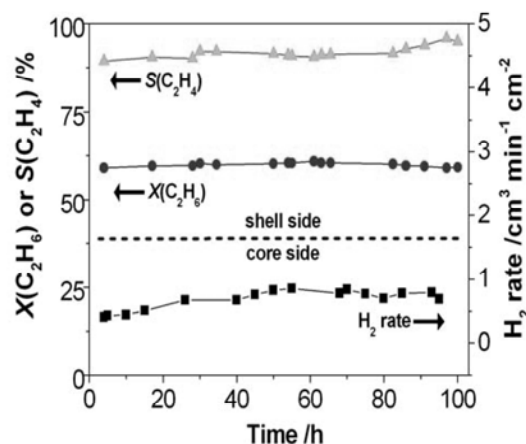
counter diffusion of electrons. Thus, the produced oxygen can be continuously removed via the BCFZ membrane, and more hydrogen from water splitting can be produced even under equilibium-controlled conditions. Simultaneously, ethylene can be obtained after steam condensation on the shell side of the membrane. The advantage of this coupling strategy is that the produced hydrogen from water splitting and the ethylene from ethane oxi-dehydrogenation are inherently separated in the membrane reactor.

It was experimentally found that the hydrogen production rate from water splitting on the core side is very low (< 0.025 cm^3 min^{-1} cm^{-2}) at temperatures below 950 °C if only the inert sweep gas He was applied on the shell side of the BCFZ hollow fiber membrane to reduce the oxygen partial pressure.[19] However, significant amounts of hydrogen were obtained on the steam side even at moderate temperatures (700-800 °C) when coupling the water dissociation with the ethane oxi-dehydrogenation. As shown in Figure 2a, by feeding 7.5 vol% C_2H_6 to the shell side, the hydrogen production rate from water splitting increases from 0.1 to 0.4 cm^3 min^{-1} cm^{-2} when the temperature rises from 700 to 800 °C. With rising the temperature, the equilibrium of the endothermic water splitting is shifted towards oxygen and hydrogen as products. Moreover, the oxygen permeation rate of BCFZ membrane increased with increasing temperature according to Wagner theory.[23,24] The fast

removal of the produced oxygen from water splitting causes further water to dissociate and thus the equilibrium constraint for the hydrogen production is overcome.
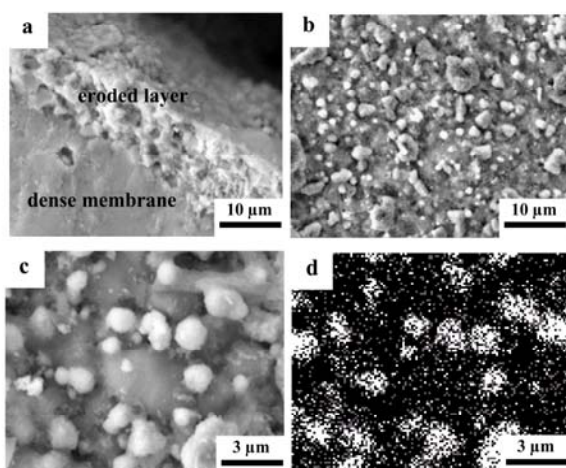
Besides operating temperature and membrane thickness, according to Wagner theory,[23,24] the oxygen permeation rate is related to the oxygen partial pressure gradient across the membrane. By feeding more ethane to the shell side of the BCFZ membrane, a larger driving force was provided for the fast removal of oxygen from the steam side, thus increasing the hydrogen production rate. Figure 2 presents the temperature dependence of the hydrogen production rate when feeding 7.5 vol% and 20 vol% ethane to the shell side, respectively. Compared to the case (a) of feeding 7.5 vol% ethane to consume the permeated oxygen, the hydrogen production rate in the case (b) of feeding 20 vol% ethane on the shell side is always higher at all temperatures investigated. It can be seen from Figure 2b that the hydrogen production rate reaches 1.2 cm^3 min^{-1} cm^{-2} at 800 °C.

The permeated oxygen from water splitting can be utilized for the oxidative dehydrogenation of ethane (ODE) to ethylene on the shell side of the membrane. As shown in Table 1, the ethane conversion increased from 6 % to 59 % and the ethylene selectivity increased from 67 % to 89 % when rising the temperature from 700 to 800 °C. At 700 °C, only a very small amount of hydrogen is detected on the shell side (< 0.15 % H_2), indicating that the ODE process ($C_2H_6 + O^{2-} \rightarrow C_2H_4 + H_2O + 2e$) is dominating compared with the thermal dehydrogenation of ethane (TDE: $C_2H_6 \leftrightarrows C_2H_4 + H_2$). Because only traces of CO_x were detected and the permeated oxygen mainly reacted with hydrogen forming water, the amount of water produced on the shell side can be estimated based on the difference of flow rates between H_2 and C_2H_4 at exit. The rate of water produced on the shell side is 0.06 cm^3 min^{-1} cm^{-2} at 700 °C and 0.5 cm^{-3} min^{-1} cm^{-2} at 800 °C, which is almost equal to that of water consumed on the core side. At 800 °C, the TDE process cannot be neglected, and it occurs parallel to the ODE process.[25-27] Consequently, ethylene, hydrogen, water, and non-reacted ethane were present on the shell side, and the ethylene yield is around 55 % at 800 °C. As a reference experiment, the dehydrogenation of ethane in the presence of water was also investigated in a fixed-bed reactor

Table 1 Ethane conversion $X(C_2H_6)$ and ethylene selectivity $S(C_2H_4)$ on the shell side of BCFZ membrane at different temperatures.

Temperature /°C	$X(C_2H_6)$ /%	$S(C_2H_4)$ /%
700	6	67
750	20	89
775	37	88
800	59	89

Core side: 40 cm^3 min^{-1} (F_{H2O} = 30 cm^3 min^{-1} and F_{He} = 10 cm^3 min^{-1}). Shell side: 40 cm^3 min^{-1} (F_{C2H6} = 3 cm^3 min^{-1}, F_{He} = 36 cm^3 min^{-1} and F_{Ne} = 1 cm^3 min^{-1}).

2

filled with BCFZ perovskite. At 800 °C, an ethylene yield of 47 % was obtained with the ethylene selectivity of 71 % in the fixed-bed reactor (see Table S1 in the Supporting Information). Obviously, more ethylene was obtained based on the coupling strategy in BCFZ membrane reactor.

Figure 3 presents the simultaneous production of hydrogen and ethylene in the BCFZ hollow fiber membrane reactor as a function of time. During a period of 100 h, about 60 % ethane conversion and 90 % ethylene selectivity were obtained. Simultaneously, the hydrogen production rate on the steam side reaches 0.8 cm^3 min^{-1} cm^{-2}. It is should be pointed out that the BCFZ hollow fiber membrane is still gas-tight after 100 h when we had to stop the test. SEM was used to characterize the spent hollow fiber. Although the membrane surface was eroded on the ethane side, there is no development of crack in the middle dense part of the membrane. Different to the reported layered porous membranes,[28,29] the BCFZ dense membrane only allows the transport of oxygen ions with infinite selectivity and therefore, there is no permeation of other gases incl. water through the membrane.[13,22] Figure 4a shows the cross section of the spent BCFZ hollow fiber with an about 10 μm eroded layer on the membrane surface exposed to ethane side. Small particles of 0.2-1.0 μm were well dispersed on the membrane surface (Figure 4b and 4c). EDXS (Figure 4d) indicates that the small particles are mainly composed of cobalt oxide. The cobalt extraction by reduction of cobalt cations from the perovskite resulting in cobalt-enriched surface particles has been reported previously.[30] Here, due to the reducing atmosphere, cobalt cations of the perovskite BCFZ lattice might be partly reduced, leading to the formation of the surface eroded layer with the thickness of about 10 μm.

Hydrogen can also be produced from water by electrolysis or photo-catalysis.[31-33] Water electrolysis is commercially available today for small-scale hydrogen production. The main obstacle in commercial exploitation of this technology for large-scale hydrogen production is the high cost of electricity and the noble metal catalysts.[31,32] The main feature of the photo-electrolysis and photo-catalytic process is the use of solar energy. Current research efforts involve overcoming the low efficiency and the unsatisfactory stability.[32,33] Compared to the water splitting by electrolysis or photo-catalysis, the direct thermal hydrogen production would require heating water above 2500 °C to obtain appreciable yields, which is a difficult temperature to reach and maintain from the materials perspective. By coupling water splitting with the ODE process on the two opposite sides of the BCFZ oxygen-permeable membrane reactor, the equilibrium constraint of water splitting was overcome and the operating temperature to obtain a hydrogen production rate of around 1.0 cm^3 min^{-1} cm^{-2} was lowered to 800 °C. Simultaneously, the permeated oxygen from water splitting can be utilized to convert ethane to ethylene on the other side of the membrane. It should be pointed out that the membrane-based hydrogen production from water splitting is still in its early stage and more laboratory efforts should be given to improve the properties and membrane stability in the near future.

In conclusion, we demonstrate a novel coupling strategy to produce hydrogen and ethylene in a BCFZ hollow fiber membrane reactor. By coupling water splitting and ethane oxi-dehydrogenation on the opposite sides of the oxygen-permeable membrane, not only a hydrogen production rate of around 1.0 cm^3 min^{-1} cm^{-2} was achieved at 800 °C, but also an ethylene yield of around 55 % was obtained on the other side of the membrane. To the best of our knowledge, this is the first report on the coupling of water splitting and ethane dehydrogenation in a membrane reactor. Compared to the reported coupling strategy in the fixed-bed reactor,[8,9] the hydrogen from water splitting and the ethylene from ethane oxi-dehydrogenation together with non-reacted ethane and hydrogen as the main products are inherently separated based on the coupling strategy in the membrane reactor.

Experimental Section

The dense BCFZ hollow fiber membranes were fabricated by phase inversion spinning followed by sintering.[34] The sintered fiber had a wall thickness of around 0.17 mm with an outer diameter of 1.10 mm and an inner diameter of 0.76 mm. In order to obtain the isothermal condition, two ends of the above fiber were coated by Au paste followed by sintering at 950 °C and thus a dense Au film that is not permeable to oxygen was obtained. Here, the length of the uncoated middle part is 3 cm, and the effective membrane area is 0.86 cm^2. The measurements were carried out in a high-temperature reactor as described in our previous work.[19-21] Figure S1 in the Supporting Information shows a schematic diagram of the membrane reactor used in this work. The Au-coated hollow fiber was sealed by silicon rubber ring and the uncoated part which is permeable to the oxygen was kept in the middle of the oven. H_2O diluted by He was fed to the core side and a mixture of C_2H_6, Ne and He was fed to the shell side. C_2H_6, He and Ne flow rates were controlled by gas mass flow controllers (Bronkhorst). H_2O flow rate was controlled by the liquid mass flow controller (Bronkhorst) and was completely evaporated at 180 °C before it was fed to the reactor. All gas lines to the reactor and the gas chromatograph were heated to 180 °C. The concentrations of the gases at the exit of the reactor were determined by an on-line gas chromatograph (Agilent 6890). Assuming that the oxygen from water splitting on the core side was totally removed and the flow rate at the outlet is equal to that at the inlet, and H_2 production rate on the core side was calculated from the total flow rate F_{core} (cm^3 min^{-1}), the hydrogen concentration $c(H_2)$, and the effective membrane area S (cm^2) based on the following equation:

$$J(H_2) = \frac{F_{core} \times c(H_2)}{S}$$

The C_2H_6 conversion $X(C_2H_6)$ and the C_2H_4 selectivity $S(C_2H_4)$ were calculated as:

$$X(C_2H_6) = \left(1 - \frac{F(C_2H_6, out)}{F(C_2H_6, in)}\right) \times 100\%$$

Figure 4. SEM images of the ethane side of the BCFZ hollow fiber membrane after measurement. (a) Cross section, (b) and (c) top views, and (d) the corresponding elemental distribution image of cobalt.

3

$$S(C_2H_4) = \frac{F(C_2H_4, out)}{F(C_2H_6, in) - F(C_2H_6, out)} \times 100\%$$

where F(i) is the flow rate of species i on the shell of the hollow fiber membrane.

The surface morphology of the spent fiber was characterized using a field-emission Scanning Electron Microscopy (SEM) of the type JEOL JSM-6700F. An Energy Dispersive X-ray (EDX) spectrometer of the type Oxford Instruments INCA-300 was used for the elemental analysis.

[1] S. A. Bhat, J. Sadhukhan, *AIChE Journal* **2009**, *55*, 408 – 422.

[2] J. Pére-Ramirez, B. Vigeland, *Angew. Chem.* **2005**, *117*, 1136 – 1139; *Angew. Chem. Int. Ed.* **2005**, *44*, 1112 – 1116.

[3] V. R. Choudhary, B. S. Uphade, S. A. R. Mulla, *Angew. Chem.* **1995**, *107*, 721 – 723; *Angew. Chem. Int. Ed.* **1995**, *34*, 665 – 666.

[4] R. C. Ramaswamy, P. A. Ramachandran, M. P. Dudukovic, *Chem. Eng. Sci.* **2008**, *63*, 1654 – 1667.

[5] J. H. Blank, J. Beckers, P. E. Collignon, F. Clerc, G. Rothenberg, *Chem. Eur. J.* **2007**, *13*, 5121 – 5128.

[6] T. M. Moustafa, S. S. E. H. Elnashaie, *J. Membr. Sci.* **2000**, *178*, 171 – 184.

[7] M. H. Khademi, A. Jahanmiri, M. R. Rahimpour, *Int. J. Hydrog. Energy* **2009**, *34*, 5091 – 5107.

[8] M. E. E. Abashar, *Chem. Eng. Proc.* **2004**, *43*, 1195 – 1202.

[9] E. V. Kondratenko, O. Ovsitser, *Angew. Chem.* **2008**, *120*, 3271 – 3273; *Angew. Chem. Int. Ed.*, **2008**, *47*, 3227.

[10] D. Lu, T. Takata, N. Saito, Y. Inoue, K. Domen, *Nature* **2006**, *440*, 295 – 297.

[11] O. Coskuner, E. A. A. Jarvis, T. C. Allison, *Angew. Chem.* **2007**, *119*, 7999 – 8001; *Angew. Chem. Int. Ed.* **2007**, *46*, 7853 – 7855.

[12] H. H. Wang, Z. Cong, W. S. Yang, *Chem. Commun.* **2002**, 1468 – 1469.

[13] J. Sunarso, S. Baumann, J. M. Serra, W. A. Meulenberg, S. Liu, Y. S. Lin, J. D. Costa, *J. Membr. Sci.* **2008**, *320*, 13 – 41.

[14] Y. T. Liu, X. Y. Tan, K. Li, *Catal. Rev -Sci. Eng.* **2006**, *48*, 145 – 198.

[15] C. Chen, S. J. Feng, S. Ran, D. C. Zhu, W. Liu, H. J. M. Bouwmeester, *Angew. Chem.* **2003**, *115*, 5354 – 5356; *Angew. Chem. Int. Ed.* **2003**, *42*, 5196 – 5198.

[16] J. Caro, K.J. Caspary, C. Hamel, B. Hoting, P. Kölsch, B. Langanke, K. Nassauer, T. Schiestel, A. Schmidt, R. Schomäcker, A. Seidel-Morgenstern, E. Tsotsas, I. Voigt, H.H. Wang, R. Warsitz, S. Werth, A. Wolf, *Ind. Eng. Chem. Res.* **2007**, *46*, 2286 – 2294.

[17] H. Naito, H. Arashi, *Solid State Ionics* **1995**, *79*, 366 – 370.

[18] U. Balachandran, T.H. Lee, S.E. Dorris, *Int. J. Hydrog. Energy* **2007**, *32*, 451 – 456.

[19] H. Q. Jiang, H. H. Wang, S. Werth, T. Schiestel, J. Caro, *Angew. Chem.* **2008**, *120*, 9481 – 9484; *Angew. Chem. Int. Ed.* **2008**, *47*, 9341 – 9344.

[20] H. Q. Jiang, L. Xing, O. Czuprat, H. H. Wang, S.Schirrmeister, T. Schiestel, J. Caro, *Chem. Commun.* **2009**, 6738 – 6740.

[21] H. Q. Jiang, H. H. Wang, F. Y. Liang, S. Werth, T. Schiestel, J. Caro, *Angew. Chem.* **2009**, *121*, 3027 – 3030; *Angew. Chem. Int. Ed.* **2009**, *48*, 2983 – 2986.

[22] H. H. Wang, S. Werth, T. Schiestel, J. Caro, *Angew. Chem.* **2005**, *117*, 7066 – 7069; *Angew. Chem. Int. Ed.*, **2005**, *44*, 6906 – 6909.

[23] M. Schroeder, *Phys. Chem. Chem. Phys.* **2005**, *7*, 166 – 172.

[24] R. Merkle, J. Maier, H. J. M. Bouwmeester, *Angew. Chem.* **2004**, *116*, 5179 – 5183; *Angew. Chem. Int. Ed.* **2004**, *43*, 5069 – 5073.

[25] S. Gaab, M. Machli, J. Find, R. K. Grasselli, J. A. Lercher, *Topics in Catal.* **2003**, *23*, 151 – 158.

[26] F. Cavani, N. Ballarini, A. Cericola, *Catal. Today* **2007**, *127*, 113 – 131.

[27] O. Czuprat, S. Werth, S. Schirrmeister, T Schiestel, J. Caro, *ChemCatChem* **2009**, *1*, 401 – 405

[28] A. V. Gaikwad, V. Boffa, J. E. ten Elshof, G. Rothenberg, *Angew. Chem.* **2008**, *120*, 5487 – 5490; *Angew. Chem. Int. Ed.* **2008**, *47*, 5407 – 5410.

[29] R. Kreiter, M. D. A. Rietkerk, H. L. Castricum, H. M. van Veen, J. E. ten Elshof, J. F. Vente, *ChemSusChem* **2009**, *2*, 158 – 160.

[30] L. Bedel, A. C. Roger, C. Estournes, A. F. Sammels, *Catal. Today* **2003**, *85*, 207 – 218.

[31] M. C. Petri, B. Yildiz, A. E. Klickman, *Int. J. Nuclear Hydrogen Production and Application* **2006**, *1*, 79 – 91.

[32] J. D. Holladay, J. Hu, D. L. King, Y. Wang, *Catal. Today* **2009**, *139*, 244 – 260.

[33] R. M. Navarro, M. C. Sánchez-Sánchez, M. C. Alvarez-Galvan, F. del Valle, J. L. G. Fierro, *Energy Environ. Sci.* **2009**, *2*, 35 – 34

[34] T. Schiestel, M. Kilgus, S. Peter, K. J. Caspary, H. H. Wang, J. Caro, *J. Membr. Sci.* **2005**, *258*, 1 – 4.

4

Supporting Information for

A coupling strategy to produce hydrogen and ethylene in a membrane reactor[**]

Heqing Jiang[*a], Zhengwen Cao[a], Steffen Schirrmeister[b], Thomas Schiestel[c], and Jürgen Caro[*a]

[a]*Institute of Physical Chemistry and Electrochemistry, Leibniz University of Hannover, Callinstr. 3A, D-30167 Hannover, Germany*

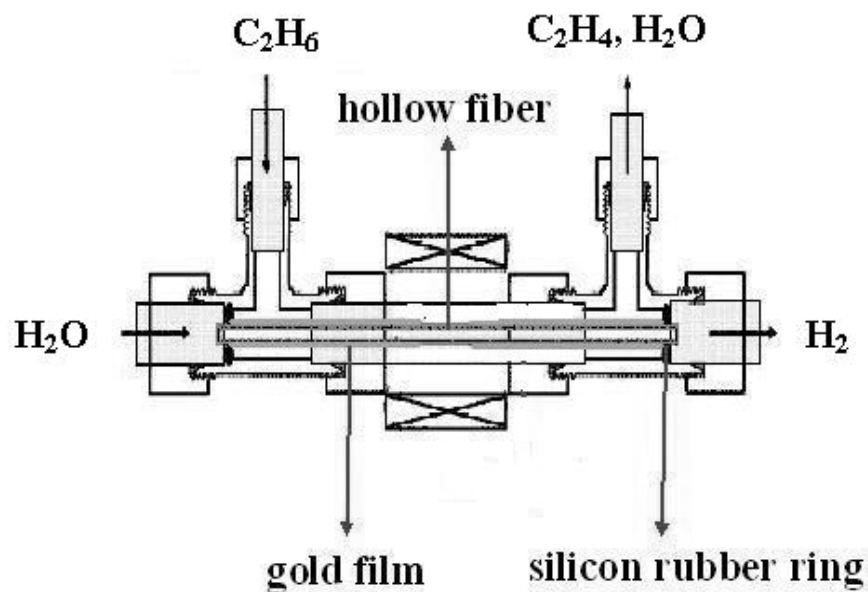[b]*Uhde GmbH, Friedrich-Uhde-Str. 15, D-44141 Dortmund, Germany*

[c]*Fraunhofer Institute of Interfacial Engineering and Biotechnology (IGB), Nobelstr 12, D-70569 Stuttgart, Germany*

Figure S1 Schematic diagram of the membrane reactor used in this work

Table S1 Ethane conversion $X(C_2H_6)$ and ethylene selectivity $S(C_2H_4)$ at different temperatures in presence of water in a fixed-bed reactor filled with the perovskite BCFZ.

Temperature /°C	$X(C_2H_6)$ /%	$S(C_2H_4)$ /%
700	14	24
750	30	59
775	47	69
800	66	71

Conditions: F_{C2H6} = 3 cm^3 min^{-1}, F_{H2O} = 6 cm^3 min^{-1}, F_{He} = 30 cm^3 min^{-1}, and F_{Ne} = 1 cm^3 min^{-1}.

Chapter 3

Kinetic coupling for nitrogen oxides decomposition

3.1 Summary

It was found that the decomposition of NO or N_2O over perovskite BCFZ is inhibited by oxygen. In this chapter, the effective NO and N_2O decomposition was demonstrated by in situ removing the inhibitor oxygen via the BCFZ hollow fiber membrane.

The first article presents the NO decomposition coupled with the POM on the opposite sides of the BCFZ hollow fiber membrane. It was found that NO conversion on the core side is below 5 % when no sweep gas was applied on the shell side. However, when feeding methane in combination with Ni-based catalyst to the shell side, the direct decomposition of NO over the inner surface of the BCFZ hollow fiber membrane was achieved with NO conversion of almost 100 % and N_2 yield of around 95 % even with coexisting 3 % oxygen in the feed.

The second article demonstrates the N_2O decomposition coupled with the POM to synthesis gas in the BCFZ oxygen-permeable membrane reactor. By in situ removing the inhibitor oxygen, N_2O with concentration of up to 50 % was completely treated at 875 °C. Moreover, this system can tolerate the coexistence of 15 % oxygen in the feed. Simultaneously, the permeated oxygen was utilized to produce synthesis gas on the shell side. A methane conversion of over 90 % and a CO selectivity of 90 % were obtained at 875 °C with the simultaneous complete conversion of N_2O in the coexistence of 5 % O_2 in the feed.

In the third article, the effect of oxygen permeability of the BCFZ hollow fiber membrane on the reactor performance for water splitting and N_2O decomposition are discussed, and much attention was given to the effect of oxygen partial pressure of the N_2O side on the N_2O decomposition. It was found that the oxygen partial pressure on the N_2O side can be decreased by increasing the operating temperature or the pressure difference across the membrane, or by feeding reducing gases like methane or ethane on permeate side. By removing the oxygen via the BCFZ membrane, the oxygen partial pressure on N_2O side was kept at a very low lever, and a complete conversion of N_2O was obtained. Moreover, the permeated oxygen was used to produce synthesis gas by the POM or ethylene by the dehydrogenation of ethane on the shell side. An ethane conversion of 85 % and an ethylene selectivity of 86 % were obtained at 850 °C.

3.2 Highly effective NO decomposition by in situ removal of inhibitor oxygen using an oxygen transporting membrane

Heqing Jiang, Lei Xing, Oliver Czuprat, Haihui Wang, Steffen Schirrmeister, Thomas Schiestel, and Jürgen Caro

Highly effective NO decomposition by *in situ* removal of inhibitor oxygen using an oxygen transporting membrane†

Heqing Jiang,[a] Lei Xing,[a] Oliver Czuprat,[a] Haihui Wang,*[ab] Steffen Schirrmeister,[c] Thomas Schiestel[d] and Jürgen Caro*[a]

Due to the *in situ* removal of the inhibitor oxygen using an oxygen transporting membrane, a complete conversion of NO to N_2 was achieved for the first time in a catalytic perovskite membrane reactor.

Nitrogen oxides (NO_x, $x = 1, 2$), which are mainly produced by automobiles and stationary power plants, are among the major atmospheric pollutants. Several methods have been employed to reduce NO emission, such as non-selective catalytic reduction (NSCR), selective catalytic reduction (SCR) with NH_3 or hydrocarbon, and direct catalytic decomposition of NO.[1–3] Considering the costs, however, the direct catalytic decomposition of NO into molecular N_2 and O_2, which is thermodynamically favored at temperatures up to about 1000 °C,[4] looks more promising. Several catalysts such as perovskite-type oxides,[5] Cu-ZSM-5 zeolites,[6] metal-doped Co_3O_4[7] and Pd/Al_2O_3[8] have been exploited for the direct decomposition of NO. Among them, perovskite-type oxides show special potential for use as catalysts for NO decomposition, because they become active above 500 °C and are sustainable for long-term operation at the higher temperatures required for NO decomposition.[9,10] However, NO decomposition over perovskites is strongly inhibited by the produced oxygen, leading to a lower NO conversion. For example, Iwakuni *et al.* investigated the catalytic activities of $BaMnO_3$-based perovskites towards NO decomposition, and found that the highest N_2 yield was achieved on $Ba_{0.8}La_{0.2}Mn_{0.8}Mg_{0.2}O_3$ and the N_2 yield was decreased from 75% to 60% by the coexistence of 1% O_2 at 850 °C.[10]

Dense perovskite membranes with mixed oxygen ion and electron conductivity have attracted increasing attention due to their potential applications in the separation of oxygen from air, conversion of natural gas to synthesis gas and selective oxidation of light hydrocarbons.[11] Recently, we

developed a novel $BaCo_xFe_yZr_{1-x-y}O_{3-\delta}$ (BCFZ) perovskite hollow fiber membrane and exploited its applications in the production of oxygen-enriched air or as the membrane reactor for N_2O abatement and water dissociation.[12] In this contribution, the decomposition of NO is investigated in the BCFZ membrane reactor. A complete NO conversion with around 95% N_2 yield was achieved in this reactor due to the *in situ* removal of the inhibitor oxygen *via* the BCFZ oxygen-permeable membrane. The computer simulation of the NO decomposition in a membrane reactor[13a] and the electrochemical removal of NO using a solid electrolyte membrane reactor[13b,c] have been reported previously. However, to our knowledge, there is no experimental study of NO decomposition with such high NO conversion and N_2 yield in perovskite membrane reactors reported up to now.

Fig. 1 shows the concept of NO decomposition in the BCFZ perovskite hollow fiber membrane reactor. First, the adsorbed NO is catalytically decomposed on the surface of the BCFZ membrane into N_2 and surface oxygen (O*) based on the reaction:[14,15]

$$NO \rightarrow \tfrac{1}{2} N_2 + O^*$$
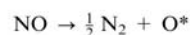
Then, the surface O* is removed as oxygen ions (O^{2-}) *via* the perovskite oxygen transporting membrane, and local charge neutrality is maintained by the counter diffusion of electrons (e^-). Thus, the surface oxygen (O*) can be continuously removed *via* the BCFZ membrane once it is generated from NO decomposition, which will result in not only a kinetic acceleration of NO decomposition, but also in the prevention of NO_2 formation.
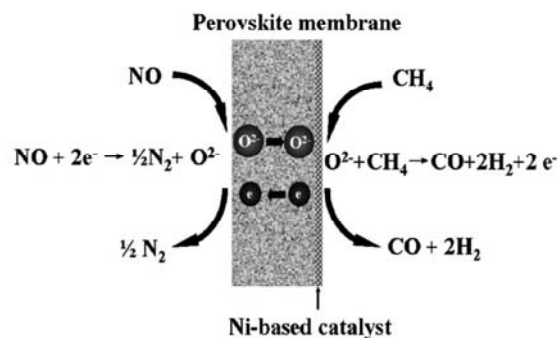
[a] *Institute of Physical Chemistry and Electrochemistry, Leibniz University of Hannover, Callinstr. 3-3A, D-30167 Hannover, Germany. E-mail: juergen.caro@pci.uni-hannover.de; Fax: +49-511-76219121; Tel: +49-511-7623175*
[b] *College of Chemistry and Chemical Engineering, South China University of Technology, Guangzhou, 510640, PR China. E-mail: hhwang@scut.edu.cn; Fax: +86-20-87110131; Tel: +86-20-87110131*
[c] *Uhde GmbH, Friedrich-Uhde-Str. 15, D-44141 Dortmund, Germany*
[d] *Fraunhofer Institute of Interfacial Engineering and Biotechnology (IGB), Nobelstr. 12, D-70569 Stuttgart, Germany*
† Electronic supplementary information (ESI) available: Fig. S1 Schematic diagram of the membrane reactor used in this work. See DOI: 10.1039/b912269a

Fig. 1 Schematic diagram of NO decomposition with *in situ* removal of oxygen *via* perovskite membrane.

Table 1 shows the NO conversion with and without oxygen removal at different temperatures in a BCFZ membrane reactor.‡ When NO was fed to the core side of the BCFZ hollow fiber, it was catalytically decomposed into N_2 and surface O*.[14,15] In the case that no sweep gas was applied on the shell side, the driving force for oxygen transport was found to be very low, the surface O* on the core side could not be removed, and the catalytically active sites for NO decomposition on the membrane surface were blocked by the surface O* which led to the inhibition of the NO decomposition. As shown in Table 1(a), NO conversion without oxygen removal is below 5%. If methane was fed to the shell side, the surface O* from the NO side could be removed *in situ* by oxygen transport to the shell side where oxygen was quickly consumed by methane oxidation. Thus, the reaction rate of NO decomposition was accelerated and a higher NO conversion could be achieved. It can be seen from Table 1(b) that the conversion of NO decomposition was significantly enhanced compared to the case without oxygen removal in Table 1(a). Clearly, the NO conversion in the membrane reactor directly depends on the rate of oxygen removal from the NO side. According to the Wagner equation,[11,12] the oxygen permeation rate increases with increasing temperature. At relatively low temperature (<875 °C), NO conversion is limited by oxygen mobility and NO cannot be completely converted due to the low oxygen mobility. However, for temperatures ≥ 875 °C, NO is already completely decomposed, as shown in Table 1(b). Moreover, the undesired consecutive reaction of NO oxidation to NO_2 was prevented since the surface oxygen generated by the NO decomposition was effectively drained off through the BCFZ membrane before it could be desorbed and form NO_2 in a homogeneous gas phase reaction. Consequently, the selectivity of N_2 reached almost 100%. Hwang *et al.* used an electro-chemically driven membrane reactor to abate NO, but only 70% NO conversion at a current density of 230 mA/cm^2 was obtained.[13b] Obviously, the BCFZ membrane reactor used in this work gave higher NO conversion and N_2 selectivity compared to refs. 13 and 16.

However, industrial off-gases to be de-NO_x-ed often contain O_2. Simulating this O_2 content, an additional amount of O_2 was added to the NO as co-feed on the core side. One could expect that NO_2 will be quickly formed. However, in our case, both NO and NO_2 decompose into N_2 and O_2 at high temperature, and the produced O_2 can be removed *in situ* by the BCFZ membrane. Table 2 shows the variation of NO conversion and N_2 selectivity with the additional oxygen concentration in the NO/O_2 co-feed gas. It can be seen that a complete conversion of NO is always achieved for oxygen

Table 2 NO conversion and N_2 selectivity for the case that the NO feed gas contains different amounts of oxygen at 875 °C

$C(O_2)$ in the NO/O_2 co-feed gas/vol.%	X(NO)/%	$S(N_2)$/%
0	100	91
2	100	99
3	100	95
5	87	100

Core side: 30 cm^3 min^{-1} (F_{NO} = 1.5 cm^3 min^{-1}, F_{O_2} = 0.6–1.5 cm^3 min^{-1}, F_{Ne} = 1 cm^3 min^{-1}, F_{He} = balance). Shell side: 50 cm^3 min^{-1} (F_{CH_4} = 8 cm^3 min^{-1}, F_{He} = 37 cm^3 min^{-1} and F_{H_2O} = 5 cm^3 min^{-1}). 0.5 g Ni-based catalyst packed on shell side.

concentrations up to 3 vol% in the co-feed gas. However, under our experimental conditions a concentration above 5% will lead to a decrease of the NO conversion, which might be caused by the competitive adsorption of the co-fed oxygen and NO. It was also found that there is no oxygen in the off-gas of the core side, indicating that both the additional oxygen and the oxygen from the NO decomposition were completely removed by the BCFZ membrane. The N_2 selectivity of NO decomposition in this experiment was found to be around 95%, revealing that the removal of oxygen can suppress the undesired NO_2 formation.

Fig. 2 shows the influence of NO concentration in the feed gas on the NO conversion and N_2 selectivity at 875 °C. It can be seen that NO conversion is reduced from 100% to 50% for increasing NO concentrations in the feed gas from 5% to 20%. Moreover, the N_2 selectivity of the NO decomposition decreased from 97% to 69%. With increasing NO concentration, more surface O* will form, and the membrane cannot completely remove these high O* concentrations, which will block the NO decomposition and lead to a decrease of NO conversion. Also, some of the surface O* will desorb as O_2 that reacts homogeneously with NO to form NO_2, leading to a decrease of the N_2 selectivity. It should be pointed out that the NO concentration in practice-relevant off-gases is usually below 1%. For such conditions we could demonstrate in the membrane-supported NO decomposition that not only a NO conversion of 100% can be achieved, but also the formation of NO_2 can be prevented.

In this work, methane was fed to the shell side to consume the permeated oxygen from the NO side. When the catalyst NiO/Al_2O_3 was packed around the BCFZ fiber on the shell side, synthesis gas (a mixture of CO and H_2) can be formed according to $CH_4 + \frac{1}{2}O_2 \rightarrow CO + 2H_2$. From synthesis gas, Fischer Tropsch products (diesel) or methanol as transportable fuels can be produced. Fig. 3 presents the variation of CH_4 conversion and CO selectivity with rising temperatures. It can

Table 1 Conversion of NO at different temperatures without and with oxygen removal using methane as oxygen consuming sweep gas

Temperature/°C	(a): X(NO)/% without O_2 removal	(b): X(NO)/% with O_2 removal
800	1	29
850	1	60
875	1	100
900	3	100
925	3	100

Core side: 30 cm^3 min^{-1} (F_{NO} = 3 cm^3 min^{-1}, F_{Ne} = 1 cm^3 min^{-1}, F_{He} = 26 cm^3 min^{-1}). Shell side: (a) no sweep gas applied, and (b) methane as oxygen consuming sweep gas, 50 cm^3 min^{-1} (F_{CH_4} = 8 cm^3 min^{-1}, F_{He} = 37 cm^3 min^{-1} and F_{H_2O} = 5 cm^3 min^{-1}). 0.5 g Ni-based catalyst packed on shell side.
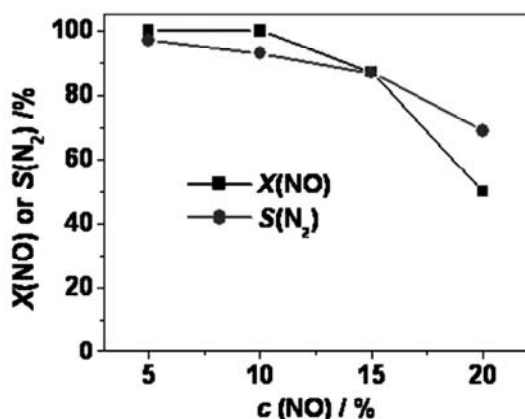
Fig. 2 Influence of the NO concentration in the fed gases on the NO conversion and N_2 selectivity at 875 °C. Core side: 30 cm^3 min^{-1} ($F_{NO} = 1.5$–6 cm^3 min^{-1}, $F_{Ne} = 1$ cm^3 min^{-1}, $F_{He} =$ balance). Shell side: 50 cm^3 min^{-1} ($F_{CH_4} = 8$ cm^3 min^{-1}, $F_{He} = 37$ cm^3 min^{-1} and $F_{H_2O} = 5$ cm^3 min^{-1}). 0.5 g Ni-based catalyst packed on shell side.

be seen that both methane conversion and CO selectivity gradually increased with increasing temperature. A methane conversion of 93% and CO selectivity of 80% were obtained at 900 °C.

In conclusion, we demonstrate a novel membrane-based route for NO decomposition, which can overcome the inhibition by oxygen. By *in situ* removal of the inhibitor oxygen, the direct decomposition of NO over the inner surface of the BCFZ hollow fiber membrane was achieved with NO conversion of almost 100% and N_2 yield of around 95% even with coexisting 3% O_2 in the feed. To the best of our knowledge, this is the first report on the direct decomposition with such high NO conversion and N_2 yield.
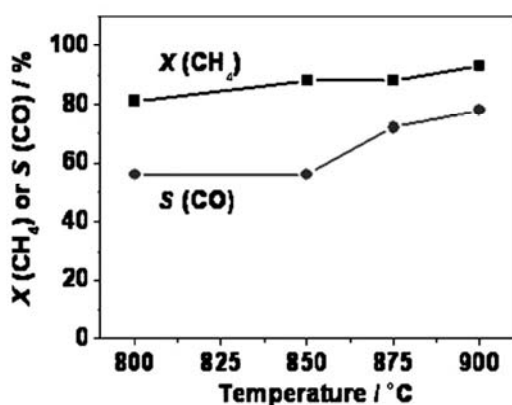
Fig. 3 CH$_4$ conversion and CO selectivity on shell side as a function of temperature. Core side: 30 cm^3 min^{-1} ($F_{NO} = 3$ cm^3 min^{-1}, $F_{He} = 27$ cm^3 min^{-1}). Shell side: 50 cm^3 min^{-1} ($F_{CH_4} = 8$ cm^3 min^{-1}, $F_{H_2O} = 5$ cm^3 min^{-1}, $F_{Ne} = 1$ cm^3 min^{-1}, and $F_{He} = 36$ cm^3 min^{-1}). 0.5 g Ni-based catalyst packed on shell side.

Notes and references

‡ **Experimental:** The dense BCFZ hollow fiber membranes were manufactured by phase inversion spinning followed by sintering.[17] A BCFZ porous layer was deposited onto the outer surface of the central 3 cm of the hollow fiber membrane to improve the catalytic activity towards methane oxidation. In order to obtain the isothermal condition, two ends of the above fiber were coated with Au paste followed by sintering at 950 °C and thus a dense Au film that is not permeable to oxygen was obtained. NO decomposition experiments were carried out in a high-temperature reactor as described in our previous work.[12] Fig. S1 in the Supporting Information shows a schematic diagram of the membrane reactor used in this work.† NO diluted by He was fed to the core side and a mixture of CH$_4$, steam and He was fed to the shell side. The commercial NiO/Al$_2$O$_3$ steam reforming catalyst G-90 with a grain size of 0.3–0.5 mm was applied as a packed bed on the shell side of the hollow fiber membrane. The concentrations of the gases at the exit of the reactor were determined with an on-line gas chromatograph (Agilent 6890).

1 (*a*) Y. Nishihata, J. Mizuki, T. Akao, H. Tanaka, M. Uenishi, M. Kimura, T. Okamoto and N. Hamada, *Nature*, 2002, **418**, 164; (*b*) R. M. Heck, *Catal. Today*, 1999, **53**, 519; (*c*) P. Sazama and B. Wichterlova, *Chem. Commun.*, 2005, 4810.
2 (*a*) S. Brandenberger, O. Kröcher, A. Tissler and R. Althoff, *Catal. Rev. Sci. Eng.*, 2008, **50**, 492; (*b*) R. Burch, *Catal. Rev. Sci. Eng.*, 2004, **46**, 271.
3 (*a*) J. Perez-Ramirez, J. M. Garcia-Cortes, F. Kapteijn, G. Mul, J. A. Moulijn and C. S. M. de Lecca, *Appl. Catal., B*, 2001, **29**, 285; (*b*) E. V. Kondratenko, V. A. Kondratenko, M. Richter and R. Fricke, *J. Catal.*, 2006, **239**, 23; (*c*) G. Centi and G. E. Arena, *J. Mol. Catal. A: Chem.*, 2003, **204–205**, 663.
4 M. Shelef, *Chem. Rev.*, 1995, **95**, 209.
5 C. Tofan, D. Klvana and J. Kirchnerova, *Appl. Catal., A*, 2002, **223**, 275.
6 (*a*) G. Moretti, G. Ferraris, G. Fierro, M. L. Jacono, S. Morpurgo and M. Faticanti, *J. Catal.*, 2005, **232**, 476; (*b*) M. V. Konduru and S. S. Chuang, *J. Phys. Chem. B*, 1999, **103**, 5802; (*c*) M. H. Groothaert, K. Lievens, H. Leeman, B. M. Weckhuysen and R. A. Schoonheydt, *J. Catal.*, 2003, **220**, 500.
7 M. Haneda, G. Tsuboi, Y. Nagao, Y. Kintaichi and H. Hamada, *Catal. Lett.*, 2004, **97**, 145.
8 M. Haneda, Y. Kintaichi, I. Nakamura, T. Fujitani and H. Hamada, *Chem. Commun.*, 2002, 2816.
9 N. Imanaka, T. Masui and H. Masaki, *Adv. Mater.*, 2007, **19**, 3660.
10 H. Iwakuni, Y. Shinmyou, H. Yano, H. Matsumoto and T. Ishihara, *Appl. Catal., B*, 2007, **74**, 299.
11 (*a*) W. S. Yang, H. H. Wang, X. F. Zhu and L. W. Lin, *Top. Catal.*, 2005, **35**, 155; (*b*) J. Sunarso, S. Baumann, J. M. Serra, W. A. Meulenberg, S. Liu, Y. S. Lin and J. D. Costa, *J. Membr. Sci.*, 2008, **320**, 13; (*c*) Y. T. Liu, X. Y. Tan and K. Li, *Catal. Rev. Sci. Eng.*, 2006, **48**, 145; (*d*) C. Chen, S. J. Feng, S. Ran, D. C. Zhu, W. Liu and H. J. M. Bouwmeester, *Angew. Chem.*, 2003, **115**, 5354.
12 (*a*) H. Q. Jiang, H. H. Wang, S. Werth, T. Schiestel and J. Caro, *Angew. Chem., Int. Ed.*, 2008, **47**, 9341; (*b*) H. H. Wang, C. Tablet, T. Schiestel, S. Werth and J. Caro, *Catal. Commun.*, 2006, **7**, 907; (*c*) H. H. Wang, S. Werth, T. Schiestel and J. Caro, *Angew. Chem., Int. Ed.*, 2005, **44**, 6906; (*d*) H. Q. Jiang, H. H. Wang, F. Y. Liang, S. Werth, T. Schiestel and J. Caro, *Angew. Chem., Int. Ed.*, 2009, **48**, 2983.
13 (*a*) G. Dixon, W. R. Moser and Y. H. Ma, *Ind. Eng. Chem. Res.*, 1994, **33**, 3015; (*b*) H. J. Hwang, J. Moon and M. Awano, *J. Eur. Ceram. Soc.*, 2004, **24**, 1325; (*c*) H. J. Hwang, J. Moon and J. Moon, *J. Am. Ceram. Soc.*, 2005, **88**, 79.
14 R. Burch, *Top. Catal.*, 2003, **24**, 97.
15 R. Burch, P. J. Millington and A. P. Walker, *Appl. Catal., B*, 1994, **4**, 65.
16 T. Yasutake, M. Yusuke and K. Shuichi, *Catalysts Catalysis*, 2000, **42**, 133.
17 T. Schiestel, M. Kilgus, S. Peter, K. J. Caspary, H. H. Wang and J. Caro, *J. Membr. Sci.*, 2005, **258**, 1.

61

3.3 Direct decomposition of nitrous oxide to nitrogen by in situ oxygen removal with a perovskite membrane

Heqing Jiang, Haihui Wang, Fangyi Liang, Steffen Werth, Thomas Schiestel, and Jürgen Caro

N₂O Decomposition

Direct Decomposition of Nitrous Oxide to Nitrogen by In Situ Oxygen Removal with a Perovskite Membrane**

Heqing Jiang, Haihui Wang,* Fangyi Liang, Steffen Werth, Thomas Schiestel, and Jürgen Caro*

Nitrous oxide (N₂O) has recently received much attention as it greatly contributes to the greenhouse effect[1] and causes severe destruction of the ozone layer in the stratosphere.[2] N₂O is produced by both natural and anthropogenic sources;[3–5] N₂O emissions that can be reduced in the short term are associated with chemical and energy industries.[6,7] The major N₂O emission of chemical production comes from adipic acid and nitric acid plants. In the past decades, significant efforts have been devoted to the development of technologies for N₂O reduction. Possible methods include: 1) non-selective catalytic reduction (NSCR), 2) selective catalytic reduction (SCR), and 3) catalytic decomposition of N₂O to O₂ and N₂. NSCR has been developed for NO$_x$ removal and has shown potential for reducing N₂O. However, NSCR is not the optimum choice because of high secondary emissions of CO$_x$ and high cost of the reductant.[8,9] SCR of N₂O with hydrocarbons has been extensively investigated over iron-based zeolites.[10–13] The major drawback of this process are also the high costs associated with the consumption of reductants.[7]

Direct catalytic decomposition of N₂O without addition of reducing agents is an attractive and economical option to reduce N₂O emission. Catalysts, including supported noble metals, metal oxides, and perovskites, are active in direct catalytic N₂O decomposition.[14–16] The commercial iron–zeolite catalysts perform quite well in the presence of other gases, such as O₂, NO$_x$, or H₂O, even in the presence of CO₂ and SO₂.[17] However, metal oxide catalysts suffer from oxygen inhibition, and a low reaction rate of the N₂O decomposition is observed.

To avoid inhibition by adsorbed oxygen, the O₂ formed can be directly removed from the reaction zone by an oxygen-selective membrane. A novel perovskite membrane,[18–27] which also acts as the catalyst, has the composition $BaCo_xFe_yZr_{1-x-y}O_{3-\delta}$ (BCFZ) with hollow-fiber geometry.[18–21]

The basic concept is shown in the Figure 1: N₂O catalytically decomposes on the perovskite membrane surface to N₂ and surface oxygen (O*) according to Equation (1).

$$N_2O \rightarrow N_2 + O^* \tag{1}$$

Afterwards, O* is removed as oxygen ions (O^{2-}) through the membrane, and local charge neutrality is maintained by counterdiffusion of electrons (e$^-$). To ensure a sufficient driving force for the oxygen transport through the membrane, and thus rapid removal of oxygen, methane is fed to the permeate side of the membrane to consume the permeated oxygen by the partial oxidation of methane (POM) to synthesis gas according to $CH_4 + O^{2-} \rightarrow CO + 2H_2 + 2e^-$. As a result, surface oxygen (O*) can be quickly removed by the membrane once it is generated from N₂O decomposition. Therefore, the average amount of adsorbed oxygen (O*) is decreased on the catalyst surface, and a higher reaction rate of the N₂O decomposition is obtained.

[*] Prof. Dr. H. Wang
School of Chemistry & Chemical Engineering
South China University of Technology
Wushan Road, Guangzhou 510640 (China)
Fax: (+86) 208-711-0131
E-mail: hhwang@scut.edu.cn

Dr. S. Werth
Uhde GmbH
Friedrich-Uhde-Strasse 15, 44141 Dortmund (Germany)
Fax: (+49) 212-6455872
E-mail: steffen.werth@werthnetz.de

H. Jiang, F. Liang, Prof. Dr. J. Caro
Institute of Physical Chemistry and Electrochemistry
Leibniz University of Hannover
Callinstrasse 3–3A, 30167 Hannover (Germany)
Fax: (+49) 511-762-19121
E-mail: juergen.caro@pci.uni-hannover.de

Dr. T. Schiestel
Fraunhofer Institute of Interfacial Engineering and Biotechnology (IGB)
Nobelstrasse 12, 70569 Stuttgart (Germany)
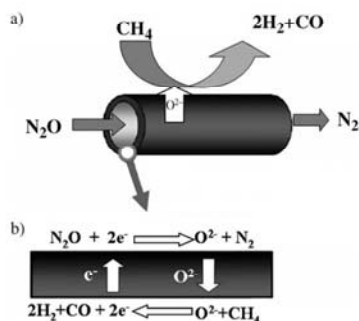
Figure 1. a) Mechanism of the direct decomposition of N₂O to N₂ with in situ removal of the rate-inhibiting surface oxygen by a perovskite hollow fiber membrane. b) Details of the membrane reaction.

Communications

To demonstrate this concept, we carried out experiments with and without oxygen removal using a BCFZ perovskite hollow fiber membrane. In the first set of experiments, N_2O was fed to the core side and no sweep gas was applied at the shell side, so that none of the oxygen surface species produced by the decomposition of N_2O were removed by permeation through the membrane (Supporting Information, Figure S1). The BCFZ membrane thus functions as a catalyst only.

The results of these investigations are shown in Figure 2a. The N_2O decomposition increases with increasing temperature; however, the conversion is relatively low ($< 30\%$ even
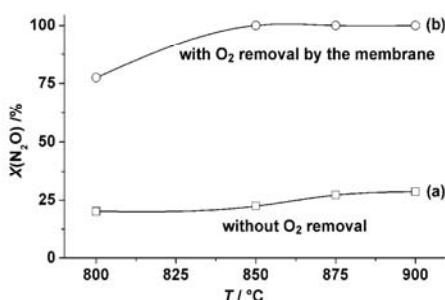
Figure 2. Conversion of N_2O at different temperatures with or without oxygen removal by the membrane. Core side: 30 cm³ min⁻¹ ($F_{N_2O} = 6$ cm³ min⁻¹, $F_{He} = 24$ cm³ min⁻¹). Shell side: a) no oxygen-consuming sweep gas applied, b) with methane as oxygen-consuming sweep gas, 40 cm³ min⁻¹ ($F_{CH_4} = 8$ cm³ min⁻¹, $F_{Ne} = 12$ cm³ min⁻¹, $F_{H_2O} = 20$ cm³ min⁻¹). Membrane area: 0.86 cm². Amount of nickel-based catalyst on shell side: 1.2 g.

at 900 °C). The catalytic decomposition of N_2O on the perovskite membrane surface proceeds mainly in two steps: 1) decomposition of N_2O into N_2 and adsorbed surface oxygen (O*) according to Equation (1), and 2) desorption of surface oxygen as O_2 to the gas phase according to Equation (2).

$$O^* \rightleftharpoons {}^1/_2 O_2 + {}^* \qquad (2)$$

Equation (2), that is, the oxygen–oxygen recombination, is known to be the rate-limiting step in N_2O decomposition.[28,29] As the surface oxygen O* generated by the N_2O decomposition occupies the surface active sites for the decomposition of N_2O, only a low N_2O conversion is obtained.

In the second set of experiments, methane was fed to the shell side (Supporting Information, Figure S1). In contrast to the poor conversion of the first set, in the second set, the N_2O decomposition is significantly improved (Figure 2b). At a temperature of 850 °C, N_2O is already completely decomposed. The reason for this enhanced conversion is an increased removal of the adsorbed surface oxygen. In contrast to the first experiment, the adsorbed surface oxygen, along with desorption to the gas phase, can be also removed directly by the perovskite material functioning as a membrane. The active centers are thus less occupied by adsorbed oxygen on the catalyst surface and therefore the reaction rate is increased.

In the direct catalytic decomposition of N_2O, most of the metal oxide catalysts cannot tolerate the coexistence of oxygen in the feed because the oxygen inhibits the N_2O decomposition. However, oxygen as co-feed has no negative effect on the N_2O decomposition in the membrane reactor. Table 1 shows the N_2O conversion and oxygen concentration

Table 1: Oxygen concentration in the off-gas as a function of the oxygen concentration in the mixed N_2O/O_2 feed gas at 100% N_2O conversion.[a]

$C(O_2)$ in the fed N_2O of the core side [vol. %]	$C(O_2)$ in the exit of the core side [vol. %]
0	0.011
5	0.014
7.5	0.019
15	0.022

[a] At 875 °C. Core side: 30 cm³ min⁻¹ ($F_{N_2O} = 6$ cm³ min⁻¹, $F_{O_2} = 1.5$–4.5 cm³ min⁻¹, $F_{He} =$ balance). Shell side: 40 cm³ min⁻¹ ($F_{CH_4} = 18$ cm³ min⁻¹, $F_{H_2O} = 22$ cm³ min⁻¹). Membrane area: 0.86 cm². Amount of nickel-based catalyst on shell side: 1.2 g.

at the reactor outlet as a function of oxygen concentration in a mixed N_2O/O_2 feed. A complete conversion of N_2O is always achieved, which does not change with increasing oxygen concentration in the range studied in the feed, as both the co-fed and the produced oxygen are removed continuously by the membrane.

Figure 3 shows the influence of the N_2O concentration on the N_2O decomposition. Both low (5%) and high (50%) N_2O concentrations can be effectively treated (conversion of $N_2O > 99.9\%$) using the BCFZ membrane reactor.

The membrane approach presented herein involves the in situ removal of pure oxygen, which could then be utilized. An attractive option for the use of this oxygen is in the production of N_2-free synthesis gas. In Figure 4, N_2O in the core side was completely converted. Simultaneously, synthesis gas is obtained by partial oxidation of methane. Using suitable reaction conditions, a methane conversion of over 90% and a CO selectivity of 90% was achieved for at least 60 h of operation. The technology is more feasible when the concen-
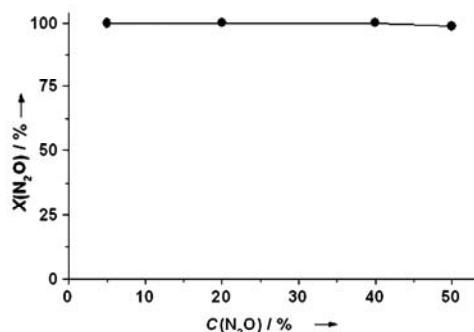
Figure 3. Influence of the N_2O concentration in the fed gas on the N_2O conversion at 875 °C. Core side: 30 cm³ min⁻¹ ($F_{N_2O} = 1.5$–15 cm³ min⁻¹, $F_{He} =$ balance). Shell side: 40 cm³ min⁻¹ ($F_{CH_4} = 8$ cm³ min⁻¹, $F_{Ne} = 12$ cm³ min⁻¹, $F_{H_2O} = 20$ cm³ min⁻¹). Membrane area: 0.86 cm². Amount of nickel-based catalyst on shell side: 1.2 g.
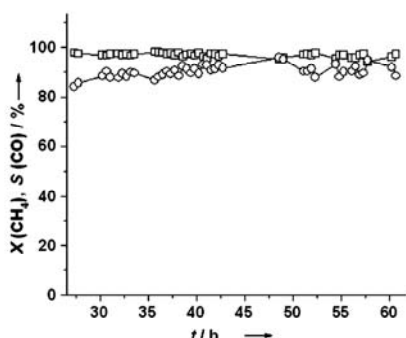
Figure 4. Methane conversion $X(CH_4)$ (□) and CO selectivity $S(CO)$ (○) as a function of time on-stream at 875 °C with 100% N_2O conversion. Core side: 30 cm^3 min^{-1} (F_{N_2O} = 6 cm^3 min^{-1}, F_{O_2} = 1.5 cm^3 min^{-1}, F_{He} = 22.5 cm^3 min^{-1}). Shell side: 40 cm^3 min^{-1} (F_{CH_4} = 23 cm^3 min^{-1}, F_{H_2O} = 17 cm^3 min^{-1}). Membrane area: 0.86 cm^2. Amount of nickel-based catalyst on shell side: 1.2 g.

trations of nitrous oxide in the off-gas are sufficient high, such as in adipic acid plants.

In conclusion, a perovskite membrane reactor is proposed for the N_2O abatement from exhaust gases. The ceramic membrane fulfills a double role: it catalyzes the decomposition of N_2O on the membrane surface, and it increases the reaction rate by overcoming the rate-limiting removal of surface oxygen, thus increasing the number of active surface sites required for the N_2O decomposition. A reducing agent has to be used; this agent, for example methane, can however be used for the production of N_2-free synthesis gas by partial oxidation using the removed oxygen from N_2O decomposition as an oxidant.

The work presented herein is the new concept to enhance the reaction rate of heterogeneous catalytic processes, in which the recombination and/or desorption of one of the reaction products is the rate-limiting step. Using a semi-permeable membrane, which facilitates in situ removal of an inhibiting species on a catalyst or catalyst support, helps to effectively reduce the surface concentration of the inhibiting species and therefore increases the reaction rate.

Experimental Section

The dense BCFZ perovskite hollow-fiber membranes were manufactured by phase inversion spinning followed by sintering.[18–21] Figure S1 (Supporting Information) shows diagrams of the membrane reactor used in this study. Two ends of the hollow fiber were coated by commercially available gold paste. After sintering at 950 °C, a dense gold film, which is not permeable to oxygen, was obtained. Such gold-coated hollow fibers can be sealed by silicon rubber rings and the uncoated part of the fiber (3.0 cm) that is permeable to oxygen can be kept in the middle of the oven, ensuring isothermal conditions. A mixture of N_2O and helium was fed to the core side and a mixture of CH_4 and helium was fed to the shell side. A nickel-based steam reforming catalyst (Süd-Chemie AG) was packed around and behind the hollow fiber membrane. To avoid coke formation on the catalyst, H_2O was also fed to the shell side. The H_2O flow rate was controlled by a liquid mass flow controller (Bronkhorst) and completely evaporated at 180 °C before it was fed to the reactor. All gas lines to the reactor and the gas chromatograph were heated to 180 °C to

avoid condensation. The concentrations of the gases at the exit of the reactor were determined by on-line gas chromatography (Agilent 6890 with a carboxen 1000 column, which was periodically switched from the core-side to the shell-side of the membrane to measure the gas compositions on both sides of the membrane). The CH_4 conversion $X(CH_4)$, the CO selectivity $S(CO)$ and the N_2O conversion were calculated as shown in Equations (3)–(5).

$$X(CH_4) = \left(1 - \frac{F(CH_4,\text{out})}{F(CH_4,\text{in})}\right) \times 100\% \tag{3}$$

$$S(CO) = \frac{F(CO,\text{out})}{F(CH_4,\text{in}) - F(CH_4,\text{out})} \times 100\% \tag{4}$$

$$X(N_2O) = \left(1 - \frac{F(N_2O,\text{out})}{F(N_2O,\text{in})}\right) \times 100\% \tag{5}$$

In these equations, $F(i)$ is the flow rate of species i on the shell or core side of the hollow fiber membrane.

[1] R. E. Dickinson, R. J. Cicerone, *Nature* **1986**, *319*, 109.
[2] M. J. Prather, *Science* **1998**, *279*, 1339.
[3] S. J. Hall, P. A. Matson, *Nature* **1999**, *400*, 152.
[4] J. E. Dore, B. N. Popp, D. M. Karl, F. J. Sansone, *Nature* **1998**, *396*, 63.
[5] T. Nobukawa, K. Sugawara, K. Okumura, K. Tomishige, K. Kunimori, *Appl. Catal. B* **2007**, *70*, 342.
[6] F. Kapteijn, J. Rodriguez-Mirasol, J. A. Moulijn, *Appl. Catal. B* **1996**, *9*, 25.
[7] J. Pérez-Ramírez, F. Kapteijn, K. Schöffel, J. A. Moulijn, *Appl. Catal. B* **2003**, *44*, 117.
[8] M. Schwefer, R. Maurer, M. Groves in *Proceedings of the International Conference and Exhibition on Nitrogen*, Vienna, 12–14 March **2000**, pp. 60–81.
[9] C. Pophal, T. Yogo, K. Yamada, K. Segawa, *Appl. Catal. B* **1998**, *16*, 177.
[10] M. Kögel, R. Moenning, W. Schwieger, A. Tissler, T. Turek, *J. Catal.* **1999**, *182*, 470.
[11] Z. S. Rak, M. J. F. M. Verhaak, B. Bos, G. Centi (ECN), WO99/49954, **1999**.
[12] M. Schwefer, R. Mauer, T. Turek, M. Kögel (Krupp Uhde), WO0151182, **2001**.
[13] J. Pérez-Ramírez, F. Kapteijn, G. Mul, J. A. Moulijn, *Chem. Commun.* **2001**, 693.
[14] G. Centi, A. Galli, B. Montanari, S. Perathoner, A. Vaccari, *Catal. Today* **1997**, *35*, 113.
[15] N. Russo, D. Fina, G. Saracco, V. Specchia, *Catal. Today* **2007**, *119*, 228.
[16] N. Gunasekaran, S. Rajadurai, J. J. Carberry, *Catal. Lett.* **1995**, *35*, 373.
[17] J. Pérez-Ramírez, F. Kapteijn, G. Mul, J. A. Moulijn, *Appl. Catal. B* **2002**, *35*, 227.
[18] T. Schiestel, M. Kilgus, S. Peter, K. J. Caspary, H. H. Wang, J. Caro, *J. Membr. Sci.* **2005**, *258*, 1.
[19] H. H. Wang, S. Werth, T. Schiestel, J. Caro, *Angew. Chem.* **2005**, *117*, 7066; *Angew. Chem. Int. Ed.* **2005**, *44*, 6906.
[20] H. H. Wang, P. Kölsch, T. Schiestel, C. Tablet, S. Werth, J. Caro, *J. Membr. Sci.* **2006**, *284*, 5.

65

Communications

[21] C. Hamel, A. Seidel-Morgenstern, T. Schiestel, S. Werth, H. H. Wang, C. Tablet, J. Caro, *AIChE J.* **2006**, *52*, 3118.

[22] J. Y. Ren, Y. Q. Fan, F. N. Egolfopoulos, T. T. Tsotsis, *Chem. Eng. Sci.* **2003**, *58*, 1043.

[23] R. Merkle, J. Maier, H. J. M. Bouwmeester, *Angew. Chem.* **2004**, *116*, 5179; *Angew. Chem. Int. Ed.* **2004**, *43*, 5069.

[24] J. Pérez-Ramírez, B. Vigeland, *Angew. Chem.* **2005**, *117*, 1136; *Angew. Chem. Int. Ed.* **2005**, *44*, 1112.

[25] Z. P. Shao, W. S. Yang, Y. Cong, H. Dong, J. H. Tong, G. X. Xiong, *J. Membr. Sci.* **2000**, *172*, 177.

[26] C. Chen, S. J. Feng, S. Ran, D. C. Zhu, W. Liu, H. J. M. Bouwmeester, *Angew. Chem.* **2003**, *115*, 5354; *Angew. Chem. Int. Ed.* **2003**, *42*, 5196.

[27] F. T. Akin, Y. S. Lin, *AIChE J.* **2002**, *48*, 2298.

[28] D. A. Bulushev, L. Kiwi-Minsker, A. Renken, *J. Catal.* **2004**, *222*, 389.

[29] S. Bennici, A. Gervasini, *Appl. Catal. B* **2006**, *62*, 336.

66

N₂O-Zersetzung

Zersetzung von Lachgas in die Elemente mit In-situ-Entfernung des Sauerstoffs durch eine Perowskitmembran**

Heqing Jiang, Haihui Wang,* Fangyi Liang, Steffen Werth,* Thomas Schiestel und Jürgen Caro*

Distickstoffmonoxid (N₂O) hat wegen seiner Wirkung als Treibhausgas und seines Einflusses auf die Ozonschicht in jüngster Vergangenheit erhebliche Aufmerksamkeit erfahren.[1,2] Abgesehen von natürlichen Emissionen wird N₂O beispielsweise von Anlagen zur Produktion von Adipinsäure oder Salpetersäure freigesetzt. Diese anthropogenen Quellen bilden die Hauptansatzpunkte für eine Emissionssenkung.[3–7] In den vergangenen Jahrzehnten wurde erheblicher Aufwand in die Entwicklung von Konzepten zur N₂O-Reduktion investiert. Die verfügbaren Verfahren umfassen: 1) nichtselektive katalytische Reduktion (NSCR), 2) selektive katalytische Reduktion (SCR) und 3) katalytische Zersetzung von N₂O in die Elemente O₂ und N₂. Die NSCR – ursprünglich entwickelt für den NO$_x$-Abbau – zeigt ein erhebliches Potenzial für die N₂O-Zersetzung, erkauft dieses jedoch durch hohe CO₂-Folgeemissionen sowie entsprechende Kosten für das Reduktionsmittel.[8,9] Die SCR von N₂O mit Kohlenwasserstoffen an Fe-Zeolithen wurde ebenfalls intensiv untersucht und erzielt im industriellen Einsatz hervorragende Ergebnisse;[10–13] auch dieses Verfahren benötigt jedoch ein Reduktionsmittel.[7]

Die direkte katalytische Zersetzung von N₂O ohne Zugabe eines weiteren Reduktionsmittels oder zumindest mit stofflicher Nutzung des Reduktionsmittels ist daher eine interessante Option zur Verringerung von N₂O-Emissionen.

Bei der direkten Zersetzung wurden Edelmetall- und Metalloxid- sowie Perowskit-Katalysatoren untersucht.[14–16] Die derzeit kommerziell eingesetzten Fe-Zeolith-Katalysatoren verfügen über hervorragende Standzeiten auch in Gegenwart von anderen Gasen wie O₂, NO$_x$, H₂O, CO₂ oder SO₂. Oxid-Katalysatoren zeigen wegen einer starken Adsorption des gebildeten Sauerstoffs an ihren aktiven Zentren jedoch nur vergleichsweise geringe Reaktionsgeschwindigkeiten.[17]

Eine Möglichkeit, die Inhibition durch adsorbierten Sauerstoff zu umgehen, ist die direkte Entfernung von gebildetem O₂ aus der Reaktionszone durch eine sauerstoffselektive Membran. Als Membran – und gleichzeitig als Katalysator – dient dabei eine neuartige Perowskit-Hohlfaser der Zusammensetzung BaCo$_x$Fe$_y$Zr$_{1-x-y}$O$_{3-\delta}$ (BCFZ).[18–27]

Das Grundkonzept ist in Abbildung 1 dargestellt: N₂O wird an der Membranoberfläche gemäß Gleichung (1) zu elementarem Stickstoff und adsorbiertem Sauerstoff (O*) zersetzt.

$$N_2O \rightarrow N_2 + O^* \tag{1}$$

Der adsorbierte Sauerstoff wird in einem Folgeschritt in ionischer Form (O²⁻) durch die Membran abtransportiert, wobei die elektrische Neutralität des Systems durch eine gleichzeitige Gegendiffusion von Elektronen (e⁻) gewahrt wird. Um eine hinreichende Triebkraft für die Permeation zu schaffen – und somit einen schnellen Sauerstoffabtransport zu erzielen –, wird der durch die Membran transportierte Sauerstoff auf der Permeatseite in der partiellen Oxidation von Methan (POM) zu Synthesegas gemäß CH₄ + O²⁻ → CO + 2H₂ + 2e⁻ umgesetzt. Als Ergebnis dieses Sauerstoffabtransports wird die mittlere Konzentration an adsorbiertem Sauerstoff (O*) auf der Membran (respektive der Katalysa-

[*] Prof. Dr. H. Wang
School of Chemistry & Chemical Engineering
South China University of Technology
Wushan Road, Guangzhou 510640 (China)
Fax: (+86) 20-87110131
E-Mail: hhwang@scut.edu.cn

Dr. S. Werth
Uhde GmbH
Friedrich-Uhde-Straße 15, 44141 Dortmund (Deutschland)
Fax: (+49) 212-6455872
E-Mail: steffen.werth@werthnetz.de

H. Jiang, F. Liang, Prof. Dr. J. Caro
Institut für Physikalische Chemie und Elektrochemie
Leibniz-Universität Hannover
Callinstraße 3–3A, 30167 Hannover (Deutschland)
Fax: (+49) 511-762-19121
E-Mail: juergen.caro@pci.uni-hannover.de

Dr. T. Schiestel
IGB, Nobelstraße 12, 70569 Stuttgart (Deutschland)
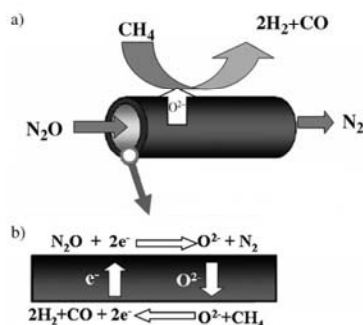
Abbildung 1. a) Konzept der direkten Zersetzung von N₂O mit Entfernung des gebildeten Sauerstoffs durch eine Perowskit-Hohlfasermembran. b) Details der Reaktionen an der Membran.

Zuschriften

toroberfläche) gesenkt. Dadurch sind mehr aktive Zentren verfügbar, und die Reaktionsgeschwindigkeit ist folglich erhöht.

Dieses Konzept wurde anhand von Untersuchungen in einem Membranreaktor mit und ohne Sauerstoffentfernung durch eine BCFZ-Hohlfasermembran überprüft. In einer ersten Versuchsreihe wurde dabei N_2O auf der Innenseite der Membran vorgelegt. Auf der Außenseite der Membran wurde kein Spülgas vorgegeben, sodass keine Triebkraft für einen Abtransport des Sauerstoffs durch die Membran gegeben war (siehe Abbildung S1). Die BCFZ-Membran wirkte daher ausschließlich als Katalysator.

Die Ergebnisse dieser Versuche sind in Abbildung 2A dargestellt. Es zeigt sich, dass der N_2O-Umsatz mit zunehmender Temperatur steigt, jedoch bei den gewählten Ver-
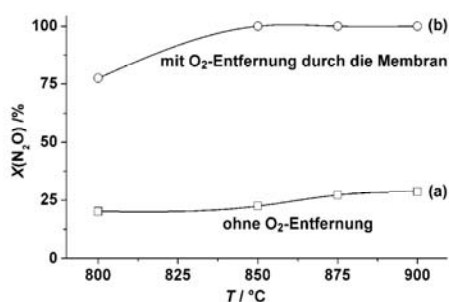
Abbildung 2. N_2O-Umsatz bei verschiedenen Temperaturen mit und ohne Sauerstoffabfuhr durch die Membran. Faserinnenseite: 30 cm³ min⁻¹ (F_{N_2O} = 6 cm³ min⁻¹, F_{He} = 24 cm³ min⁻¹). Faseraußenseite: a) kein oxidierbares Medium, b) Methan als oxidierbares Spülgas, 40 cm³ min⁻¹ (F_{CH_4} = 8 cm³ min⁻¹, F_{Ne} = 12 cm³ min⁻¹ und F_{H_2O} = 20 cm³ min⁻¹). Membranfläche: 0.86 cm². Menge des Nickelkatalysators: 1.2 g.

weilzeiten auch bei 900°C unterhalb von 30% liegt. Die katalytische Zersetzung von N_2O umfasst dabei im Wesentlichen zwei Schritte: 1) Zersetzung von adsorbiertem N_2O in N_2 und eine an der Oberfläche adsorbierte Sauerstoffspezies (O*) entsprechend Gleichung (1) und 2) Desorption von O* als elementarer Sauerstoff in die Gasphase gemäß Gleichung (2).

$$O^* \;\rightleftharpoons\; {}^1/_2\,O_2 + {}^* \tag{2}$$

Es wird vermutet, dass die in Gleichung (2) dargestellte Rekombination und anschließende Desorption des adsorbierten Sauerstoffs den geschwindigkeitsbestimmenden Schritt der Umsetzung darstellt.[28,29] Gleichzeitig verringert auf der Katalysatoroberfläche adsorbierter Sauerstoff die Zahl an aktiven Zentren, die für die Umsetzung von N_2O zur Verfügung stehen, sodass nur geringe effektive Reaktionsgeschwindigkeiten und somit (im Rahmen der gewählten Verweilzeiten) nur geringe Umsätze erzielt werden.

In einer zweiten Versuchsreihe wurde nun Methan auf der Außenseite der Hohlfaser zugegeben. Durch die partielle Oxidation von Methan wird in diesem Bereich Sauerstoff verbraucht, was eine Triebkraft für die weitere Sauerstoff-

permeation durch die Membran erzeugt (siehe Abbildung S1). Die Ergebnisse dieser Versuche sind in Abbildung 2B dargestellt. Es zeigt sich ein gegenüber dem Versuch ohne Sauerstoffabfuhr durch die Membran deutlich erhöhter Umsatz (und entsprechend eine höhere effektive Reaktionsgeschwindigkeit). So wurde bereits bei 850°C ein vollständiger N_2O-Umsatz erzielt. Der Grund hierfür ist die beschleunigte Abfuhr von adsorbiertem Oberflächensauerstoff: Anders als beim Vergleichsversuch kann nun der adsorbierte Oberflächensauerstoff neben der Desorption in die freie Gasphase auch direkt durch das Katalysatormaterial, respektive die Membran, abgeführt werden. Dadurch ergibt sich eine verringerte Belegung der aktiven Zentren auf der Katalysatoroberfläche durch adsorbierten Sauerstoff und damit eine erhöhte effektive Reaktionsgeschwindigkeit.

Aufgrund der beschriebenen Blockierung aktiver Zentren durch Sauerstoff sind Oxid-Katalysatoren häufig ungeeignet für die N_2O-Zersetzung, sobald Sauerstoff im Ausgangsgemisch enthalten ist. Bei Versuchen im Membranreaktor mit einem reaktiven Spülgas ist dies jedoch erwartungsgemäß nicht der Fall, wie die Ergebnisse in Tabelle 1 zeigen. Es ist

Tabelle 1: Sauerstoffkonzentration im Produktgas in Abhängigkeit von der Sauerstoffkonzentration des Ausgangsgemischs bei vollständigem N_2O-Umsatz.[a]
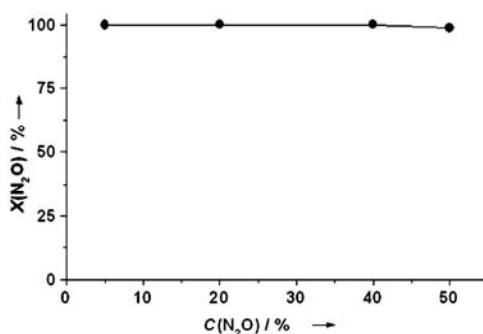
$C(O_2)$ im Ausgangsgemisch an der Faserinnenseite [Vol.-%]	$C(O_2)$ am Reaktoraustritt der Faserinnenseite [Vol.-%]
0	0.011
5	0.014
7.5	0.019
15	0.022

[a] Bei 875°C. Faserinnenseite: 30 cm³ min⁻¹ (F_{N_2O} = 6 cm³ min⁻¹, F_{O_2} = 1.5–4.5 cm³ min⁻¹, F_{He} = Rest). Faseraußenseite: 40 cm³ min⁻¹ (F_{CH_4} = 18 cm³ min⁻¹, F_{H_2O} = 22 cm³ min⁻¹). Membranfläche: 0.86 cm². Menge des Nickelkatalysators: 1.2 g.

vielmehr offensichtlich, dass auch mit zunehmender Sauerstoffkonzentration im Ausgangsgemisch ein vollständiger Umsatz erreicht wird und keine messbare Verringerung der Reaktionsgeschwindigkeit auftritt. Dieser Effekt ist damit zu erklären, dass sowohl der während der Reaktion gebildete als auch der bereits im Gemisch vorhandene Sauerstoff durch die Membran abgeführt wird.

Abbildung 3 zeigt den Einfluss der N_2O-Konzentration auf den Zersetzungsprozess: Im BCFZ-Membranreaktor werden sowohl bei geringen (5%) als auch hohen N_2O-Konzentrationen (50%) Umsätze über 99.9% erreicht.

Der vorgestellte Membranansatz beruht auf der In-situ-Entfernung von reinem Sauerstoff, der anschließend stofflich genutzt werden kann. Eine interessante Option zur Verwendung dieses Sauerstoffs ist die Gewinnung von stickstofffreiem Synthesegas. Abbildung 4 zeigt das Ergebnis eines derartigen Versuchs. Auf der Innenseite der keramischen Hohlfaser wurde das Lachgas vollständig zersetzt, während der permeierende Sauerstoff für die Gewinnung von Synthesegas auf der Außenseite der Hohlfaser durch die partielle Oxidation von Methan genutzt wurde. Unter geeigneten Reaktionsbedingungen konnte ein Methanumsatz von 90% bei

68

Abbildung 3. Einfluss der N_2O-Konzentration im Ausgangsgemisch auf den N_2O-Umsatz bei 875 °C. Faserinnenseite: 30 cm³ min⁻¹ ($F_{N_2O} = 1.5$–15 cm³ min⁻¹, $F_{He} =$ Rest). Faseraußenseite: 40 cm³ min⁻¹ ($F_{CH_4} = 8$ cm³ min⁻¹, $F_{Ne} = 12$ cm³ min⁻¹ und $F_{H_2O} = 20$ cm³ min⁻¹). Membranfläche: 0.86 cm². Menge des Nickelkatalysators: 1.2 g.
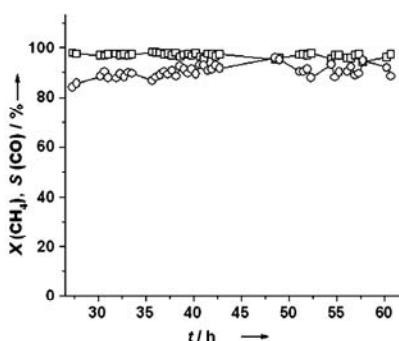
Abbildung 4. Methan-Umsatz $X(CH_4)$ (□) und CO-Selektivität $S(CO)$ (○) als Funktion der Versuchsdauer bei 875 °C und vollständigem N_2O-Umsatz. Ursprüngliches Diagramm (a) wurde entfernt, da X-(N_2O) stets 100 %. Faserinnenseite: 30 cm³ min⁻¹ ($F_{N_2O} = 6$ cm³ min⁻¹, $F_{O_2} = 1.5$ cm³ min⁻¹, $F_{He} = 22.5$ cm³ min⁻¹). Faseraußenseite: 40 cm³ min⁻¹ ($F_{CH_4} = 23$ cm³ min⁻¹, $F_{H_2O} = 17$ cm³ min⁻¹). Membranfläche: 0.86 cm². Menge des Nickelkatalysators: 1.2 g.

einer CO-Selektivität von 90 % über einen Zeitraum von 60 h erzielt werden. Diese Option ist naturgemäß besonders interessant, wenn die N_2O-Konzentration im Ausgangsgemisch hinreichend hoch ist (beispielsweise bei Anlagen zur Adipinsäure-Produktion).

Als Fazit bleibt festzuhalten, dass ein Perowskitmembranreaktor eine interessante Option für die Verringerung des N_2O-Gehalts von Abgasen darstellt. Die keramische Membran erfüllt dabei zwei Funktionen: 1) Sie katalysiert die Zersetzung von N_2O auf der Membranoberfläche, und 2) sie erhöht die Zahl an verfügbaren aktiven Zentren auf der Oberfläche (und damit die effektive Reaktionsgeschwindigkeit) durch eine kontinuierliche Abfuhr des adsorbierten Sauerstoffs. Auch dieser Ansatz zur N_2O-Zersetzung benötigt ein Reduktionsmittel, das jedoch räumlich getrennt von dem zu behandelnden Abgasstrom eingesetzt und damit stofflich genutzt werden kann – im Fall des Reduktionsmittels Methan beispielsweise durch partielle Oxidation zu Synthesegas.

Das vorgestellte Konzept zeigt darüber hinaus eine neue reaktionstechnische Option zur Beschleunigung heterogenkatalytischer Prozesse, deren geschwindigkeitsbestimmender Schritt die Desorption eines Reaktionsprodukts von der Katalysatoroberfläche ist. Parallel zu der ohnehin stattfindenden Desorption wird bei Verwendung einer für die adsorbierte Spezies permeablen Membran als Katalysator oder Katalysatorträger ein zusätzlicher Weg zur Entfernung der adsorbierten Spezies von der Katalysatoroberfläche etabliert. Als Resultat beschleunigt sich die Freigabe der aktiven Zentren durch die adsorbierte Spezies, mit dem Ergebnis einer im Mittel größeren Zahl an freien aktiven Zentren und folglich einer höheren effektiven Reaktionsgeschwindigkeit.

Experimentelles

Die dichten BCFZ-Hohlfasern wurden durch ein Phaseninversionsspinnverfahren hergestellt[18–21] und anschließend in den in Abbildung S1 dargestellten Reaktoren verwendet. Um isotherme Messungen zu ermöglichen, wurden die beiden Enden der jeweiligen Faser vor dem Einbau in den Reaktor mit einer kommerziell erhältlichen Goldpaste beschichtet. Nach Sintern bei 950 °C erhielt man im beschichteten Faserteil eine dichte Goldschicht, die jegliche Sauerstoffpermeation unterbindet. Die derart vorbereiteten Fasern wurden anschließend mithilfe von Silicondichtungen in den Reaktor eingebaut, sodass der mittlere, unbeschichtete Teil der Faser (3 cm) im isothermen Bereich des Ofens angeordnet war. Während des Versuchs wurde entsprechend den jeweiligen Reaktionsbedingungen eine Mischung aus N_2O und He an die Innenseite der Faser sowie gegebenenfalls eine Mischung aus CH_4 und He an die Außenseite der Faser geleitet. Ein Nickel-Steamreformingkatalysator (Süd-Chemie) wurde als Festbett um die Faser gepackt. Um Koksbildung zu vermeiden, wurde gegebenenfalls zusätzlich Wasserdampf zur Außenseite der Faser geleitet. Zur Vermeidung von Kondensationen wurden sämtliche Gasleitungen auf 180 °C erwärmt. Die Konzentrationen an den jeweiligen Reaktoraustritten wurden mit einem Gaschromatograph (Agilent 6890/Carboxen 1000) bestimmt, wobei periodisch zwischen den beiden Reaktoraustritten umgeschaltet wurde. Der Methanumsatz $X(CH_4)$, die CO-Selektivität $S(CO)$ sowie der N_2O-Umsatz wurden nach Gleichung (3)–(5) berechnet.

$$X(CH_4) = \left(1 - \frac{F(CH_4, out)}{F(CH_4, in)}\right) \times 100\% \qquad (3)$$

$$S(CO) = \frac{F(CO, out)}{F(CH_4, in) - F(CH_4, out)} \times 100\% \qquad (4)$$

$$X(N_2O) = \left(1 - \frac{F(N_2O, out)}{F(N_2O, in)}\right) \times 100\% \qquad (5)$$

Hierbei ist $F(i)$ der Volumenstrom der Spezies i an der Innen- oder Außenseite der Hohlfasermembran.

[1] R. E. Dickinson, R. J. Cicerone, *Nature* **1986**, *319*, 109.
[2] M. J. Prather, *Science* **1998**, *279*, 1339.
[3] S. J. Hall, P. A. Matson, *Nature* **1999**, *400*, 152.

Zuschriften

[4] J. E. Dore, B. N. Popp, D. M. Karl, F. J. Sansone, *Nature* **1998**, *396*, 63.

[5] T. Nobukawa, K. Sugawara, K. Okumura, K. Tomishige, K. Kunimori, *Appl. Catal. B* **2007**, *70*, 342.

[6] F. Kapteijn, J. Rodriguez-Mirasol, J. A. Moulijn, *Appl. Catal. B* **1996**, *9*, 25.

[7] J. Pérez-Ramírez, F. Kapteijn, K. Schöffel, J. A. Moulijn, *Appl. Catal. B* **2003**, *44*, 117.

[8] M. Schwefer, R. Maurer, M. Groves in *Proceedings of the International Conference and Exhibition on Nitrogen*, Wien, 12.–14. März **2000**, S. 60–81.

[9] C. Pophal, T. Yogo, K. Yamada, K. Segawa, *Appl. Catal. B* **1998**, *16*, 177.

[10] M. Kögel, R. Moenning, W. Schwieger, A. Tissler, T. Turek, *J. Catal.* **1999**, *182*, 470.

[11] Z. S. Rak, M. J. F. M. Verhaak, B. Bos, G. Centi (ECN), WO99/49954, **1999**.

[12] M. Schwefer, R. Mauer, T. Turek, M. Kögel (Krupp Uhde), WO0151182, **2001**.

[13] J. Pérez-Ramírez, F. Kapteijn, G. Mul, J. A. Moulijn, *Chem. Commun.* **2001**, 693.

[14] G. Centi, A. Galli, B. Montanari, S. Perathoner, A. Vaccari, *Catal. Today* **1997**, *35*, 113.

[15] N. Russo, D. Fina, G. Saracco, V. Specchia, *Catal. Today* **2007**, *119*, 228.

[16] N. Gunasekaran, S. Rajadurai, J. J. Carberry, *Catal. Lett.* **1995**, *35*, 373.

[17] J. Pérez-Ramírez, F. Kapteijn, G. Mul, J. A. Moulijn, *Appl. Catal. B* **2002**, *35*, 227.

[18] T. Schiestel, M. Kilgus, S. Peter, K. J. Caspary, H. H. Wang, J. Caro, *J. Membr. Sci.* **2005**, *258*, 1.

[19] H. H. Wang, S. Werth, T. Schiestel, J. Caro, *Angew. Chem.* **2005**, *117*, 7066; *Angew. Chem. Int. Ed.* **2005**, *44*, 6906.

[20] H. H. Wang, P. Kölsch, T. Schiestel, C. Tablet, S. Werth, J. Caro, *J. Membr. Sci.* **2006**, *284*, 5.

[21] C. Hamel, A. Seidel-Morgenstern, T. Schiestel, S. Werth, H. H. Wang, C. Tablet, J. Caro, *AIChE J.* **2006**, *52*, 3118.

[22] J. Y. Ren, Y. Q. Fan, F. N. Egolfopoulos, T. T. Tsotsis, *Chem. Eng. Sci.* **2003**, *58*,1043.

[23] R. Merkle, J. Maier, H. J. M. Bouwmeester, *Angew. Chem.* **2004**, *116*, 5179; *Angew. Chem. Int. Ed.* **2004**, *43*, 5069.

[24] J. Pérez-Ramírez, B. Vigeland, *Angew. Chem.* **2005**, *117*, 1136; *Angew. Chem. Int. Ed.* **2005**, *44*, 1112.

[25] Z. P. Shao, W. S. Yang, Y. Cong, H. Dong, J. H. Tong, G. X. Xiong, *J. Membr. Sci.* **2000**, *172*, 177.

[26] C. Chen, S. J. Feng, S. Ran, D. C. Zhu, W. Liu, H. J. M. Bouwmeester, *Angew. Chem.* **2003**, *115*, 5354; *Angew. Chem. Int. Ed.* **2003**, *42*, 5196.

[27] F. T. Akin, Y. S. Lin, *AIChE J.* **2002**, *48*, 2298.

[28] D. A. Bulushev, L. Kiwi-Minsker, A. Renken, *J. Catal.* **2004**, *222*, 389.

[29] S. Bennici, A. Gervasini, *Appl. Catal. B* **2006**, *62*, 336.

70

Supporting Information for

Direct decomposition of nitrous oxide to nitrogen by in-situ oxygen removal with a perovskite membrane**

Heqing Jiang[a], Haihui Wang[a,b,*], Fangyi Liang[a], Steffen Werth[c], Thomas Schiestel[d], Jürgen Caro[a,*]

[a]Institute of Physical Chemistry and Electrochemistry, Leibniz University of Hannover, Callinstr. 3-3A,

D-30167 Hannover, Germany

[b] School of Chemistry and Chemical Engineering, South China University of Technology, Guangzhou,

510640, PR China

[c]Uhde GmbH, Friedrich-Uhde-Str. 15, D-44141 Dortmund, Germany

[d]Fraunhofer Institute of Interfacial Engineering and Biotechnology (IGB), Nobelstr 12, D-70569 Stuttgart,

Germany

[*]Corresponding author.
  E-mail address: hhwang@scut.edu.cn or juergen.caro@pci.uni-hannover.de
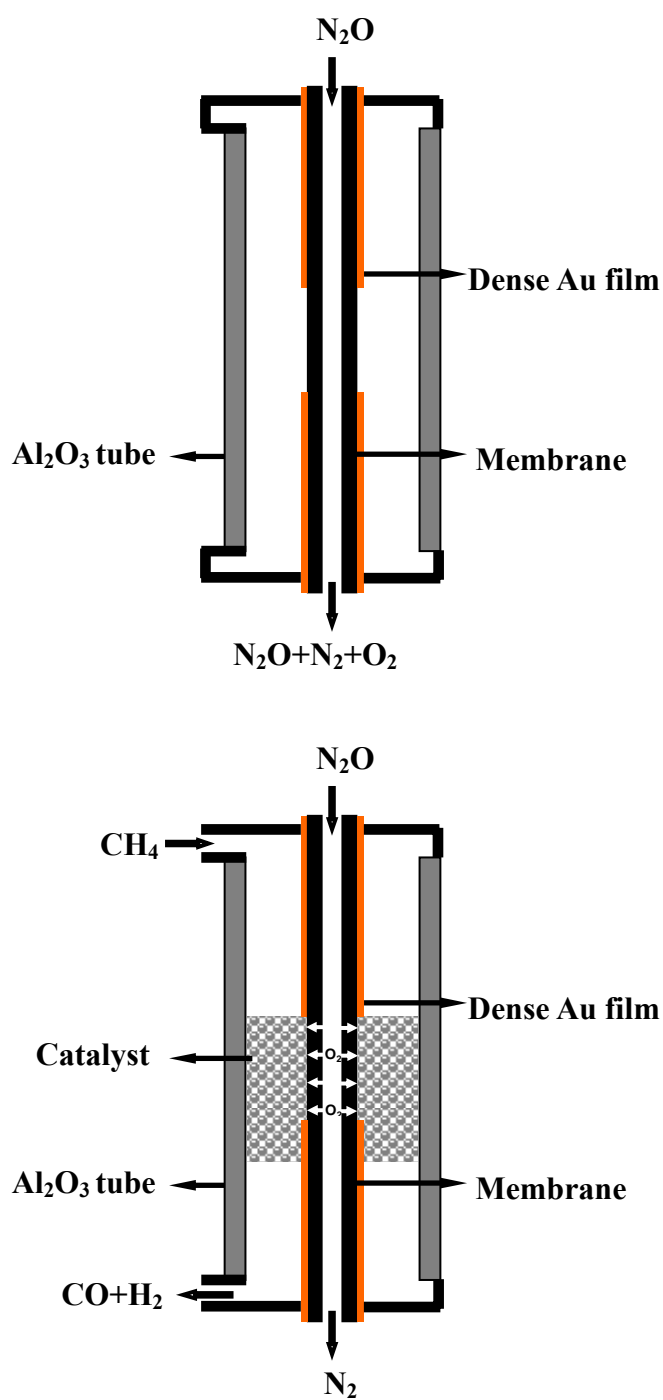
Figure S1 Comparative study of N₂O catalytic decomposition in different operation modes.

top: Membrane operation mode without oxygen removal.

bottom: Membrane operation mode with in-situ oxygen removal.

3.4 Improved water dissociation and nitrous oxide decomposition by in situ oxygen removal in perovskite catalytic membrane reactor

Heqing Jiang, Haihui Wang, Fangyi Liang, Steffen Werth, Steffen Schirrmeister, Thomas Schiestel, and Jürgen Caro

ARTICLE IN PRESS

Improved water dissociation and nitrous oxide decomposition by in situ oxygen removal in perovskite catalytic membrane reactor

Heqing Jiang[a,*], Haihui Wang[b], Fangyi Liang[a], Steffen Werth[a], Steffen Schirrmeister[c], Thomas Schiestel[d], Jürgen Caro[a,*]

[a] *Institute of Physical Chemistry and Electrochemistry, Leibniz University of Hannover, Callinstr. 3A, D-30167 Hannover, Germany*
[b] *College of Chemistry and Chemical Engineering, South China University of Technology, Guangzhou, 510640, PR China*
[c] *Uhde GmbH, Friedrich-Uhde-Str. 15, D-44141 Dortmund, Germany*
[d] *Fraunhofer Institute of Interfacial Engineering and Biotechnology (IGB), Nobelstr 12, D-70569 Stuttgart, Germany*

ARTICLE INFO

ABSTRACT

The equilibrium controlled water dissociation and the kinetically controlled nitrous oxide (N$_2$O) decomposition were studied in the perovskite BaCo$_x$Fe$_y$Zr$_{1-x-y}$O$_{3-\delta}$ (BCFZ) oxygen-permeable membrane reactor. By increasing the temperature or pressure difference and by feeding reducing gases like methane or ethane to the permeate side to consume the permeated oxygen, hydrogen production rate or N$_2$O conversion could be enhanced. A hydrogen production rate of 3.1 cm^3 min^{-1} cm^{-2} was obtained at 950 °C. When methane was used as the reducing gas on the shell side, the oxygen concentration on the N$_2$O side can be kept at a low level, thus avoiding the inhibition of the N$_2$O decomposition by adsorbed surface oxygen species. A complete decomposition of N$_2$O for gas streams containing 20 vol.% N$_2$O was achieved on the core side at 850 °C. Simultaneously, methane on the shell side was converted into synthesis gas with CO yield of above 80%. When feeding ethane to the shell side, the hydrogen from the thermal dehydrogenation of ethane can consume the permeated oxygen. At 850 °C, an ethane conversion of 85% and an ethylene selectivity of 86% were obtained.

1. Introduction

In the past two decades, membrane reactors, as devices combining chemical reactions and a membrane separation in one unit, have attracted more and more attention [1–3]. One of the major advantages of membrane reactors is that the equilibrium constraint of many reversible reactions can be overcome by removal of one or more product(s) through the membrane, thus further increasing the conversion. For example, the equilibrium constant of water dissociation is very small even at a relatively high temperature. However, significant amounts of H$_2$ from water splitting can be obtained at moderate temperatures if an oxygen-permeable membrane [4–7] is used to remove O$_2$ as it is generated [8–10]. In another application, a higher conversion can be obtained in membrane reactor if the reaction is kinetically limited and inhibited by one of the products. For example, for the catalytic decomposition of nitrous oxide (N$_2$O) [11–14] over perovskite catalysts, most of the catalysts cannot tolerate the co-existence of O$_2$ because adsorbed oxygen blocks the catalytically active sites for the N$_2$O decompo-

sition [15,16]. However, the total decomposition of N$_2$O can be obtained in a perovskite catalytic membrane reactor if the inhibitor oxygen is continually removed from the N$_2$O side of the membrane [17].

Obviously, the performance of the membrane reactor used for water splitting or N$_2$O decomposition depends directly on the rate of oxygen removal from the system. In this work, a novel BaCo$_x$Fe$_y$Zr$_{1-x-y}$O$_{3-\delta}$ (BCFZ) hollow fiber perovskite membrane was employed to in situ remove O$_2$ from water dissociation or N$_2$O decomposition. This BCFZ hollow fiber membrane exhibits a high oxygen permeation rate and has already been used, for example, in the production of oxygen-enriched air [18] and the partial oxidation of hydrocarbons [19,20]. Special attention was given to the effect of oxygen permeability of the BCFZ membrane on the reactor performance for water splitting or N$_2$O decomposition.

2. Experimental

The dense BCFZ perovskite hollow fiber membranes were manufactured by a phase inversion process [21]. After sintering, the fiber has a thickness of around 0.17 mm with outer diameter of 1.10 mm and inner diameter of 0.76 mm. Fig. 1 shows a schematic diagram of the membrane reactor used in this study. Two ends of the hol-

* Corresponding author. Tel.: +49 511 7622942; fax: +49 511 76219121.
E-mail addresses: heqing.jiang@pci.uni-hannover.de, hq.jiang@yahoo.com (H. Jiang), juergen.caro@pci.uni-hannover.de (J. Caro).

ARTICLE IN PRESS
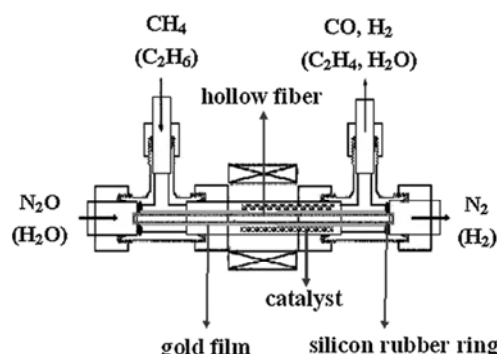
Fig. 1. Schematic diagram of membrane reactors for water splitting and N_2O decomposition.

Fig. 2. Concept of water splitting and N_2O decomposition in a perovskite oxygen-permeable membrane reactor.

low fiber were coated by Au paste (C5754, Heraeus GmbH) and then sintered at 950 °C for 5 h. The coating and sintering procedure were repeated three times and a dense Au film which is not permeable to oxygen was obtained on BCFZ membrane surface. Such Au-coated hollow fiber can be sealed by silicon rubber ring and the uncoated part (the effective length is 3 cm, and the effective membrane area is 0.86 cm^2) which is permeable to the oxygen can be kept in the middle of the oven ensuring isothermal conditions. The mixture of N_2O (or H_2O) and He was fed to the core side and a mixture of CH_4 (or C_2H_6). Ne and He was fed to the shell side. A Ni-based steam reforming (SR) catalyst (Süd Chemie AG) was packed around and behind the hollow fiber membrane when methane was used as the reducing gas on the shell side. N_2O, CH_4, C_2H_6, He and Ne flow rates were controlled by gas mass flow controllers (Bronkhorst). H_2O flow rate was controlled by the liquid mass flow controller (Bronkhorst) and was completely evaporated at 180 °C before it was fed to the reactor. All gas lines to the reactor and the gas chromatograph were heated to 180 °C. The concentrations of the gases at the exit of the reactor were determined by an on-line gas chromatograph (Agilent 6890). Only very small amounts of oxygen (below 0.001%) and also nitrogen (below 0.007%) were detected, which probably come from the residual air in the metal lines. So, it was assumed that the oxygen from water splitting on the core side was totally removed and the flow rate at the outlet is equal to that at the inlet, and H_2 production rate on the core side was calculated from the total flow rate F_{core} (cm^3 min^{-1}), the hydrogen concentration c (H_2), and the effective membrane area S (cm^2) based on the following equation:

$$J(H_2) = \frac{F_{core} \times c(H_2)}{S}$$

The N_2O conversion $X(N_2O)$, the C_2H_6 conversion $X(C_2H_6)$, and the C_2H_4 selectivity $S(C_2H_4)$ were calculated as

$$X(N_2O) = \left(1 - \frac{F(N_2O, \text{ out})}{F(N_2O, \text{ in})}\right) \times 100\%$$

$$X(C_2H_6) = \left(1 - \frac{F(C_2H_6, \text{ out})}{F(C_2H_6, \text{ in})}\right) \times 100\%$$

$$S(C_2H_4) = \frac{F(C_2H_4, \text{ out})}{F(C_2H_6, \text{ in}) - F(C_2H_6, \text{ out})} \times 100\%$$

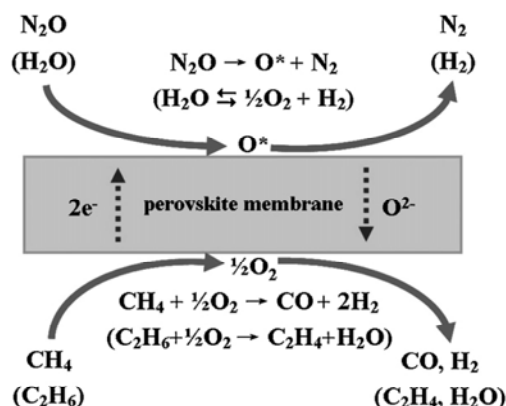where $F(i)$ is the flow rate of species i on the shell or core side of the hollow fiber membrane.

3. Results and discussion

### 3.1. The concept of water splitting and N_2O decomposition in membrane reactor

Water dissociation into hydrogen and oxygen is a reversible reaction, and the equilibrium constant of this reaction is very small even at a relatively high temperature. According to the low equilibrium constant of $K_p \approx 2 \times 10^{-8}$ at 950 °C [22], only very low equilibrium concentrations of $P_{O2} \approx 4.6 \times 10^{-6}$ bar and $P_{H2} \approx 9.2 \times 10^{-6}$ bar can be obtained. However, when this reaction is performed in the perovskite oxygen-permeable membrane reactor, as shown in Fig. 2, oxygen can permeate to the other side of the membrane where it is consumed by the partial oxidation of methane (POM) to form synthesis gas. Thus, oxygen and hydrogen become separated and the equilibrium of the water dissociation is continuously shifted to the product side.

Different to the equilibrium controlled water dissociation, the decomposition of N_2O is kinetically limited and inhibited by the product molecule oxygen. As shown in Fig. 2, the inhibitor O^* can be removed as oxygen ion (O^{2-}) via the membrane as it is generated from N_2O on perovskite membrane surface according to $N_2O \rightarrow N_2 + O^*$. The local charge neutrality can be maintained by the counter diffusion of electrons (e^-). To increase the driving force for the oxygen transport through the membrane, methane or ethane can be fed to the permeate side to consume the permeated oxygen.

3.2. Hydrogen production from water splitting

It was experimentally found that, if only inert gas was used as sweep on the shell side, the H_2 production rate on the steam side is very low. As shown in H_2 chromatograms (the inset of Fig. 3), hydrogen is hardly detectable even at 900 °C. However, H_2 was observed when feeding methane in combination with a Ni-based catalyst to the shell side, which is more effective to consume the permeated O_2 and establish a larger O_2 partial pressure gradient across the membrane. Because H_2 production rate depends directly on the rate of O_2 removal from water dissociation, it can be increased by increasing the temperature or a steeper oxygen partial pressure gradient across the membrane according to Wagner theory [23,24]. It can be seen from Fig. 3 that the hydrogen production rate increases from 0.7 to 3.1 cm^3 min^{-1} cm^{-2} as the temperature rises from 800 to 950 °C. Moreover, it was also found that increasing the concen-
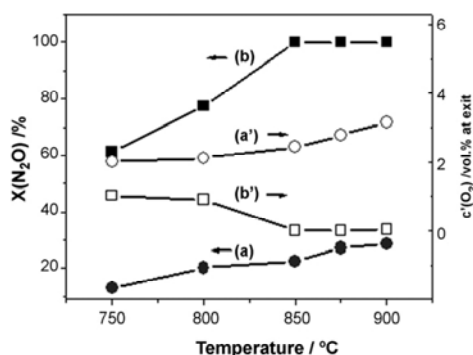
ARTICLE IN PRESS
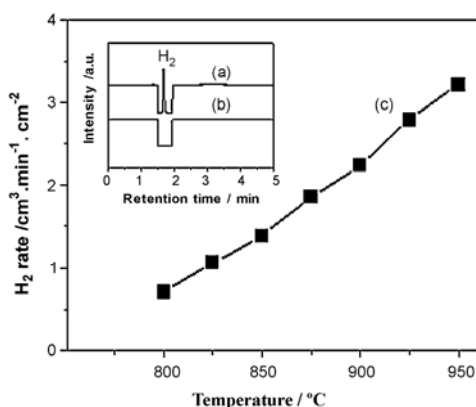
Fig. 3. H_2 production rate on the core side as a function of temperature. The inset shows H_2 chromatograms at $900\,°C$. Core side (a, b and c): $F_{H2O} = 30\,cm^3\,min^{-1}$ and $F_{He} = 10\,cm^3\,min^{-1}$. Shell side (a and c): $50\,cm^3\,min^{-1}$ ($F_{He} = 45\,cm^3\,min^{-1}$, $F_{Ne} = 3\,cm^3\,min^{-1}$ and $F_{CH4} = 2\,cm^3\,min^{-1}$). Shell side (b): $50\,cm^3\,min^{-1}$ ($F_{He} = 47\,cm^3\,min^{-1}$ and $F_{Ne} = 3\,cm^3\,min^{-1}$). Amount of packed bed Ni/Al$_2$O$_3$ catalyst: 0.8 g.
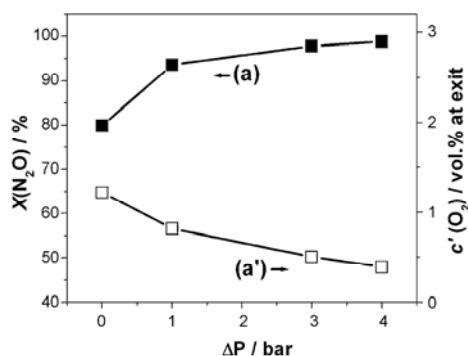
tration of steam in the feed gas will shift the equilibrium towards the water dissociation and more H_2 can be produced.

3.3. Direct decomposition of N_2O coupled with partial oxidation of methane

Fig. 4 presents N_2O conversion and oxygen concentration at the exit of N_2O side at different temperatures without and with oxygen removal. It can be seen that the conversion of N_2O increases with increasing temperature. When there is no sweep gas flow on the shell side, however, the conversion is relatively low (below 30% even at $900\,°C$) since the produced oxygen from the N_2O decomposition was not removed and – as a result – the oxygen concentration at the exit of N_2O side increases when the temperature rises from 750 to $900\,°C$, as shown in Fig. 4a′. To obtain a higher conversion of N_2O decomposition, the adsorbed surface oxygen O* should be removed fast. As shown in Fig. 4b′, when diluted methane was fed to the shell side, the oxygen concentration at the exit of N_2O side decreases with increasing temperature because the oxygen from N_2O decomposition can be effectively removed in this case. Accordingly, the conversion of N_2O decomposition was sig-
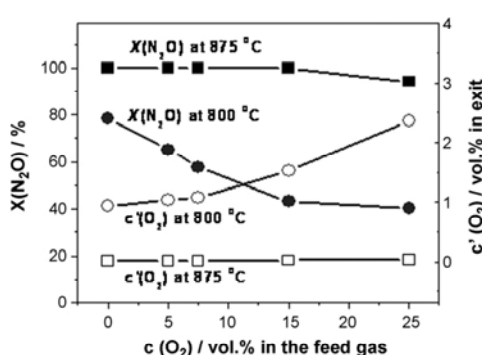

Fig. 5. N_2O conversion (a) and oxygen concentration (a′) at the exit of N_2O side as a function of pressure difference. Core side: $F_{N2O} = 6\,cm^3\,min^{-1}$, $F_{He} = 24\,cm^3\,min^{-1}$, $P = 1.0–5.0\,bar$. Shell side: $40\,cm^3\,min^{-1}$ ($F_{CH4} = 8\,cm^3\,min^{-1}$, $F_{Ne} = 12\,cm^3\,min^{-1}$ and $F_{H2O} = 20\,cm^3\,min^{-1}$), $P = 1\,bar$, $T = 800\,°C$. Amount of packed bed Ni/Al$_2$O$_3$ catalyst: 1.2 g.

nificantly improved, as shown in Fig. 4b. When the temperature reaches $850\,°C$, N_2O in a concentration of 20 vol.% on the core side was totally decomposed.

As mentioned above, the conversion of N_2O decomposition is related to the oxygen permeability of the membrane. According to Wagner equation, the oxygen permeation rate can be improved by increasing the oxygen partial pressure gradient across the membrane. Fig. 5 shows the influence of pressure difference on the N_2O conversion and oxygen concentration at the exit of N_2O side at $800\,°C$. It can be seen that N_2O conversion increases with rising pressure difference because more oxygen from N_2O decomposition can be transported to the other side of the membrane in the case of a steeper oxygen partial pressure gradient. It was found that the N_2O conversion increased from 80% to 99% when changing the pressure difference from 0 to 4 bar. Accordingly, the oxygen concentration at exit of N_2O side decreased gradually with increasing pressure difference due to the depletion of N_2O, as shown in Fig. 5a′.

In order to investigate the effect of the presence of external oxygen in the feed gas on N_2O abatement in this membrane reactor, different amounts of oxygen were added to the N_2O/He co-feed on the core side. From Fig. 6, we can see that N_2O conversion decreased with increasing oxygen concentration in the N_2O/O_2 co-feed gas at $800\,°C$. Oxygen cannot become totally removed due to the limited oxygen permeability of this membrane at this temperature, which

Fig. 4. N_2O conversion and oxygen concentration at exit of N_2O side as a function of temperature without (a and a′) or with (b and b′) oxygen removal. Core side: $F_{N2O} = 6\,cm^3\,min^{-1}$, $F_{He} = 24\,cm^3\,min^{-1}$. Shell side: (a and a′) no feed gas or (b and b′) $40\,cm^3\,min^{-1}$ ($F_{CH4} = 8\,cm^3\,min^{-1}$, $F_{Ne} = 12\,cm^3\,min^{-1}$ and $F_{H2O} = 20\,cm^3\,min^{-1}$). Amount of packed bed Ni/Al$_2$O$_3$ catalyst: 1.2 g.

Fig. 6. N_2O conversion and oxygen concentration at the exit of N_2O side as a function of oxygen concentration in the N_2O/O_2 co-feed gas. Core side: $30\,cm^3\,min^{-1}$ ($F_{N2O} = 6\,cm^3\,min^{-1}$, $F_{O2} = 1.5–7.5\,cm^3\,min^{-1}$, $F_{He} = balance$). Shell side: $40\,cm^3\,min^{-1}$ ($F_{CH4} = 18\,cm^3\,min^{-1}$, $F_{H2O} = 22\,cm^3\,min^{-1}$). Amount of packed bed Ni/Al$_2$O$_3$ catalyst: 1.2 g.

ARTICLE IN PRESS

Table 1
C_2H_6 conversion $X(C_2H_6)$, C_2H_4 selectivity $S(C_2H_4)$ and N_2O conversion $X(N_2O)$ at different temperatures.

Temperature/°C	$X(C_2H_6)$/%	$S(C_2H_4)$/%	$X(N_2O)$/%
800	57	88	68
850	85	86	100
875	91	80	100

Core side: F_{N2O} = 1.5 cm^3 min^{-1}, F_{He} = 28.5 cm^3 min^{-1}. Shell side: 50 cm^3 min^{-1} (F_{C2H6} = 11.5 cm^3 min^{-1}, F_{Ne} = 1 cm^3 min^{-1}, F_{He} = 32.5 cm^3 min^{-1} and F_{H2O} = 5 cm^3 min^{-1}).

can be further confirmed by the fact that the oxygen concentration at exit increased with increasing oxygen concentration in the co-feed gas. The excess oxygen will produce an inhibition effect on N_2O decomposition. However, N_2O conversion reached 99% and did not change with increasing oxygen concentration in the co-feed gas at 875 °C. According to the high oxygen permeability of BCFZ membrane at this temperature, all the oxygen can be removed from the N_2O side as shown in Fig. 6. These results show that the active surface of BCFZ membrane employed for N_2O abatement was not poisoned by adsorbed oxygen at high temperatures.

The permeated oxygen from N_2O decomposition can be used to produce synthesis gas by the POM on the shell side. According to a previous study [19], the so-called POM process using a Ni-based catalyst is first a total oxidation of methane to H_2O and CO_2, which is followed by steam and CO_2 reforming. A methane conversion of over 90% and CO selectivity of 90% were obtained at 875 °C. When oxygen is provided by thermal splitting of water, only limited amounts of oxygen were transported to methane side due to the very low equilibrium constant of water dissociation, and it was found that only 2 cm^3 min^{-1} methane can be converted into synthesis gas with methane conversion of 70% and CO selectivity of 60% [10]. Here, it was found that around 20 cm^3 min^{-1} methane can be converted into synthesis gas with CO yield of above 80% when N_2O was used to provide oxygen, indicating that N_2O decomposes easier than water to provide oxygen in the membrane reactor.

3.4. Direct decomposition of N_2O coupled with dehydrogenation of ethane

From the above discussion, to achieve the total decomposition of N_2O, a reducing gas should be used on the permeate side to consume the permeated oxygen, thus ensuring a large driving force for the fast oxygen removal from N_2O side. Besides methane, ethane was also used as the reducing gas in this paper. At high temperature, the thermal dehydrogenation of ethane leads to the formation of ethylene and hydrogen according to Eq. (1).

$$C_2H_6 \leftrightharpoons C_2H_4 + H_2 \tag{1}$$

The produced hydrogen can be used to consume the permeated oxygen from N_2O side based on Eq. (2).

$$H_2 + 1/2O_2 \rightarrow H_2O \tag{2}$$

From Table 1, it can be found that, on increasing the temperature from 800 to 875 °C, ethane conversion increases from about 57% to 91%. Besides C_2H_4, H_2, H_2O and C_2H_6, CO and CO_2 were also detected in the effluents. Simultaneously, with rising temperature, N_2O conversion increased from 68% to almost 100% due to the increasing oxygen permeation rate. The ethylene selectivity decreases from 88% to 80%, the concentrations of CO increase from 1% to 4%, and the concentrations of CO_2 increase from 0.4% to 0.7%. An increasing amount of methane was also found in the product stream from the shell side of BCFZ membrane. In the dehydrogenation of C_2H_6 to C_2H_4, in addition to the combustion of hydrogen by

the permeated oxygen, the deep oxidation of C_2H_4 to CO and CO_2 could not be avoided in the hollow fiber membrane reactor.

4. Conclusions

By using a perovskite-type BCFZ oxygen-permeable hollow fiber membrane, oxygen from water dissociation can be continually removed, and the equilibrium of this reaction is continuously shifted to the product side. When feeding methane to the permeate side, a larger driving force was provided for oxygen transport through the membrane, and accordingly significant amounts of hydrogen can be produced. A hydrogen production rate of 3.1 cm^3 min^{-1} cm^{-2} was obtained at 950 °C. For the decomposition of N_2O over perovskite BCFZ, the surface adsorbed oxygen acts as an inhibitor. To obtain a higher N_2O conversion, the oxygen concentration on N_2O side should be kept at a very low level, which can be achieved by in situ removing the inhibitor oxygen via BCFZ hollow fiber membrane. It was found that the oxygen concentration on N_2O side can be kept at a low level by increasing the temperature or the pressure difference and by feeding reducing gases like methane or ethane on permeate side. Benefiting from the effective oxygen removal via the oxygen-permeable membrane, a complete decomposition of N_2O with the concentration of 20 vol.% was obtained at 850 °C. Moreover, the permeated oxygen was used to produce synthesis gas by the POM or ethylene by the dehydrogenation of ethane on the shell side. An ethane conversion of 85% and an ethylene selectivity of 86% were obtained at 850 °C.

References

[1] R. Dittmeyer, J. Caro, in: G. Ertl, H. Knözinger, F. Schüth, J. Weitkamp (Eds.), Handbook of Heterogeneous Catalysis, vol. 4, Wiley-VCH, Weinheim, 2008, p. 2221.
[2] J. Sunarso, S. Baumann, J.M. Serra, W.A. Meulenberg, S. Liu, Y.S. Lin, J.D. Costa, J. Membr. Sci. 320 (2008) 13.
[3] K. Sirkar, P. Shanbhag, A. Kovvali, Ind. Eng. Chem. Res. 38 (1999) 3715.
[4] Y.T. Liu, X.Y. Tan, K. Li, Catal. Rev.-Sci. Eng. 48 (2006) 145.
[5] C. Chen, S.J. Feng, S. Ran, D.C. Zhu, W. Liu, H.J.M. Bouwmeester, Angew. Chem. Int. Ed. 115 (2003) 5354.
[6] W.S. Yang, H.H. Wang, X.F. Zhu, L.W. Lin, Top. Catal. 35 (2005) 155.
[7] F.T. Akin, Y.S. Lin, AIChE. J. 48 (2002) 2298.
[8] U. Balachandran, T.H. Lee, S. Wang, S.E. Dorris, Int. J. Hydrogen Energy 29 (2004) 291.
[9] U. Balachandran, T.H. Lee, S.E. Dorris, Int. J. Hydrogen Energy 32 (2007) 4451.
[10] H.Q. Jiang, H.H. Wang, S. Werth, T. Schiestel, J. Caro, Angew. Chem. Int. Ed. 47 (2008) 9341.
[11] J. Pérez-Ramírez, F. Kapteijn, G. Mul, J.A. Moulijn, Chem. Commun. 11 (2001) 693.
[12] G. Centi, A. Galli, B. Montanari, S. Perathoner, A. Vaccari, Catal. Today 35 (1997) 113.
[13] N. Russo, D. Fina, G. Saracco, V. Specchia, Catal. Today 119 (2007) 228.
[14] E.V. Kondratenko, O. Ovsitser, Angew. Chem. Int. Ed. 47 (2008) 2983.
[15] N. Gunasekaran, S. Rajadurai, J.J. Carberry, Catal. Lett. 35 (1995) 373.
[16] N. Russo, D. Mescia, D. Fino, G. Saracco, V. Specchia, Ind. Eng. Chem. Res. 46 (2007) 4226.
[17] H.Q. Jiang, H.H. Wang, F.Y. Liang, S. Werth, T. Schiestel, J. Caro, Angew. Chem. Int. Ed. 48 (2009) 2983.
[18] H.H. Wang, S. Werth, T. Schiestel, J. Caro, Angew. Chem. Int. Ed. 44 (2005) 6906.
[19] H.H. Wang, C. Tablet, T. Schiestel, S. Werth, J. Caro, Catal. Commun. 7 (2006) 907.
[20] H.H. Wang, C. Tablet, J. Caro, Catal. Today 118 (2006) 98.
[21] T. Schiestel, M. Kilgus, S. Peter, K.J. Caspary, H.H. Wang, J. Caro, J. Membr. Sci. 258 (2005) 1.
[22] S. Ihara, Bull. Electrotech. Lab. 41 (1977) 259.
[23] M. Schroeder, Phys. Chem. Chem. Phys. 7 (2005) 166.
[24] R. Merkle, J. Maier, H.J.M. Bouwmeester, Angew. Chem. Int. Ed. 43 (2004) 5069.

Chapter 4

Conclusions

In this thesis, the coupling of energy/environment related reactions in the perovskite catalytic membrane reactor has been demonstrated. Specifically, the equilibrium controlled water splitting and the kinetically controlled NO and N_2O decomposition were studied in the perovskite BCFZ hollow fiber membrane reactor that allows the selective permeation of oxygen. It is found that both the hydrogen production rate and the conversion of NO and N_2O on the core side directly depend on the rate of oxygen removal from the core side to the shell side of the BCFZ membrane. The effective hydrogen production or nitrogen oxides abatement were achieved by coupling water dissociation or nitrogen oxides decomposition with a series of oxygen-consuming reactions on the opposite sides of the BCFZ hollow fiber membrane reactor.

To produce more hydrogen from the equilibrium controlled water splitting on the core side of BCFZ membrane, the simultaneously produced oxygen should be quickly removed from the steam side to the other side. In other words, a higher oxygen permeation rate should be achieved, which can be realized by establishing a larger gradient of oxygen partial pressure across the membrane. Three oxygen-consuming reactions were employed to couple with water splitting for the effective hydrogen production in the perovskite BCFZ hollow fiber membrane.

First, methane combustion was employed to couple with water splitting. When a blank BCFZ hollow fiber was used as the reactor, the membrane itself shows a poor catalytic activity towards methane combustion. This was confirmed by the fact that much un-reacted methane and oxygen were detected from the effluent of the shell side when methane and air were, respectively, fed to the shell side and core side of the BCFZ membrane. To improve the catalytic activity of the membrane surface and thus the oxygen permeation rate, a catalytic BCFZ-Pd porous layer was deposited onto the outer surface of the dense BCFZ hollow fiber membrane. It is found that under the catalysis of the BCFZ-Pd porous layer, almost all the permeated oxygen was consumed by methane combustion. Due to the establishment of a larger gradient of oxygen partial pressure across the membrane, the oxygen permeation rate

was increased by 3.5 times as compared to that of the blank BCFZ membrane. Accordingly, the hydrogen production rate from water splitting was increased from 0.7 to 2.1 mL min^{-1} cm^{-2} at 950 °C after depositing a BCFZ-Pd porous layer onto the BCFZ membrane.

Second, the POM to synthesis gas was coupled with water splitting. In this work, a Ni-based reforming catalyst was packed around and behind the BCFZ hollow fiber membrane on the shell side. The permeated oxygen first reacted with methane to form CO_2 and H_2O. In the presence of Ni-based reforming catalyst, the produced CO_2 and H_2O were converted with methane to give CO and H_2 by dry reforming and steam reforming. Thus, synthesis gas was on-line produced, which shows stronger ability to consume the permeated oxygen. A hydrogen production rate of 3.1 cm^3 min^{-1} cm^{-2} was obtained at 950 °C on the core side of BCFZ membrane. Moreover, CO_2 and H_2O will convert with the residual methane into CO and H_2 in the presence of Ni-based reforming catalyst behind the active zone of the BCFZ hollow fiber membrane. Thus, synthesis gas was obtained on the shell side of the BCFZ membrane.

In the third work, water splitting was coupled with ODE process. Compared to the POM process, the ODE normally takes place at even lower temperatures. It is found that significant amounts of hydrogen were obtained at moderate temperatures (700-800 °C) by coupling water splitting with the ODE process on the opposite sides of the BCFZ hollow fiber membrane. At 800 °C, a hydrogen production rate of around 1.0 cm^3 min^{-1} cm^{-2} was achieved on the steam side, and a ethylene yield of 55 % was obtained on the other side of the BCFZ membrane. Moreover, the operation for the simultaneous production of hydrogen from water splitting on the side and ethylene on the shell side

The decomposition of NO or N_2O into N_2 and O_2 over the perovskite BCFZ is inhibited by oxygen. To obtain a highly effective abatement of nitrogen oxides, the oxygen partial pressure should be kept at a very low lever, which can be achieved by in situ removing the inhibitor oxygen via the perovskite BCFZ oxygen-permeable membrane. It was found that the conversion of NO or N_2O on the core side is very low when no sweep gas was applied on the shell side. However, when feeding methane in combination with Ni-based catalyst to the shell side, the direct decomposition of NO over the inner surface of the BCFZ hollow fiber membrane was achieved with NO conversion of almost 100 % even with coexisting 3 % oxygen in the feed. Moreover, benefiting from the in situ removal of oxygen, the undesired

NO_2 formation by the consecutive reaction between NO and O_2 can effectively be prevented. The N_2 selectivity of NO decomposition was found to be around 95 %.

For the N_2O decomposition in the BCFZ membrane reactor, the conversion was enhanced by increasing the operating temperature or the pressure difference across the membrane or by feeding reducing gases like methane or ethane on the permeate side. When methane was used as the reducing gas on the shell side, the oxygen concentration on the N_2O side can be kept at a low level, thus avoiding the inhibition of the N_2O decomposition by adsorbed surface oxygen species. A complete decomposition of N_2O with the concentration of up to 50 % was achieved at 875 °C. Moreover, the permeated oxygen was utilized to produce synthesis gas by the POM or ethylene by the ODE on the shell side. A methane conversion of over 90 % and a CO selectivity of 90 % were obtained at 875 °C with the simultaneous complete decomposition of 20 % N_2O.

In summary, this Ph. D. work presented the effective hydrogen production from water splitting and nitrogen oxides abatement by in situ removing oxygen via a perovskite BCFZ hollow fiber membrane. In the presented coupling strategies, not only the reactions on both sides of the membrane reactor are energy/environment related and industrially interesting, but also the reactor performance has been significantly improved, which contributes to the concept of process intensification.

82

Publications and Conferences

Publications included in this thesis

1. <u>Heqing Jiang</u>, Zhengwen Cao, Steffen Schirrmeister, Thomas Schiestel, and Jürgen Caro, *A coupling strategy to produce hydrogen and ethylene in a membrane reactor*, **Angew. Chem. Int. Ed.,** 2010, **revised.**

2. <u>Heqing Jiang</u>, Fangyi Liang, Oliver Czuprat, Konstantin Efimov, Armin Feldhoff, Steffen Schirrmeister, Thomas Schiestel, Haihui Wang, and Jürgen Caro, *Hydrogen production by water dissociation in surface-modified $BaCo_xFe_yZr_{1-x-y}O_{3-\delta}$ hollow fiber membrane reactor with improved oxygen permeation*, **Chem. Eur. J.***,* 2010, **accepted**.

3. <u>Heqing Jiang</u>, Haihui Wang, Fangyi Liang, Steffen Werth, Steffen Schirrmeister, Thomas Schiestel, and Jürgen Caro, *Improved water dissociation and nitrous oxide decomposition by in situ oxygen removal in perovskite catalytic membrane reactor*, **Catal. Today**, 2010, doi: 10.1016/j.cattod.2010.02.027.

4. <u>Heqing Jiang</u>, Lei Xing, Oliver Czuprat, Haihui Wang, Steffen Schirrmeister, Thomas Schiestel, and Jürgen Caro, *Highly effective NO decomposition by in situ removal of inhibitor oxygen using an oxygen transporting membrane*, **Chem. Commun.**, 2009, 6738.

5. <u>Heqing Jiang</u>, Haihui Wang, Fangyi Liang, Steffen Werth, Thomas Schiestel, and Jürgen Caro, *Direct decomposition of nitrous oxide to nitrogen by in situ oxygen removal with a perovskite membrane*, **Angew. Chem.,** 2009, *121*, 3027; **Angew. Chem. Int. Ed.,** 2009, *48*, 2983.
    (Selected as **Front Cover**; Highlighted by **Nature,** 2009, *457*, 639**.**)

6. <u>Heqing Jiang</u>, Haihui Wang, Steffen Werth, Thomas Schiestel, and Jürgen Caro, *Simultaneous production of hydrogen and synthesis gas by combining water splitting with partial oxidation of methane in a hollow-fiber membrane reactor*, **Angew. Chem**., 2008, *120*, 9481; **Angew. Chem. Int. Ed.,** 2008, *47*, 9341.
    (Reported by **Chemistry World**, 2008, 5 (12) as the News: "*Double reactor makes hydrogen and syngas*").

Publications not included in this thesis

7. <u>Heqing Jiang</u>, Fangyi Liang, Armin Feldhoff, Steffen Schirrmeister, Thomas Schiestel, and Jürgen Caro, *Design of nanostructure catalytic coating onto the ceramic membrane for synthesis gas production*, In preparation.

8. Huixia Luo, Bingbing Tian, Yanying Wei, Haihui Wang, <u>Heqing Jiang</u>, and Jürgen Caro, *Oxygen permeability and structural stability of a novel tantalum-doped perovskite* $BaCo_{0.7}Fe_{0.2}Ta_{0.1}O_{3-\delta}$, **AIChE Journal,** 2010, *56*, 604.

9. Huixia Luo, Yanying Wei, <u>Heqing Jiang</u>, Wenhui Yuan, Yangxiao Lv, Jürgen Caro, and Haihui Wang, *Performance of a ceramic membrane reactor with high oxygen flux Ta-containing perovskite for the partial oxidation of methane to syngas*, **J. Mem. Sci.**, 2010, *350*, 154.

10. Hongjun Chen, Yuling Wang, <u>Heqing Jiang</u>, Baifeng Liu, and Shaojun Dong, *Spontaneous formation of two-dimensional gold networks at the air−water interface and their application in surface-enhanced Raman scattering (SERS)*, **Crystal Growth & Design**, 2007, *7*, 1771.

11. Minghua Huang, <u>Heqing Jiang</u>, Junfeng Zhai, Baifeng Liu, and Shaojun Dong, *A simple route to incorporate redox mediator into carbon nanotubes/Nafion composite film and its application to determine NADH at low potential*, **Talanta**, 2007, *74*, 132.

12. <u>Heqing Jiang</u>, Xuping Sun, Minghua Huang, Yuling Wang, Dan Li, and Shaojun Dong. *Rapid self-assembly of oligo(o-phenylenediamine) into one-dimensional structures through a facile reprecipitation route,* **Langmuir**, 2006, *22*, 3358.

13. Lina Huang, <u>Heqing Jiang</u>, Jisheng Zhang, Zhijun Zhang, and Pingyu Zhang, *Synthesis of copper nanoparticles containing diamond-like carbon films by electrochemical method*, **Electrochem. Commun.**, 2006, *8*, 262.

14. Minghua Huang, <u>Heqing Jiang</u>, Xiaohu Qu, Zhiai Xu, Yuling Wang, and Shaojun Dong, *Small molecules as cross-linkers: fabrication of carbon nanotubes/thionine self-assembled multilayers on amino functionalized surfaces*, **Chem.Commun.**, 2005, 5560.

15. Minghua Huang, Yongdong Jin, <u>Heqing Jiang</u>, Xuping Sun, Hongjun Chen, Baifeng Liu, Erkang Wang, and Shaojun Dong, *Designed nanostructured Pt film for electrocatalytic activities by underpotetntial deposition combined chemical replacement techniques*, **J. Phys. Chem. B.**, 2005,*109*, 15264.

16. <u>Heqing Jiang</u>**,** Lina Huang, Zhijun Zhang, Tao Xu, and Weimin Liu. *Facile deposition of copper-doped diamond-like carbon nanocomposite films by a liquid-phase electrochemical route, **Chem. Commun.**,* 2004, 2196.

17. <u>Heqing Jiang</u>**,** Lina Huang, Shujie Wang, Zhijun Zhang, Tao Xu, and Weimin Liu, *Synthesis of diamond-like carbon films by electrolysis of dimethylsulfoxide*, **Electrochem. Solid-State Lett.**, 2004, *7*, D19.

18. <u>Heqing Jiang</u>**,** Lina Huang, Zhijun Zhang, Tao Xu, and Weimin Liu, *Deposition of nanostructured diamond-like carbon films on Al substrate by facile electrochemical route*, **Chem. Lett.,** 2004, *33,* 378.

19. <u>Heqing Jiang</u>**,** Zhijun Zhang, Tao Xu, and Weimin Liu, *Research progress on the preparation of diamond-like carbon film by the liquid phase electrodeposition technique*, **Surf. Tech.**, 2004, *33*, 4.

20. Lina Huang, <u>Heqing Jiang</u>**,** Zhijun Zhang, Tao Xu, and Weimin Liu, *Preparation of diamond-like carbon films from acetonitrile by electrochemical method, **Chem. Res.** 2004, 15*, 9.

21. <u>Heqing Jiang</u>**,** Lina Huang, Zhijun Zhang, Tao Xu, and Weimin Liu, *The composition and structure of diamond-like carbon films prepared by using liquid-phase electrodeposition technique*, **J. Funct. Mater.,** 2004, *35*, 560.

22. Raojie Tao, Shuangquan Zang, and <u>Heqing Jiang</u>, and Benyong Lou, *Synthesis, characterization and electrochemical of dioxotetraamines heterobinuclear, **Chem. Res.,** 2001, 12*, 23.

Contributions to Conferences

1. <u>Heqing Jiang</u>, Haihui Wang, Fangyi Liang, Steffen Werth, Steffen Schirrmeister, Thomas Schiestel, and Jürgen Caro. *Improved nitrous oxide decomposition and water splitting by in-situ oxygen removal in perovskite catalytic membrane reactor.* ***9th International Conference on Catalysis in membrane reactors***, 2009, S08-O3, Lyon, France. **(Talk)**.

2. <u>Heqing Jiang</u>, Haihui Wang, Fangyi Liang, Steffen Werth, Steffen Werth, Thomas Schiestel, Jürgen Caro. *Water splitting and catalytic N_2O decomposition by in-situ removing oxygen in the hollow fiber perovskite membrane reactor.* ***42nd Annual Meeting of the German Catalysis Society***, 2009, Weimar, Germany. **(Talk)**.

3. <u>Heqing Jiang</u>, Xuping Sun, Minghua Huang, Yuling Wang, Erkang Wang, and Shaojun Dong. *Bulk synthesis of poly(o-phenylenediamine) one-dimensional nanostructures by reprecipitation.* ***10th International Seminar on Electroanalytical Chemistry***, 2005, P-25, p.134, Changchun, China. **(Poster)**.

4. <u>Heqing Jiang</u>, Minghua Huang, Erkang Wang, and Shaojun Dong, *A facile electrochemical route to synthesize Au and Ag metal nanoparticles stabilized by polyoxometalates,* ***9th National Conference on Electroanalytical Chemistry***, 2005, D50, p.392; Nanjing, China. **(Talk)**.

5. <u>Heqing Jiang</u>, Lina Huang, and Zhijun Zhang. *Attempt to deposit diamond-like carbon films by electrolysis of DMSO under mild condition.* ***24th Annual Meeting of the Chinese Chemical Society***, 2004, 11-025, Changsha, China. **(Talk)**.

Curriculum Vitae

Personal data

Date of birth	September 12, 1978
Place of birth	Henan, China
Nationality	Chinese
Marital status	Married, one child

Awards

2008	Chinese Government Award for Outstanding Self-financed Students Abroad
2006	First-Class Award of Excellent Paper of Natural Science in Henan Province

Education and work experiences

Since 04/2007	**Scientific co-worker** at the group of Prof. Dr. Jürgen Caro, Institute of Physical Chemistry and Electrochemistry, Leibniz Universität Hannover, Germany
07/2004-04/2007	**Research assistant** at the group of Prof. Shaojun Dong, State Key Laboratory of Electroanalytical Chemistry, Changchun Institute of Applied Chemistry, Chinese Academy of Sciences, China
09/2001-07/2004	**Graduate student** at Key Laboratory for Special Functional Materials of Ministry of Education, Henan University, China **Degree:** Master of Science, mark: excellent
09/1997-07/2001	**Undergraduate student** at Department of Chemistry, Henan University, China **Degree:** Bachelor of Science, mark: excellent

Erklärung zur Dissertation

Hiermit erkläre ich, dass ich die vorliegende Arbeit selbstständig verfasst und nur unter Verwendung der angegebenen Quellen und Hilfsmittel angefertigt habe. Die Dissertation ist nicht schon als Diplomarbeit oder ähnliche Prüfungsarbeit verwendet worden.

Hannover, im März 2010

_____

(Unterschrift)

Name: Heqing Jiang